Investigating the neural circuitry of the Mushroom body calyx in *Drosophila melanogaster*

Dissertation

zur Erlangung des Doktorgrades (Dr. rer. nat.)

der Mathematisch-Naturwissenschaftlichen Fakultät

der Rheinischen Friedrich-Wilhelms-Universität Bonn

vorgelegt von

Philipp Ranft

aus

Hannover

Bonn, 22.04.2020

Angefertigt mit der Genehmigung der Mathematisch-Naturwissenschaftlichen Fakultät der Rheinischen Friedrich-Wilhelms Universität Bonn

1. Gutachter: Prof. Dr. rer. nat. Gaia Tavosanis
2. Gutachter: Prof. Dr. rer. nat. Michael Pankratz

Tag der mündlichen Prüfung: 07.07.2020
Erscheinungsjahr: 2020

Erklärung

Hiermit erkläre ich, dass ich die vorliegende Dissertation selbständig angefertigt habe, dass ich sie zuvor an keiner anderen Hochschule und in keinem anderen Studiengang eingereicht habe. Es wurden keine anderen als die angegebenen Quellen und Hilfsmittel benutzt. Die Stellen der Arbeit, die dem Wortlaut oder dem Sinne nach anderen Werken entnommen wurden, sind unter Angabe der Quellen kenntlich gemacht.

Table of Contents

List of Figures

List of Tables

Abstract

In *Drosophila melanogaster*, the mushroom body (MB) is essential for the formation and retrieval of olfactory associative memories. Within its input region, the MB calyx, olfactory information is delivered from second order projection neurons (PN) to MB intrinsic neurons. These cells form characteristic synaptic complexes called Microglomeruli (MGi). Previous studies suggest that MGi include modulatory neurons, which connect the calyx with other brain regions. However, these studies were unable to identify the cell types and to which extent they contribute to the MG complex. Furthermore, studies in other insect models suggest that the organization of the MB calyx underlies plastic changes induced by experience and changes in the sensory environment.

This thesis consists of three projects with the aim to help understand the function and the structure of the MB calyx in *Drosophila*. First, a complete reconstruction of a Microglomerulus (MG) synaptic complex identified all neurons and their local pre- and postsynaptic connections. This local connectome suggests that MGi are complex local microcircuits that include modulatory GABAergic neurons. Second, the possibility of learning induced plastic changes in the organization of the MB calyx was investigated. By visualizing the pre- and postsynaptic partners within MGi, we could reveal a structural reorganization of the calyx accompanied by the formation of new MGi following olfactory conditioning. In a second approach, the odors were substituted by manipulating neuronal activity with light-sensitive cation channels. This approach however, could not induce memory. The third project gives a first description of a neuron found in the MG reconstruction, called mushroom body neuron 1 (MB-C1). The neuron was identified as GABAergic and to connect the MB calyx with the center for innate behavior, the Lateral horn (LH). Silencing the neuron during odor application and conditioning experiments however did not allow an unambiguous conclusion about the function of MB-C1.

Overall, the data represented here suggest that the MG is a complex local microcircuit that undergoes structural changes upon the formation of associative memory. These findings provide the basis for further studies to investigate the olfactory processing in the calyx and the cellular mechanisms involved in plasticity.

1 Introduction

A prominent and striking ability of the brain is to gain knowledge, which underlies "learning" and "forming memory". Learning is defined as an adaptive change in behavior based on experience. When an animal is able to store gained information and reproduce the learned behavior at a later time, we speak of memory. These two functions are highly conserved across many different animal species and help them to cope with drastic changes in their environment.

1.1 *Drosophila* in neurobiology

One key element in the understanding of how brains learn and retain information is the thorough mapping of the underlying neuronal circuitries. The human brain consists of approximately 86 to 100 billion neurons forming connections via estimated 100 trillion synapses for extensive review see (Herculano-Houzel 2009). Therefore it is no surprise that still in today's era of modern science our brain remains to be a great mystery to us. Recently, science has made great progress in developing imaging techniques to visualize the anatomy and some physiological processes in healthy and diseased brains. But still, for the fundamental understanding of how neuronal networks operate, we rely to a large extent on research made in simpler organisms.

A powerful and widely used model organism is the fruit fly *Drosophila melanogaster*. Unmatched by any other model organism, *Drosophila* offers a great neurogenetic tool kit with highly specific driver lines for specific neurons. The brain of the fruit fly has

approximately 100000 neurons, many of which are reproducibly identifiable across individuals. Overall, the genetic access to specific neurons in combination with modern neuroscience techniques helped greatly in defining mechanisms underlying many brain functions on the level of cellular resolution (Amin and Lin 2019). Among these techniques are optogenetic and thermogenetic manipulations of neural activity, functional imaging with genetically encoded calcium indicators, targeted patch-clamp recordings and connectome reconstruction from electron microscopy volumes.

1.1.1 How to target neurons: The UAS/GAL4 system and others

The GAL4/UAS system is particularly useful for the manipulation of defined populations of neurons. In fact, this binary system allows targeting subsets of neurons by simply crossing a GAL4 driver fly with an upstream activating sequence (UAS) reporter fly (Brand and Perrimon 1993; Phelps and Brand 1998). The GAL4 protein, which originated from yeast *Saccharomyces cerevisiae*, binds to the UAS and induces the transcription of neighboring genes. The artificial expression of GAL4 itself is put under the control of a defined native gene promoter. Consequently, GAL4 is only expressed in cells in which the native gene is active, assuring a cell-specific driver line. In turn, UAS-driven transgenes remain silent unless activated by the binding of the GAL4 protein in a given cell. This induces a UAS-driven transgene expression in GAL4 expressing cells only.

Additionally, other systems have been introduced to the field over the last years and are commonly used today. For example, as most GAL4 driver lines target a large variety of cells, a more specific yet genetically more complex alternative is offered by the splitGAL4 system. In this system two separate GAL4 driver lines are combined. However, each driver line only expresses one portion of the GAL4 protein, which is inactive by itself, yielding a full GAL4 protein only if both elements are co-expressed. Thus, only if the pattern of expression of the driver lines overlap and both portions of the GAL4 protein are translated in the same cell, a functional GAL4 protein can be reconstituted and can bind to the UAS site (Pfeiffer et al. 2010). Another alternative to the GAL4 is the LexA/lexAop system. It works similarly to but independently from the GAL4/UAS system, and can thus be used simultaneously without any interference in the same fly (Lai and Lee 2006).

1.2 Classical conditioning in *Drosophila*

First described by Ivan Pavlov, animals have the ability to form associative memories (Pavlov 1927). In a process called classical conditioning, an animal learns to associate a

neutral stimulus, the conditioned stimulus (CS), with a biological significant stimulus which elicits an innate response, the unconditioned stimulus (US). The US can be either rewarding or aversive. The association between the two stimuli leads in the future to a changed responsive behavior towards the formally neutral CS, according to the either attractive or aversive value of the US. Likewise, fruit flies are able to form such associative memories (Quinn, Harris, and Benzer 1974; Tully and Quinn 1985). For example, flies are able to form an association between a neutral odor and a US in a designed olfactory conditioning experiment (Tully and Quinn 1985). Here, flies are at first exposed to an odor alone and later exposed to a second odor paired with either a sugar reward or an electric shock. Afterwards flies are tested in a T-maze, in which they have to choose between the two odors (Tully and Quinn 1985). Standardized over the years, this paradigm has become a widely used setup in studying fruit flies' ability to form memories (Krashes and Waddell 2011).

1.3 The olfactory system of *Drosophila*

The olfactory system in insects, in particular in *Drosophila* (Fig. 1), is widely used for studying how sensory information is processed within neuronal circuits. Although the circuitry is similar to that of more complex organisms (Su, Menuz, and Carlson 2009), it is numerically smaller. The perception of extrinsic odor cues begins at the antennae, where odor molecules are detected via olfactory receptors from a large set of olfactory sensory neurons (OSNs), each of which has a particular chemical sensitivity (de Bruyne, Clyne, and Carlson 1999; de Bruyne, Foster, and Carlson 2001; Yao, Ignell, and Carlson 2005; Hallem and Carlson 2006; Benton et al. 2009). Odor molecules binding to a receptor initiate action potentials, which are transmitted into the central brain. OSNs expressing the same odor receptor project to the same functional processing units, called glomeruli, of the antennal lobe (AL) (Fig. 1A), which shares functional similarities with the vertebrate olfactory bulb. There are between 51 and 54 different glomeruli in the AL of *Drosophila* that have been identified (Couto, Alenius, and Dickson 2005; Fishilevich and Vosshall 2005). In the AL, OSNs form synapses with projection neurons (PNs) and local interneurons. The PNs project then to two higher brain centers, called mushroom body (MB) and lateral horn (LH), the insect analogues of the mammalian piriform cortex and cortical amygdala, respectively (Fig. 1B). Furthermore, in the AL, local interneurons control release from OSN presynaptic terminals onto PNs by lateral inhibition, which is suggested to improve odor discrimination (Olsen and Wilson 2008; Olsen, Bhandawat, and Wilson 2010; Root et al. 2008; Luo, Axel, and Abbott 2010).

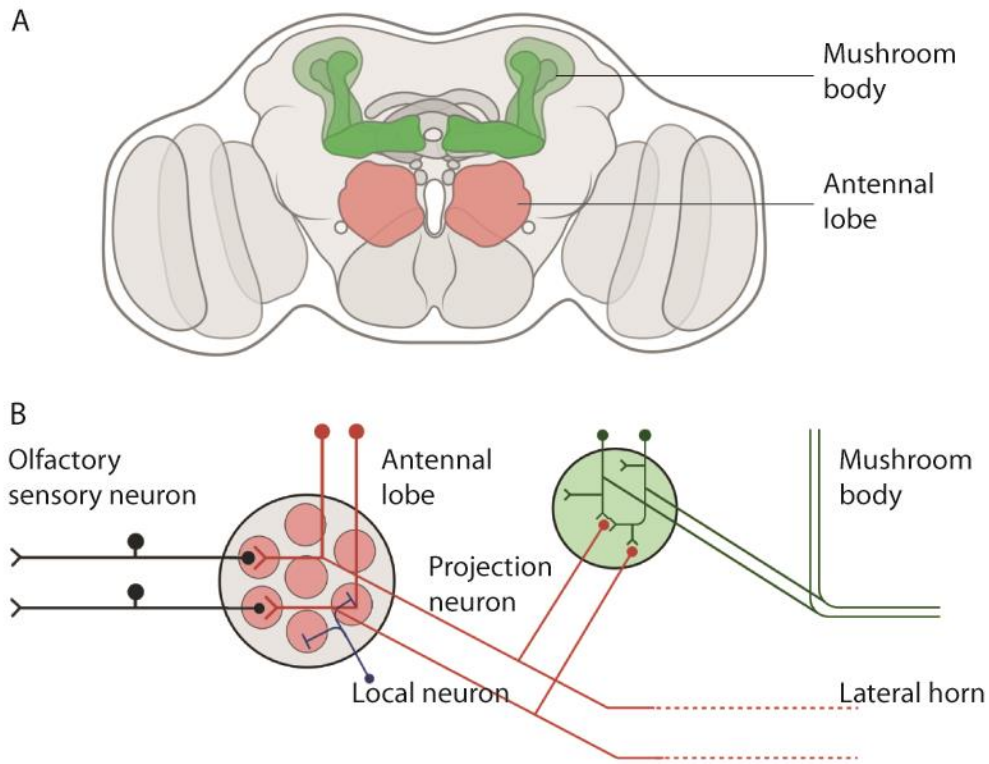

Figure 1: The olfactory system in *D. melanogaster*. **A)** Illustration of an adult fruit fly brain from an anterior view. The AL is highlighted in red, the MB in green. Created with BioRender. **B)** Simplified schematic representation of the olfactory system. OSN (black) project AL glomeruli (red circles) and form synaptic connections with PNs (red). Olfactory information is transmitted to the MB (green), where PN connect with Mushroom body intrinsic neurons (green), and the LH. Local interneurons (blue) in the AL connect different glomeruli and modulate odor processing by lateral inhibition.

1.4 The Mushroom Body

The insect MB is essential for the formation and retrieval of multiple types of memory, including olfactory associative memories (Heisenberg et al. 1985; McGuire, Le, and Davis 2001; Zars et al. 2000; de Belle and Heisenberg 1994). It does not receive direct sensory input (*e.g.* olfaction) and is not directly connected to motor neurons. Instead, olfactory information is first processed in the AL from which neurons directly project to the premotor output region. Therefore, the MB is a second order neuropil and lies in a parallel sensory-motor pathway, which resembles conditions of cortical structures like the hippocampus and the prefrontal cortex in mammalian brains (Menzel 2014). Yet, its discrete structure provides a relatively simple model to study the neuronal basis of learning and memory. First described by Félix Dujardin in 1850 (Dujardin 1850), it consists primarily of intrinsic neurons called Kenyon cells (KCs), named after Frederick C. Kenyon (Strausfeld et al. 1998).

First evidence that the MB mediates learning came from studies in honey bees, *Apis mellifera*. Locally cooling the MB after the honey bees had learned to associate an odor with sugar resulted in significant impairment of memory formation, whereas cooling other areas of the brain did not (J. Erber 1980). Later, this finding could be reproduced in experiments with flies following a similar approach. Chemical ablation of the MB in flies led to the loss of associative olfactory learning while at the same time, and most importantly, this deficit could not be attributed to a reduction in olfactory sensitivity or locomotor behavior (de Belle and Heisenberg 1994). Further experiments involving the blockage of synaptic transmission to the MB (Dubnau et al. 2001) and from the MB (McGuire, Le, and Davis 2001) confirmed these findings.

1.4.1 Neuronal structure of the MB

In *D. melanogaster*, the MB calyx, its input region, is comprised of three types of neurons: PNs delivering stimuli information, intrinsic KCs, and extrinsic neurons (EN), which connect the calyx with other brain regions. PN axons display large spherical boutons rich in presynaptic active zone (AZ) proteins and form synaptic complexes with KC claw-like dendrites, called Microglomeruli (MGi, plural of MG for Microglomerulus) (Fig. 2A, B). The name is in analogy to similar structures in the vertebrate central nervous system, including the mossy fiber/ granule cell synapse in the mammalian cerebellum (Yasuyama, Meinertzhagen, and Schurmann 2002). The overall shape of MGi is spheroidal, but they can also have more complicated, irregular shapes (Leiss et al. 2009; Butcher et al. 2012). KCs can be distinguished based on their axonal projections in the MB lobes and distinct gene expressions into three main subtypes: αβ, α'β' and γ (Crittenden et al. 1998; Strausfeld et al. 1998) (Fig. 2C). Each type has been demonstrated to play a different role in olfactory learning and memory (Zars et al. 2000; McGuire, Le, and Davis 2001; McGuire et al. 2003; Pascual and Preat 2001; Krashes et al. 2007). A split-GAL4 screen with in-depth analysis of their axonal projection patterns revealed that they can be further divided into seven cell types. Five types (αβ core, αβ surface, α'β' middle, α'β' anterior-posterior and γ main) extend their dendrites in the main calyx, whereas two have dendrites only innervating either the ventral (γ dorsal) or dorsal (αβ posterior) accessory calyx (Aso, Hattori, et al. 2014). The connections between PN axons and different subtypes of KCs appear to be random (Caron et al. 2013; Eichler et al. 2017; Gruntman and Turner 2013). This results in sparse olfactory representations, which are additionally maintained by inhibition (Papadopoulou et al. 2011).

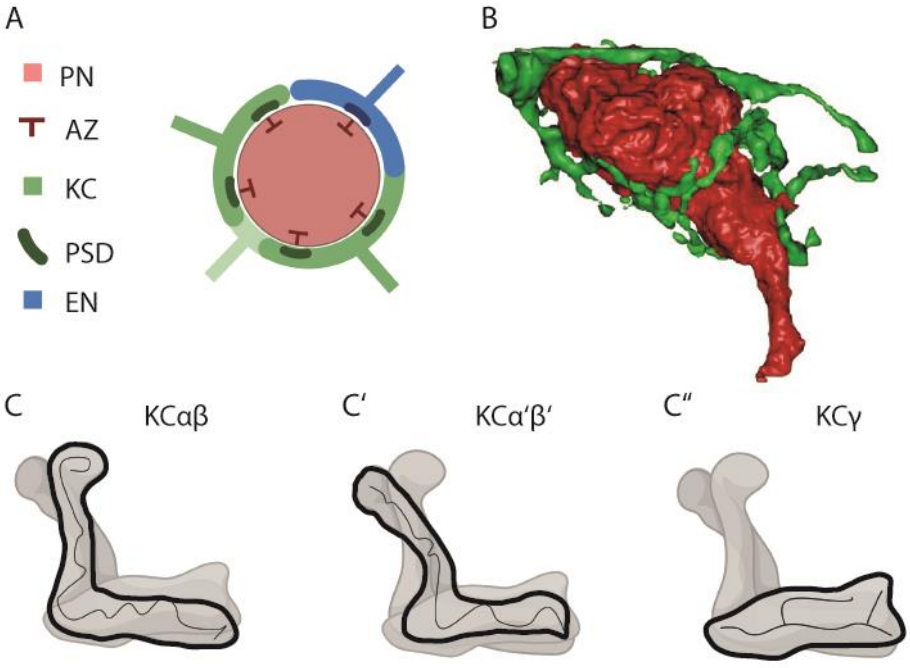

Figure 2: Structure of the MB **A)** Illustration of a MG typically found in the MB calyx. A PN bouton (red circle) is rich in presynaptic AZ (dark red T-shape). The bouton is surrounded by multiple KC claws (green) and by a few EN (blue). KCs and ENs form multiple synaptic connections with a single bouton. **B)** 3D-reconstruction of a PN bouton (red) and a single KC claw (green) from electron microscopy (EM). **C)** Illustration of the MB lobes. KCs are categorized into three types which make up the lobes. Single lobes are outlined with individual representative KCs shown in black. Created with BioRender.

1.4.2 The MB lobe compartments

The adult MB lobes can be separated into 15 different non-overlapping compartments. Each lobe (αβ, α'β' and γ) has five compartments (Tanaka, Tanimoto, and Ito 2008; Aso, Hattori, et al. 2014; Aso, Sitaraman, et al. 2014). Each one is innervated by different dopaminergic neurons (DANs) conveying either reward or punishment information. Reward coding DANs form a cluster called PAM, and punishment coding DANs form the PPL1 cluster (Aso et al. 2010; Aso and Rubin 2016; Burke et al. 2012; Claridge-Chang et al. 2009; Waddell 2010; Liu et al. 2012). Moreover, these compartments are precisely matched by the dendritic fields of different MB output neurons (MBONs), which project to other neuropils in the brain. Optogenetic activation of different MBONs is sufficient to induce approach or avoidance behaviors, suggesting MBONs are responsible for driving memory retrieval (Aso, Sitaraman, et al. 2014; Bouzaiane et al. 2015; Cohn, Morantte, and Ruta 2015; Hige et al. 2015; Owald and Waddell 2015; Perisse et al. 2016).

1.5 Associative learning in the MB

During classical olfactory conditioning, odor information is represented by an odor-specific subset of KCs. In the lobes, KC axons form synaptic connections with MBON, which either code for approach or avoidance behavior depending on the compartment. Simultaneously, information about reward or punishment is delivered by the respective DANs to the MB lobes. Dopamine release alters the strength of the synaptic connections between KCs and MBONs (Owald and Waddell 2015; Hige et al. 2015). If the DANs code for reward, the synaptic connections between KCs and avoidance driving MBONs will be effected. As the synaptic connections between KCs and approach driving MBONs stay unaffected, the balance in the network has shifted. When the fly is exposed to the odor a second time, it will approach the odor. If the DANS code for a punishment, the synaptic connections between KCs and approach driving MBONs will be weakened, thus the fly will avoid the odor (Owald and Waddell 2015; Perisse et al. 2016) (Fig. 3). Consequently, this suggests that the coincidental stimulation of KCs and DANs leads to memory formation via the dopamine induced synaptic plasticity between KCs and MBONs (Aso, Sitaraman, et al. 2014; Bouzaiane et al. 2015; Cohn, Morantte, and Ruta 2015; Hige et al. 2015; Owald and Waddell 2015; Perisse et al. 2016; Cognigni, Felsenberg, and Waddell 2018).

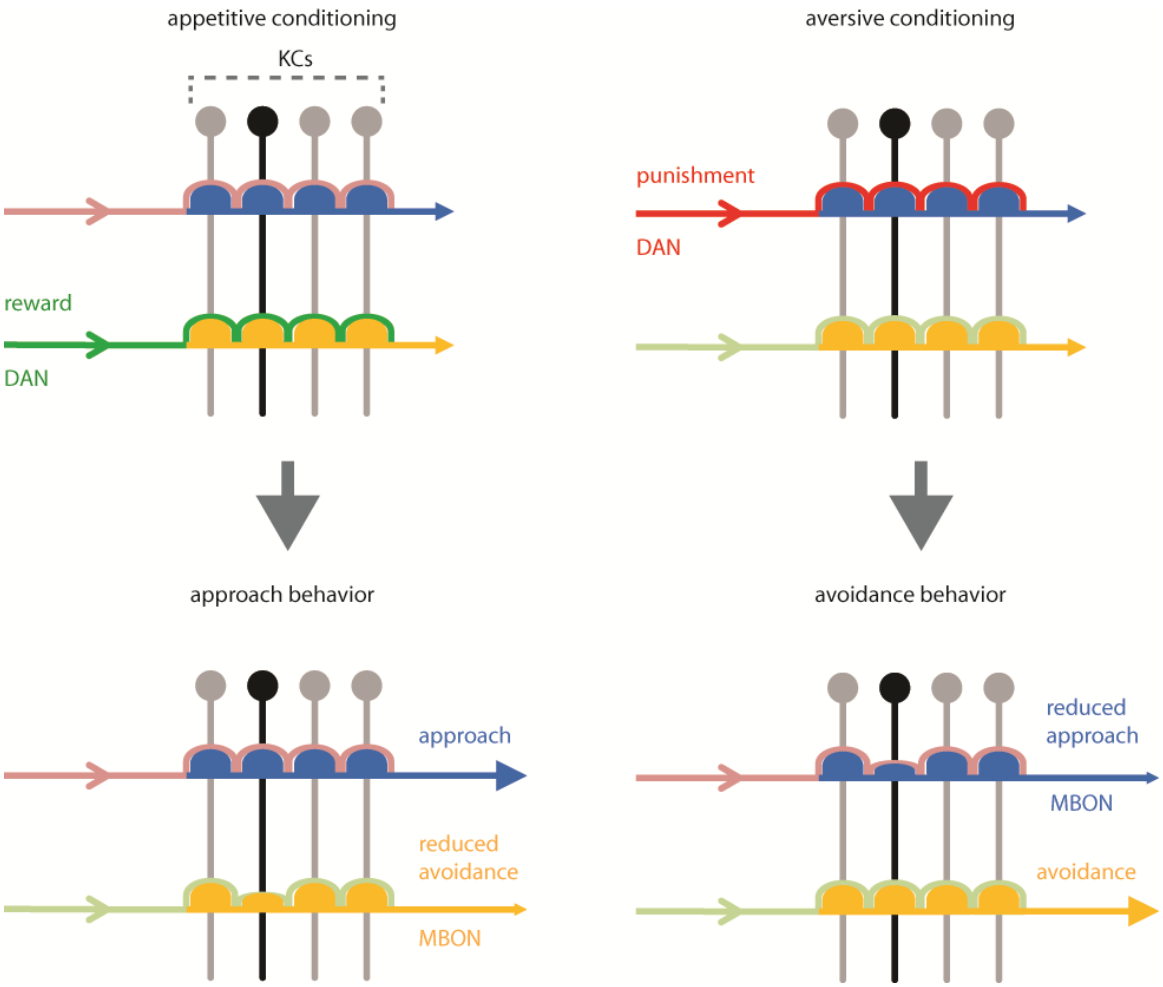

Figure 3: Model for associative learning in the MB. During classical conditioning (top), a specific set of KCs (black) is activated by the odor and simultaneously the DANs are activated by either a reward (green) or punishment (red). The release of Dopamine induces synaptic plasticity at the KC to MBON (orange and blue) synapses (semicircles). When the odor is presented a second time (below), the balance of the network has shifted (smaller semicircles) due to the Dopamine induced plasticity. In the case of appetitive conditioning, the connection between KCs and the avoidance promoting MBONs is weakened and approached behavior is induced. During aversive conditioning, the connections between KCs and the approach promoting MBONs is weakened, thus the network drives avoidance behavior. Illustration adapted from (Cognigni, Felsenberg, and Waddell 2018).

1.6 Comparing the centers for innate and learned behavior

The role of the lateral horn (LH) in innate behavior was first indicated by experiments silencing the MB or the PNs, and testing naïve odor responses. In an early study, the MB in flies was silenced by chemical ablation. When tested in an odor conditioning experiment, such flies showed greatly impaired experience-dependent olfactory responses. However, the same flies showed normal innate experience-independent olfactory responses (de Belle and Heisenberg 1994). In a subsequent study, experimenters severely reduced not only the MB through ablation, but also partially the AL. This resulted in flies missing the PNs connecting

the AL with the MB calyx, but with a cluster of PNs directly projecting to the LH remaining intact. Unable to learn, these flies still showed normal innate responses to olfactory cues (Stocker et al. 1997). On the contrary, by precisely blocking the synaptic output of all PNs, projecting to the MB and the LH, the innate responses to different odor stimulations were impaired as well (Heimbeck et al. 2001). In comparison, blocking neurotransmission of KCs by silencing their synaptic output led to suppression of memory and a reset to innate olfactory responses (Heimbeck et al. 2001; Parnas et al. 2013). Finally, more direct evidence for the LH's role in innate behavior derived from a study manipulating single and small subsets of defined LH neuron types, demonstrating that optogenetic activation of different LH neurons can drive valence or motor behaviors (Dolan et al. 2019). Taken together these results suggest that the direct PN connection from the AL to the LH is sufficient enough and necessary for initiating innate odor responses, whereas learned odor responses require the MB.

1.6.1 Stereotypic and random circuitries

The projections of PNs into the LH are stereotyped (Jefferis et al. 2007; Marin et al. 2002). This is interesting, because some PNs respond primarily to aversive or attractive odors. As PNs project to particular zones, specific LH regions can be associated with either negative or positive valence. Attractive PNs innervate medially and aversive PNs laterally in the LH, thus forming two rough valence compartments (Seki et al. 2017). Moreover, the connectivity between the PNs and the LH neurons is stereotyped as well, meaning the same PNs connect to the same LH neurons, when compared across animals (Jefferis et al. 2007; Fisek and Wilson 2014; Jeanne, Fisek, and Wilson 2018; Frechter et al. 2019). Furthermore, the LH includes a great number of genetically defined cell types, which themselves show highly stereotyped arborization (Dolan et al. 2019). Anatomical analysis of single neurons either labeled genetically or with dye fills identified 165 different cell types that seem to have a majority of their dendrites within the LH (Chiang et al. 2011; Frechter et al. 2019). In addition, another screen with cell type specific labeled neurons identified a further set of 14 non-PN cell types to provide input to the lateral horn (Dolan et al. 2019).

The PN projections into the MB calyx seem to be partly separated as well, but less distinct as in the LH. Aversive coding PNs tend to project into the center of the calyx, whereas PNs of attractive valence innervate the periphery (Seki et al. 2017). Yet unlike in the LH, the connectivity between KCs and PNs is not structured, leading to the assumption that the olfactory input into the MB calyx is random (Caron et al. 2013; Gruntman and Turner 2013).

1.6.2 Connections between MB and LH

The MB and the LH are responsible for learned and innate behavior respectively. However, this division has become more complex by recent findings that the MB also contributes to innate behaviors (Lewis et al. 2015; Tsao et al. 2018) and that olfactory aversive memory retrieval requires MB output to the LH (Dolan et al. 2018). Moreover, EM reconstruction revealed several neurons that directly connect the two neuropils (Dolan et al. 2018; Dolan et al. 2019; Bates 2020). However, these findings might only scratch the surface of how the MB and the LH really communicate with each other.

1.7 Focus on the MB calyx

In the fly, great progress has been made in understanding how odor information is integrated into higher brain centers and how the MB consolidates it into memories. Yet, most studies have focused on the MB output site, the lobes, and few on the input site, the calyx.

1.7.1 Extrinsic neuron innervation of the MB calyx

To start with, the neuronal circuitry in the calyx in the fly MB is not fully investigated. Past work using light microscopy (LM) has described various types of ENs, including modulatory and inhibitory neurons, extending projections into the calyx (Tanaka, Tanimoto, and Ito 2008; Aso, Hattori, et al. 2014). Nonetheless, these methods did not provide enough resolution to elucidate functional contacts. More recent electron microscopy studies focused locally on individual MGi. While it was revealed that they contain complex synaptic networks potentially including ENs, the neuronal types involved could not unequivocally be identified (Leiss et al. 2009; Yasuyama, Meinertzhagen, and Schurmann 2002; Butcher et al. 2012).

However, which cell types are contributing to the microglomerular circuit, where modulation and inhibition is happening, and the extent of synaptic connections is of great interest. While PNs respond strongly and broadly to odor input, only a restricted number of postsynaptic KCs will be activated. Furthermore, the responding KCs only produce few action potentials, primarily at the onset of the stimulus (Perez-Orive et al. 2002; Honegger, Campbell, and Turner 2011). This sparse coding appears to be generated by a combination of general inhibition in the calyx and intrinsic properties of KCs (Gruntman and Turner 2013; Turner, Bazhenov, and Laurent 2008). Information about individual odors is thought to be encoded in the MBs through the activation of distinct sparse subsets of KCs (Turner,

Bazhenov, and Laurent 2008). In the honey bee calyx, inhibitory neurons extend their processes within the MG, delivering inhibitory stimulus directly at the PN/ KC synapse, as shown by immuno-EM (Ganeshina and Menzel 2001)

1.7.2 MB calyx as a model for learning dependent plasticity

Another point to consider is that studies using other insect model organisms suggest that the MB calyx undergoes structural changes upon experience. Honey bees undertake a series of different tasks during their lifetime, starting with duties inside the hive, guard duties and finally foraging for pollen outside the hive. Structural analysis of the PN to KC microcircuits, the MG, revealed that during this transition from inside duties to outside foraging the number of MGi and the volume of the PN boutons increases, whereas bees prohibited from becoming a forager showed a decrease in number of MGi (Krofczik et al. 2008). Learning experiments with honey bees in an appetitive conditioning paradigm showed similar results, as the density of MGi increased in the calyx after 24 hours of training (Hourcade et al. 2010). Furthermore, desert ants, *Cataglyphis bicolor*, undergo transitions from inside to outside the hive comparable to honey bees. The transition is also accompanied by structural changes in the MB calyx, which could be linked to the animals' visual experience rather than to their age (Stieb et al. 2010).

Indirect evidence supporting these results has been found in fruit flies. Silencing the olfactory input into the calyx by inhibiting the PN output, led to an increase in MG number and size (Kremer et al. 2010).

1.8 Aims of the thesis

In the context of my research, I thus aimed to investigate three main points.

1.8.1 A detailed reconstruction of the MG circuitry

A detailed description of a MG wiring diagram at synaptic resolution with all its participants provides an anatomical guide in the understanding of sparse KC responses and the associative memory dependent plastic changes. It further allows determining whether MGi are autonomous computational relays. Therefore, with the availability of a whole brain electron microscopy (EM) volume of an adult female fly (Zheng et al. 2018), I reconstructed the complete circuitry of a MG and identified all the neurons that compose it and their local connections. Starting off from a PN bouton, I identified all cell types pre- and postsynaptic

within the MG synaptic complex by tracing to identification and annotating each synaptic connection. This allowed me to describe the local connectome of a single MG.

1.8.2 Learning dependent plastic changes in the MB calyx

Studies in honey bees and ants suggest that MGi undergo experience and memory dependent structural plasticity, which cannot be explained by development (Hourcade et al. 2010; Krofczik et al. 2008; Stieb et al. 2010). It is of great interest to investigate the possibility of learning induced plasticity in the calyx of flies as well. The calyx is located at the most posterior end of the fly brain and thus easily to access for imaging. The fruit fly offers a great genetic tool kit unmatched by any other model organisms so far, and the detailed description of the olfactory circuit makes is accessible to genetic manipulation. Thus, this project could lead the way for further investigations of the cellular mechanisms involving plasticity, as well as their genetic basis.

1.8.3 A first description of MB-C1

The description of a connectomic wiring diagram is not sufficient enough to draw functional predictions, which therefore need to be tested. Further, to interpret connectoms one has to be able to link behavioral outputs to the activity of specific neuron types. In my investigation of the MG wiring diagram, I found direct connections between PN boutons and the extrinsic MB calyx neuron 1 (MB-C1). The neuron has not been described before. In order to investigate the function of MB-C1, I performed immunohistochemical, genetic and behavioral experiments.

2 Materials and Methods

2.1 Materials

2.1.1 Caretaking

Flies were kept on standard cornmeal-based fly food. Unless otherwise stated, they were stored at either 18°C or 25°C with relative air humidity between 50% and 60% in a 12h/12h light-dark cycle. Transgenic fly lines with optogenetic insertions were kept in constant darkness.

2.1.2 Fly strains

Table 1: The following flies with their different genotypes were used.

Genotype	Source
CantonS	Bloomington #64349
yw; UASmCD8::GFP/ Cyo	Bloomington #30125
w; P(y[+t7.7]w[+mC]=13XLexAop2-mCD8::GFP)attP2	Bloomington #32203
w;UASbrp-D3::mCherry;	Gift S. Sigrist
w; 8x lexAop2-brp-short-mCherry 28E7/CyO;	Gift A. Sugie
w;;P(w[+mC]=UAS-DenMark)3	Bloomington #33061
w; UASnSyb-spGFP1-10,lexAopCD4-spGFP11/CyO	Bloomington #64314
w; lexAOP-nSyb-spGFP1-10,UASCD4-spGFP11; MRKS/TM6b	Bloomington #64315
w;;(VT043924.Gal4)attP2 (APL-GAL4)	VDRC VT043924
w; (GMR68D02-lexA)attP40;	Bloomington #54923
w;;(GMR37H08-GAL4)attP2	Bloomington #49970

w;;MB247-Dα7::GFP,UAS-brp-short-mCherry	Gift F. Leiss
SS01867	Gift Y. Aso
;UAS-CS-Chrimson_tdTomato in VK attpP40;	Gift V. Jayaraman
yw; P(w[+mW.hs]=GawB)GH146	Bloomington #30026
;R17A04-17A04_p65ADZp in attP40; R65D07-ZpGAL4DBD in attP2 (MB-C1-GAL4, GMR_MB380B)	Gift Y. Aso
;UAS-D3 UASmCD8-GFP/CyO; MKRS or TM6/+	Gift G. Marchetti
;;P(GD8508)RNAiGAD1	VDRC 32344/GD stock
yw;PBac(Disc\RFP[DsRed2.3xP3]=GH146-QF.P)53 P(w[+mC]=QUAS-mCD8-GFP.P)5B/TM6B, Tb	Bloomington #30038
Df(1)19,f[1]/C(1)RM,y[1]shi[1]f[1];;Dp(1;Y)shi[+]3,y[+] (UAS-Shibire^{ts})	Bloomington #5270
;;UASLuciferase.RNAi	Bloomington #31603
w; UASamon.RNAi69h;	Bloomington #29010
Y[1]v[1];P(y[+t7.7]v[+t1.8]=TRiP.HM05071)attP2 (amonTRIP RNAi)	Bloomington #28583
w; UASrpr.C	Bloomington #5824
w; UAShid.Z/CyO	Bloomington #65403
w; P(w[+mC]=UAS-Dcr-2.D)2	Bloomington #24650

2.1.3 Buffers and Media

Table 2: Buffers and media with their ingredients used in this thesis are listed here.

Name	Composition
Fly food	462,5 g yeast; 292,5 g agar; 1000 g molasses; 2500 g corn flour; 250 g soja flour; 1000 g baking malt; 62,5 g methylparaben; 250 ml H_3PO_4 10%; fill up to 25 L with water
Phosphate-buffered saline (PBS) 10x	100 mM Na_2HPO_4; 200 mM KH_2PO_4; 1.37 M NaCl; 27 mM KCl; pH 7.4
PBT	0.01%, 0.1% or 0.3% Triton X-100 in 1x PBS
Drosophila Ringer solution	130 mM NaCl; 5 mM KCl; 2 mM $MgCl_2$;2 mM $CaCL_2$; 36 mM sucrose, 5 mM Hepes-NaOH; pH 7,3
Ringer solution in Agar	Drosophila Ringer solution with 1.1% low melting Agar
Zamboni fixation buffer	4% formaldehyde, 1.6% glutaraldehyde, 0.2% saturated Piric acid in 1x PBS

2.1.4 Antibodies

Table 3: Primary antibodies used in the experiments.

Antiserum	Antigen	Fixation	Dilution	Source
AB152 rabbit anti-tyrosine hydroxylase	Tyrosine Hydroxylase (Dopamine)	4% FA	1:200	Chemicon

Anti-Glutamate monoclonal mouse G9282 SIGMA	L-gltamic conjugated to KLH with glutaraldehyde	Zamboni	1:5000	Sigma Aldrich
Anti-Octopamine rabbit polyclonal	Octopamine coupled to thyroglobulin	4% FA	1:1000	GeneTex
Anti-Synapsin mouse monoclonal 3C11	Synapsin	4% FA	1:100	Developmental Studies Hybridoma Bank
ChAT4B1 mouse monoclonal	Choline acetyltransferase	4% FA	1:1000	Developmental Studies Hybridoma Bank
DN -Ex #8 rat	N-cadherin	4% FA/ EDAC	1:20	Developmental Studies Hybridoma Bank
GABA polyclonal rabbit	γ-aminobutyric	4% FA	1:50	Sigma Aldrich
NC-82s monoclonal mouse	Bruchpilot	4% FA	1:50	Developmental Studies Hybridoma Bank
PAN19C polyclonal rabbit	Histamine	4% EDAC	1:500	ImmunoStar
Serotonin (5HT-H209) mouse monoclonal	5-Hydroxytryptamine hydrochloride (3-(2-aminoethyl)-5-hydroxyindole)	4% FA	1:1000	Thermo Scientific Pierce Antibodies

Table 4: Secondary antibodies used in the experiments.

Name	Host	Dilution	Source
Anti-mouse 568	Goat	1:200	Alexa Fluor
Anti-mouse 633	Goat	1:200	Alexa Fluor
Anti-rabbit 568	Goat	1:200	Alexa Fluor
Anti-rat 633	Goat	1:200	Alexa Fluor

2.1.5 Software

Table 5: The following software programs and algorithms were used to quantify data, image analysis and to prepare images.

Name	Version	Source
Fiji/ImageJ	1.52p	Wayne Rasband, National Institute of Health, USA
Excel	Microsoft Office 2010	Microsoft Cooperation, USA
Photoshop	CS5.1	Adobe Inc., USA
BioRender		www.biorender.com

Blender3D	v2.80.75	Blender Foundation
GraphPad Prism 8	8.0.1 (244)	GraphPad Software, USA
Definiens Developer XD™	2.3	Definiens Inc., USA
Illustrator	CS5.1	Adobe Inc., USA
Imaris	9.1.2	Andor Technology, Switzerland
CATMAID		Saalfeld et al. 2009 (Saalfeld et al. 2009)
NBLAST online		http://flybrain.mrc-lmb.cam.ac.uk/si/nblast/www/
TrakEM2		Cardona et al. 2012 (Cardona et al. 2012), https://imagej.net/TrakEM2
CATMAID-to-Blender		Schlegel et al 2016 (Schlegel et al. 2016), https://github.com/schlegelp/CATMAID-to-Blender

2.1.6 Hardware

Table 6: Hardware and their sources are listed here.

Name	Model	Source
T-Maze revolver	Custom made	Universität Würzburg, Germany
Mounted 625 nm LED	M625L3	Thorlabs, USA
LED driver	LEDD1B	Thorlabs, USA
ELV Puls generator	ELV UPG 100	Thorlabs, USA
Binocular	Stemi-2000C	Zeiss, Germany
Cold light source	CL 6000 LED	Zeiss, Germany
Forceps	Dumont 5, 55	Fine Science Tools, Germany
pH-meter	HI 221	Hanna Instruments, USA
acrylic glass plate	Acrylglas XT Frost LED opal weiß 6mm	Vink Kuststoffe, Germany
infrared LED	M120	Kemo Electronic GmbH, Germany
HQ camera	DCC1645C-USB CMOS	Thorlabs, Germany
Long pass filter	LP 820 HT	Schneider Kreuznach, Germany
Power and Energy meter	PM100USB	Thorlabs, USA
Standard photodiode power sensor	S121C	Thorlabs, USA
Stimulus Controller	CS-55	SYNTECH, Germany
Soldering station	digital 90 W Weller Professional WT 1012	Weller Tools GmbH, Germany
Micro pipettes	Pipetman Neo 2/20/100/200/1000µl	Gilson Inc, USA
Hot plate stirrer	RH Basic2	IKA, Germany

2.1.7 Microscopes

Table 7: The following microscopes and objectives were used for image acquisition.

Name	Model	Source
Confocal microscopes	LSM 700, LSM 780	Zeiss, Germany
2-Photon-laser-scanning microscope	TRIM Scope II	LaVision Bio Tec, Germany
LCI Plan-Apochromat 25x/ 0.8 oil immersion objective		Zeiss, Germany
C-Plan-Apochromat 63x/1.4 oil immersion objective		Zeiss, Germany
LCI Plan-Apochromat 25x/1.1 water immersion objective		Zeiss, Germany

2.1.8 Reagents and consumables

Table 8: Critical reagents and consumables, which are of great significance for establishing or the analysis of experiments, are here.

Name	Abbreviation	Source
3-octanol	Oct	Sigma Aldrich, Germany
4-methylcyclohexanol	MCH	Sigma Aldrich, Germany
Ethanol	EtOH	Sigma Aldrich, Germany
11-cis vaccenyl acetate	cVA	Cayman Chemicals, USA
Geranyl acetate	Ga	Sigma Aldrich, Germany
All-trans-Retinal		Santa Cruz Biotechnology, USA
Sucrose		VWR International, Germany
Low melting agarose		Thermo Scientific, Germany
Triton X-100		Carl Roth, Germany
Vectashield		Vector Laboratories, USA
Mineral oil, light		Sigma Aldrich, Germany
Myristic acid		Sigma Aldrich, Germany

2.2 Methods

2.2.1 Neuron reconstructions and identification

Neuron skeletons were reconstructed in a serial section transmission electron microscope (ssTEM) volume of a complete female adult fly brain (Female Adult Fly Brain, FAFB), described and published by (Zheng et al. 2018) (x, y, z resolution 4 nm x 4 nm x 40 nm). Neurons were manually traced using CATMAID, a Web-based environment for working on large image data sets (Saalfeld et al. 2009). Chemical synapses were also manually annotated and identified based on the following criteria: 1) an active zone (AZ) surrounded by vesicles, 2) a thick dark presynaptic specialization (e.g. T-bar), 3) a synaptic cleft and 4) a postsynaptic density zone (PSD), which however can be absent. If the PSD is absent, we annotated all cells along the synaptic cleft (Prokop and Meinertzhagen 2006; Zheng et al. 2018). Neuron identity is based on previously described morphologies with LM (KC subtypes (Aso, Hattori, et al. 2014), APL (Liu and Davis 2009), MB-C1 (Tanaka, Tanimoto, and Ito 2008), PN (Jefferis et al. 2007; Grabe et al. 2015)), such as dendritic branching, axonal projection and location in the neuropil, and additionally for PN subtype identification a neuron search against a LM dataset in NBLAST (Costa et al. 2016), as described in (Zheng et al. 2018).

3D reconstructions of the PN bouton and KC claws from ssTEM sections were created manually with the ImageJ plugin TrakEM2 (Cardona et al. 2012).

2.2.2 Odor conditioning

For fly conditioning, the appetitive olfactory conditioning paradigm, first established by (Tully and Quinn 1985) and standardized by (Krashes and Waddell 2011), was conducted. Groups of 2-6 day old flies were starved on wet KIMTECH wipes (Kimberly-Clark Worldwide Inc., UK) at 25°C and 60% humidity until about 10-20% died – approximately after 24 to 48 hours. For short-term memory conditioning, approximately 50 flies were exposed to a first odor (CS-) for 2 min. Following 1 min of clean air, a second odor was presented for 2 min paired with a dried filter paper previously soaked in 2M sucrose (CS+). After 1 min of clean air, memory was subsequently assessed by testing flies for their odor preference between the CS- and the CS+ odors in a T-maze for 2 min. A preference index (PI) was calculated as the number of flies in the CS+ arm of the T-maze minus the number in the CS- arm, divided by the total number of tested flies: PI= (CS+ - CS-) / (CS+ + CS-). For long-term memory conditioning, flies were trained in the same way, but were exposed to the CS- and the sugar-paired CS+ for 5 min, and tested after 24 hours retention time. The longer

feeding time assured a higher survival rate during the experiment. During the retention time flies were kept on wet KIMTECH wipes at 25°C and 60% humidity.

Transgenic flies expressing temperature-sensitive Shibire (Shi^{ts}) were raised at 18°C with 50-60% relative humidity. Experiments were performed at either 31°C to activate Shi^{ts} or at 18°C for control groups with inactive Shi^{ts}. Before behavioral testing or conditioning with active Shi^{ts} transgenic flies were incubated for 2 hours at 31°C to guarantee complete vesicle reuptake inhibition.

Table 9: The following odors and their concentrations used for appetitive odor conditioning are listed here.

Name	Source	Dilution
cVA	Cayman Chemicals, USA	1:400 in PBS with 5% EtOH (EtOH in raw product)
Ga	Sigma Aldrich, Germany	1:200 in PBS with 5% EtOH
MCH	Sigma Aldrich, Germany	1:100 in mineral oil
Oct	Sigma Aldrich, Germany	1:80 in mineral oil

2.2.3 Optogenetic conditioning

For conditioning flies with optogenetic stimulation of PNs, driver line and reporter line flies were crossed on normal fly food. Adult offspring flies were collected at 2 to 3 days of age and tipped into vials containing fly food supplemented with 100µM all-trans-retinal (SC-210778A, Santa Cruz Biotechnology, U.S.A.). After 3 days, flies were starved for 24 or, when otherwise stated, 48 hours in vials with wet KIMTECH wipes (Kimberly-Clark Worldwide Inc., UK). For training, mixed groups of 40-60 flies were gently put into a transparent vial with the upper half coated with cellulose paper (Chromatography paper 3mm, WhatmanTM, UK), soaked in 2M sucrose and dried beforehand, and illuminated for 5 minutes from below with 625 nm LED light (M625L3, Thorlabs, U.S.A.) with 1,45 mW/cm2 light intensity. Unpaired control flies were treated in the same way, but given sugar and exposed to red light separately with a 2 minute break in between. Flies were either 1) again stored for 24 hours in vials with wet KIMTECH wipes for starvation, or 2) refed with 100µM all-trans-retinal food for 3 hours and subsequently starved 21 hours – use of either protocol is stated for each respective experiment in the result section. For testing, a choice assay was performed in a circular arena. The dimensions were 9 cm in diameter and 3 mm high. The arena was placed on an acrylic glass plate (Acrylglas XT Frost LED opal weiß 6mm, Vink Kunststoffe, Germany), which was illuminated from below by infrared LEDs (M120, Kemo Electronic GmbH, Germany) and one half additionally by the 625 nm LED with the same

light intensity as before. Flies were given 30 seconds to adjust to the arena. The red light LED was turned on 10 seconds into the video recording. Videography was performed at 1 frame per second with a DCC1645C-USB CMOS HQ camera (Thorlabs) with a long-pass filter (LP 820 HT, Schneider Kreuznach, Germany).

Flies were raised and experiments were performed in the dark at 25°C with 50-60% relative humidity.

Light intensity was measured with a Power and Energy meter (PM100USB, Thorlabs, U.S.A.) connected with a Standard photodiode power sensor (S121C, Thorlabs, U.S.A.).

To locate and count flies in time lapse movies we implemented an ImageJ macro executing following processing steps: First, images were inverted in order to transform dark fly objects into bright spots. Second, a background image was obtained by a median projection over the whole time series and removed from each frame of the time series. Next, each frame was smoothed with a gaussian filter (sigma=2). As a result, we obtained a dark time series with moving bright spots, where each spot corresponded to a fly. Spot locations were identified by the local maxima detection ("Find Maxima") of ImageJ. Red light illuminated and not illuminated regions were defined by halves of a static, user-defined circular area. Spot locations were classified into "illuminated" or "not illuminated" according to their location in the image.

The preference index for the "illuminated" half of the arena was calculated in every frame as described above (chapter 2.2.2).

2.2.4 Immunohistochemistry

Throughout this study different immunohistochemistry (IHC) protocols were used. Figure 7A, 7B, 8, 11, 14 and 15 used protocol 1, Figure 7C-C", 7D-D" and 16 used protocol 2, antibody staining against Glutamate and Histamine (see table 13) used protocol 3.

Protocol 1: Fly brains were dissected in cold sodium phosphate buffered saline (PBS) with 0.01% Triton X-100 and fixed in 4% formaldehyde in PBS for 50 min. They were washed in PBS with 0.1% Triton X-100 and then incubated over night at 4°C in PBS with 0.3% Triton X-100 with the primary antibodies. Afterwards brains were washed three times in PBS with 0.3% Triton X-100 and then incubated for four hours with the secondary antibody diluted in PBS with 0.3% Triton X-100. Finally, they were washed three times in PBS with 0.3% Triton X-100 and mounted onto an objective slide in Vectashield (Vector Laboratories, Burlingame, California, U.S.A.) mounting medium.

Protocol 2: Fly brains were dissected in cold PBS with 0.01% Triton X-100 and fixed in PBS with 4% formaldehyde for 30 min. Afterwards, they were washed three times in PBS with

0.3% Triton X-100. Blocking was performed with 5% normal goat serum in PBS with 0.3% Triton X-100 overnight at 4°C. After three times of washing, primary antibodies were incubated at 4°C for 48 hours. Brains were washed three times again and incubated with the secondary antibodies at 4°C for 48 hours. After incubation, the brains were washed three times more in PBS with 0.3% Triton X-100 at room temperature. Finally, brains were mounted onto an objective slide in Vectashield mounting medium.

Protocol 3: Fly brains were dissected in cold PBS with 0.01% Triton X-100, fixed for 60 min in either Zamboni fixation buffer (4% formaldehyde, 1.6% glutaraldehyde, 0.2% saturated Piric acid in PBS) or in N-(3Dimethylaminopropyl)-N'-ethylcarbodiimide hydrochloride (EDAC; Sigma Aldrich, St. Louis, Missouri, U.S.A.) and were washed in PBS with 0.1% Triton X-100. Primary antibodies were incubated over night at 4°C diluted in PBS with 0.3% Triton X-100. Afterwards brains were washed three times in PBS with 0.3% Triton X-100 and then incubated for four hours with the secondary antibody diluted in PBS with 0.3% Triton X-100. They were washed three times again and finally mounted onto an objective slide in Vectashield mounting medium.

2.2.5 IHC Image Acquisition

All images for IHC were acquired using a Zeiss 780 Confocal Microscope (Zeiss, Jena, Germany). Overview images of whole mount brains were imaged using a LCI Plan-Apochromat 25x/NA 0.8 oil immersion objective (voxel size: 0.55µm x 0.55µm x 1µm). For higher resolution of individual cells or specific neuropils, whole mount brains were imaged using a C-Plan-Apochromat 63x/NA 1.4 oil immersion objective (voxel size: 0.09µm x 0.09µm x 0.25µm).

2.2.6 Statistics

All statistical analysis was performed in GraphPad Prism8.0.1. Data were tested for normality with a D'Agostino-Person omnibus K2 test. To compare differences between groups a two-sample t-test or a one-way analysis of variance (ANOVA) followed by pairwise multiple-comparison Bonferroni posthoc test. To compare the mean response of a group to a hypothetical value a one-sample t-test was performed. Statistical significance was defined as $p<0.05$ = *, $p<0.005$ = **, $p<0.0005$ = ***, $p<0.0001$ = ****.

3 Results

This study focuses on the MB calyx and aims to investigate its involvement in learning, memory formation and odor processing. The MB calyx is the main input site of the MB. It is located at the very posterior end of the brain and therefore provides easy access for imaging. Previous studies in honey bees (Hourcade et al. 2010) and ants (Krofczik et al. 2008) could show that upon processing new experience the calyx undergoes morphological changes, such as increased density of MGi and changes in the volume of MGi. In fruit flies, suppressing the synaptic input of the PNs induces increased volume of KC claws, the main postsynaptic sites in MGi (Kremer et al. 2010).

3.1 Microglomerulus reconstruction

To gain insight into the complexity of the microcircuit of a MG formed by a single PN and its synaptic partners in the calyx, we took advantage of the availability of a whole brain electron microscopy (EM) volume of an adult female fly (FAFB) (Zheng et al. 2018). EM constitutes the only means by which a sufficient resolution is reached to visualize fine neurites, synaptic vesicles and synaptic clefts (Fig. 4B) and so to identify all synaptic connections between definable neurons. Therefore, the reconstruction of neuronal connections is unbiased and the connectivity is certain.

3.1.1 Identification of PN

We were particularly interested in reconstructing a MG of a PN deriving from the DA1 subset, which extends its dendrites in the DA1 glomerulus of the AL. Therefore, we started tracing PNs within the medial antennal lobe tract (mALT) into the AL. Potential DA1 PN candidates were chosen based on the following three criteria: First, innervation of the AL; second, within AL only one glomerulus innervated; third, the DA1 glomerulus location in the AL, which had been previously described by (Couto, Alenius, and Dickson 2005). PNs fitting these criteria were further traced into the LH for validation of tracing identity in NBLAST (Costa et al. 2016; Zheng et al. 2018), a software that compares tracings against a LM data set. Finally, we traced into the calyx and for simplicity chose a round unilobed DA1 PN bouton rather than an elongated shape (Fig. 4C, E).

3.1.2 Projection neuron bouton and Kenyon Cells

The PN bouton has a maximum diameter of 2,66µm and a volume of 5.77µm^3, measured with TrakEM2 (Cardona et al. 2012). Within the bouton we find 33 pre synaptic active zones (AZ), each easily identifiable by a T-bar and a synaptic cleft (Fig. 4A, B). Along the cleft of the presynaptic sites we find in total 277 postsynaptic profiles, on average 8.42 with a range of 2 to 17 postsynaptic profiles per presynaptic site. KCs are the most prominent cell types comprising 248 postsynaptic profiles. In many cases, a KC claw can have more than one postsynaptic profile to the same AZ; in one case we counted four. This was not restricted to a specific subtype of KCs. Additionally we found the bouton to be post synaptic six times. Including these six postsynaptic sites, all synaptic sites are polyadic (a single presynapse connects to multiple postsynaptic sites). Only 23 (8.3%) fine dendritic postsynaptic profiles could not be traced to identification and thus are described as orphans. We also found 11 profiles along the PN bouton that do not make synaptic connections. Five are identified as KCs; six remain orphans.

We identified 14 KCs, representing all the 5 different subtypes included in the main calyx: αβc, αβs, α'β'ap, α'β'm and γmain (Fig. 4A, D, F), demonstrating for the first time that a bouton can have divergent KC downstream partners. The KCs receive between 8 to 25 presynaptic inputs from the PN bouton, which fits well with an estimated number of roughly 20 postsynaptic sites per KC claw from a previous study (Butcher et al. 2012). Each KC contacts the bouton with a single claw (Fig. 4F). Interestingly, DA1 PN boutons are reported to be located within a region of the MB calyx to be predominantly occupied by early αβ KCs (Lin et al. 2007), in this study referred to as αβs in reference to Aso et al. 2014 (Aso, Hattori,

et al. 2014). We find our DA1 PN bouton however to be presynaptic to eight γmain KCs and only three αβs, one αβc, one α'β'ap and one α'β'm. Further, we find two γmain KCs presynaptic to the bouton (Fig. 4A). In both cases, the presynaptic specialization is along the length of a dendrite and not within a claw. The synapses these two KCs form within the MG are divergent triads, including a KC, the PN bouton and a third neuron type the anterior paired lateral neuron (APL) (Fig. 4B). To our surprise, we also found two γmain KC claws with presynaptic connections to the APL.

We also found 3 KCs (γmain, α'β'ap and α'β'm one time each) extending branches through the MG complex, each forming synapses once giving input to KC claws and the APL, but otherwise have no connection to the PN bouton.

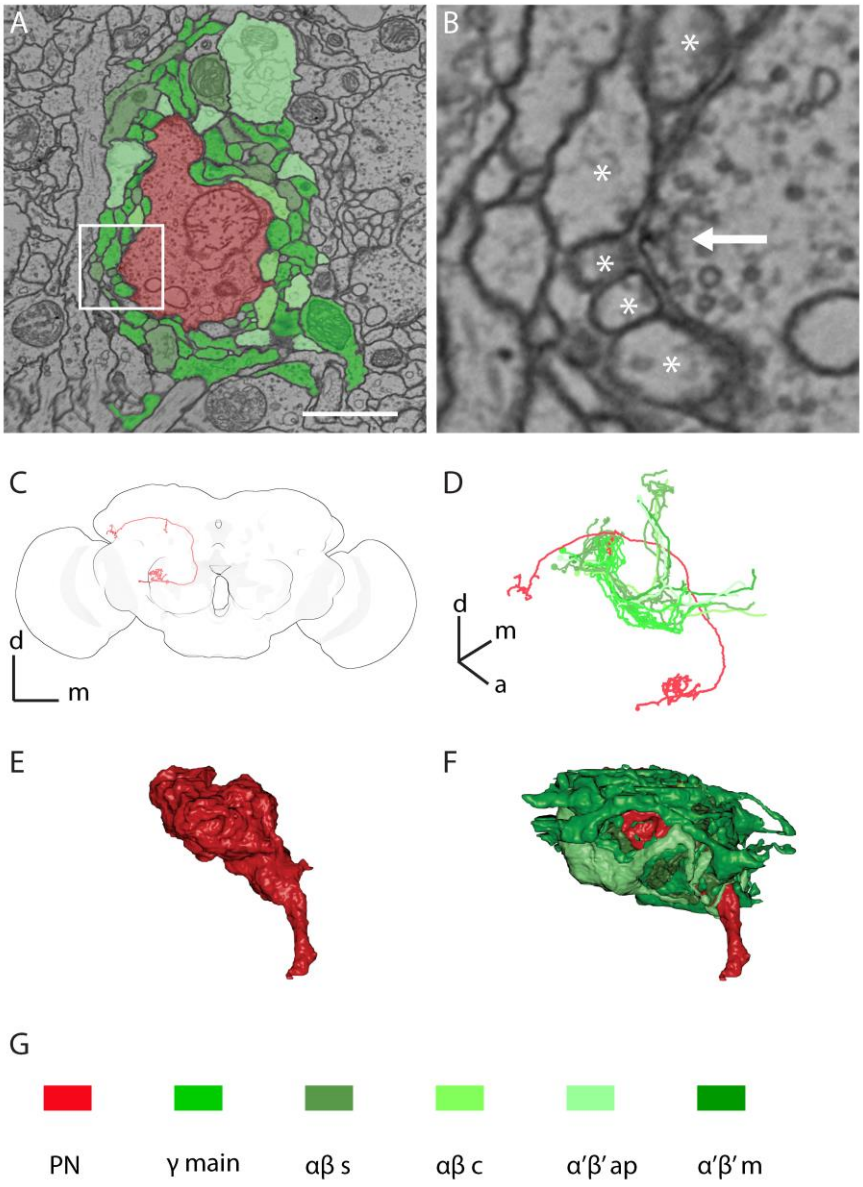

Figure 4: 3D EM reconstruction of a MG. **A)** Single EM section through the MG from the EM FAFB dataset, scale bar = 1 µm. White square is magnified in B. **B)** A synapse visible in EM. White arrow is

pointing to the T-bar structure of the AZ and white * labeling fine dendritic postsynaptic profiles of KCs. **C)** Reconstruction from FAFB EM dataset of the DA1 identified PN (red) and its location in the brain. **D)** Higher magnification of the DA1-PN (red) and the KCs (green) postsynaptic to the bouton. Different green shades represent different KC subtypes as in G. **E)** 3D reconstruction of the PN bouton and **F)** 3D reconstruction of PN bouton (red) and postsynaptic KC claws (green) from EM serial sections in TrakEM2. **G)** Legend of color code in A, D, E and F.

3.1.3 APL and MB-C1

It is known that besides PNs and KCs a number of other neurons innervate the MB calyx (Aso, Hattori, et al. 2014; Tanaka, Tanimoto, and Ito 2008). Within our MG we find two additional cell types forming synaptic connections with the bouton. These are: APL, a large GABAergic inhibitory neuron that innervates the entire MB and promotes sparse coding of olfactory stimuli (Liu and Davis 2009; Lin et al. 2014), and Mushroom Body Calyx 1 neuron (MB-C1) with two cells per hemisphere innervating the calyx and the lateral horn (Tanaka, Tanimoto, and Ito 2008).

In detail, we find APL (Fig. 5C) to be three times pre- and two times postsynaptic to the PN bouton. The APL presynaptic sites are also polyads and target 3, 6 and 10 neurons in addition to the PN bouton (Fig. 5D). Among these cells we find KC claws, MB-C1 and additional KCs not connected to the PN bouton of the γmain and αβc KC subtypes. Additionally, APL forms three synaptic connections in the periphery of the MG space, the volume of the MG defined by the postsynaptic KC claws. Here, APL is presynaptic to KC claws, additional KCs, and in one case also including MB-C1. Again the majority of KC targets were γmain with 13 cells, complemented by one αβs and one α'β'm.

We find both MB-C1 (Fig. 5E) neurons connected to our PN bouton of which one is simultaneously pre- and postsynaptic one time each, and the other cell exclusively postsynaptic but three times. Along the synaptic cleft of MB-C1's input site we find four γmain and one αβc KC, which themselves have no synaptic connection to the PN bouton or any other cell of our MG complex. The presynaptic MB-C1 also has one presynaptic connection within the periphery of the MG space, giving input to two KC claws and two additional γmain KCs.

We noticed that the presynaptic profiles of APL and MB-C1 are visibly larger than KC profiles (Fig. 5D, F), which is consistent with other studies (Butcher et al. 2012; Leiss et al. 2009). This is however not true for the postsynaptic profiles of APL and MB-C1, which can only be distinguished from postsynaptic KC profiles by tracing them back.

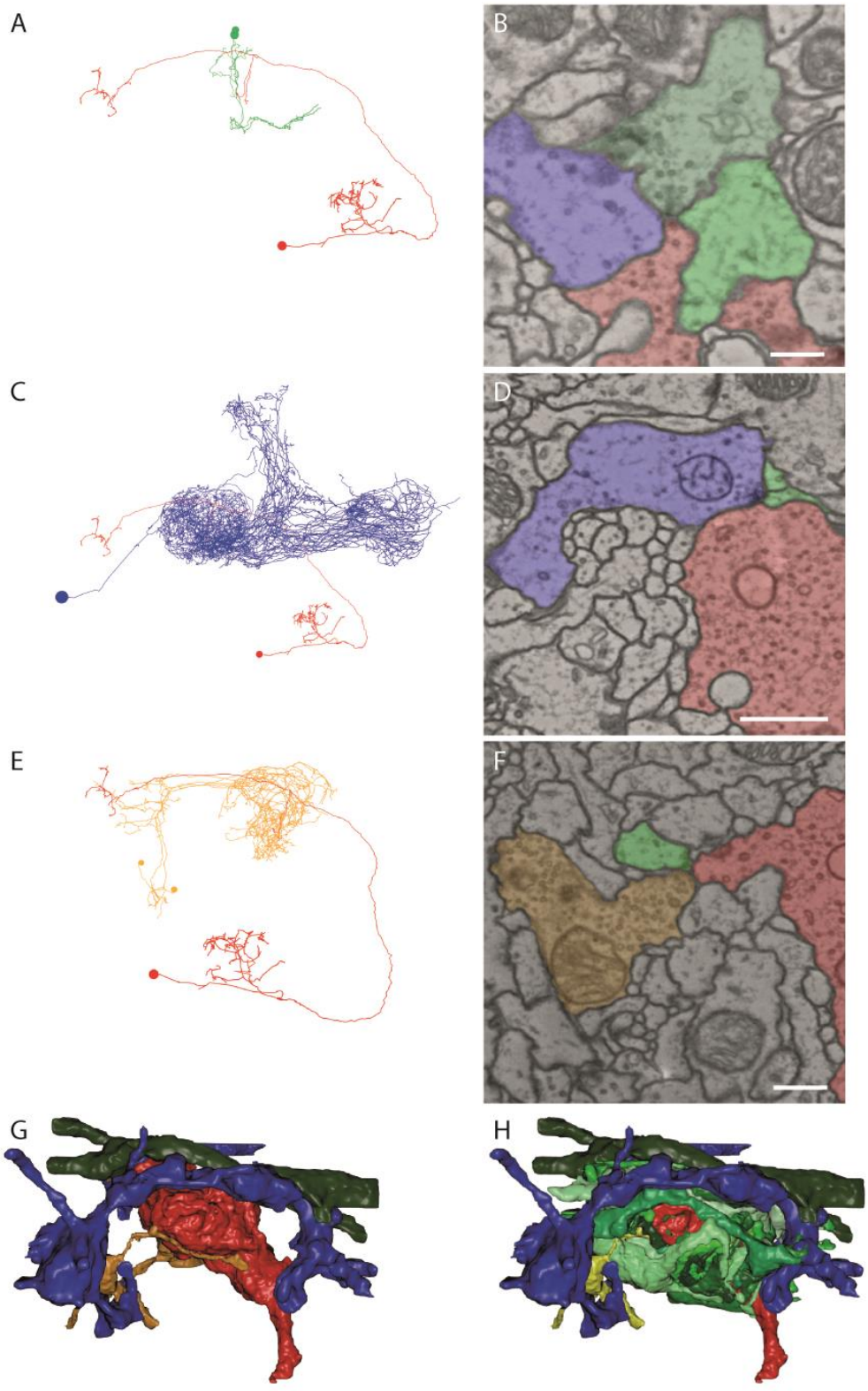

Figure 5: Presynaptic KCs and ENs in the MG complex. **A)** Tracing of the PN (red) and the two presynaptic KCs (green). **B)** Single EM section showing an example of a synaptic connection between presynaptic KC (dark green) and its postsynaptic partners, PN bouton (red), APL (blue) and a KC claw (lighter green). Scale bar is 250 nm. **C)** Tracing of APL (blue) and PN (red). **D)** Example of a synaptic connection between presynaptic APL (blue) and its postsynaptic partners, PN bouton (red), and KC claws (green). Scale bar is 500 nm. **E)** Tracing of MB-C1 neurons (orange) and PN (red). **F)** Example

of a synaptic connection between presynaptic MB-C1 (orange) and postsynaptic PN bouton (red) and KC claw (green). Scale bar is 250 nm. **G)** 3D reconstruction PN bouton (red), APL (blue), MB-C1 (orange) and presynaptic KCs (green). **H)** Complete Microglomerulus.

Taken together, the picture of a complex local circuit with large inhibitory components emerges (Fig. 6, table 10). To date, no further modulatory neurons appear to contribute to the local circuit.

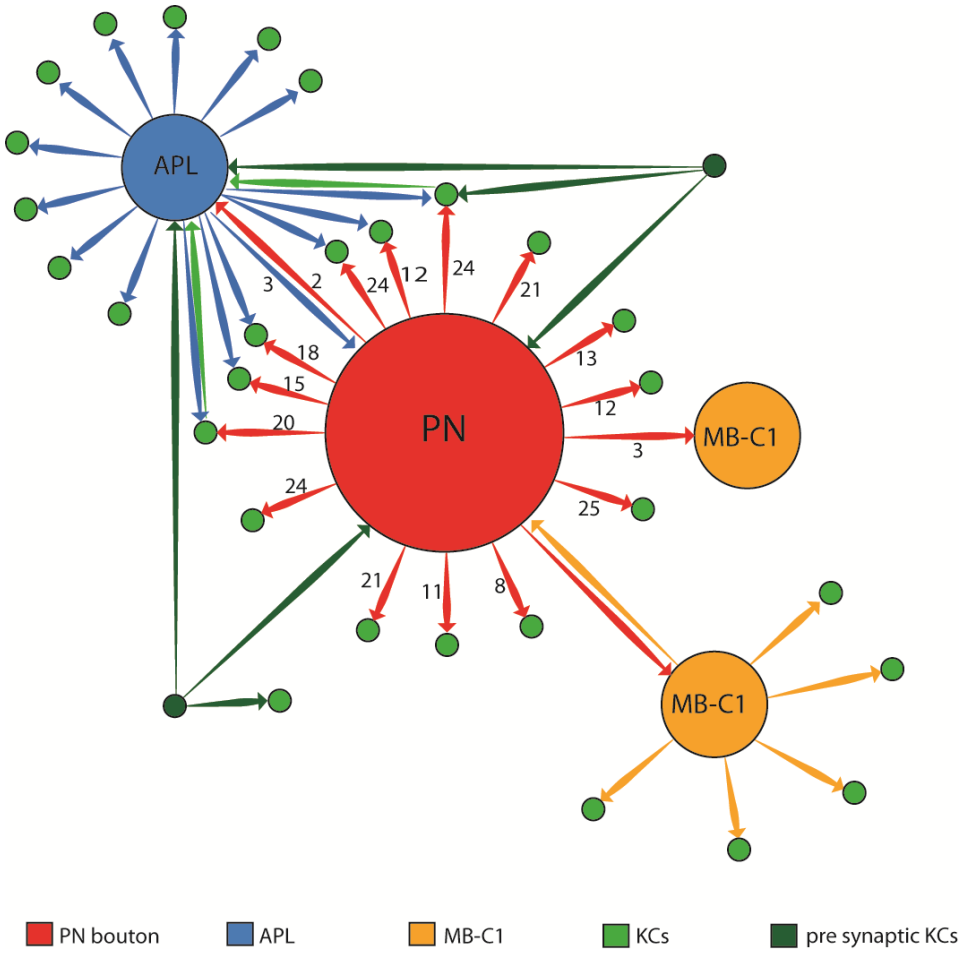

Figure 6: Complete schematic connectome of the reconstructed MG network. Numbers along the arrows indicate the quantity of synaptic connections between the indicated cells; if the arrow is not labelled with a number the quantity of synaptic connections between the cells is one. The network consists of a DA1 PN bouton (red), surrounded by the APL neuron (blue), two MB-C1 neurons (orange), 14 postsynaptic KC claws and two additional KCs (dark green), which are presynaptic to the PN bouton and the APL. APL and MB-C1 form polyadic synapsis with the PN bouton and further including KCs. Some of these are not postsynaptic to the PN bouton and therefore placed in the scheme around the respective APL or MB-C1 neuron.

Table 10: Cells and their number of synaptic connections in the MG.

Connection to PN bouton	Cell type	Number of cells	Number of synaptic connections
downstream	KC αβp	0	0
	KC αβc	1	11
	KC αβs	3	11-25
	KC α'β'ap	1	25
	KC α'β'm	1	8
	KC γmain	8	10-24
	KC γd	0	0
	APL	1	2
	MB-C1	2	1-3
upstream	KC γmain	2	1
	APL	1	3
	MB-C1	1	1

3.1.4 APL forms connections with multiple PN types

Here we show for the first time that the APL forms connections with a PN bouton. Besides, it also innervates the MB lobes, where its connections with KCs have caught great interests. APL has been suggested to be important for the maintenance of KCs sparse activity and thereby to promote odor discrimination (Lin et al. 2014). This is facilitated by a negative feedback circuit between the APL and the KCs, in which KCs activate APL and APL inhibits KCs (Lin et al. 2014). Therefore, we were interested, if APL forms connections with different types of PNs.

At this stage the reconstruction of the MB in the FAFB data set is not completed. However, we were still able to investigate the APL tracing further. In an anecdotal approach, we could identify additional MGi which form connections with APL in the same manner, with pre- and postsynaptic connections with the PN bouton and KC claws. We found 8 MGi with these types of connections (table 11) and 10 further PN boutons with direct pre- and postsynaptic connections (table 12). Yet, these tracings do not represent a complete reconstruction of the MB calyx, but prove that the APL innervation of the MG is not an individual case.

Our findings could be further strengthened by the hemibrain:v1.0.1 (Xu et al. 2020) data set, which consist of a large portion of the central fly brain that includes the AL and the MB. Its connectome was reconstructed by automated segmentation, synapse prediction and proof reading. This data set is publicly available for circuit analysis. Here, we found 105 PNs from 51 AL glomeruli and 31 multi glomerular PNs presynaptic to APL in the calyx. Since AZs in the PN collaterals in the calyx are present exclusively in boutons, these connections are part

of MGi. Presynaptic connections of APL were found onto 130 PNs of 48 AL glomeruli and 37 multi glomerular PNs.

Table 11: Additionally identified MGi in the FAFB data set showing direct pre- and postsynaptic connections with APL and indirectly via KC claws.

PN bouton	Presynaptic to APL	Postsynaptic to APL	KCs pre to APL	KCs post to APL
VA6	4	2	1	4
DM2	5	5	2	5
VA3	3	3	1	1
VC3m	3	1	1	2
DA1	3	3	2	2
VC1	2	2	1	2
VA1d	2	1	1	2
DM6	1	2	2	1

Table 12: MGi in the FAFB data set showing direct pre- and postsynaptic connections with APL but KC claws had not been traced until that point are listed here.

PN bouton	Presynaptic to APL	Postsynaptic to APL
DM2	1	1
VA2	2	1
DL1	3	1
DM1	1	2
DA1	4	1
VM1	2	1
DL2v	2	1
VC1	1	1
VM3	1	1
VM3	1	1

We additionally used activity-dependent GFP reconstitution across synaptic partners (syb::GRASP) to identify connections between APL and PNs across multiple animals (Macpherson et al. 2015). Syb::GRASP consists of two complementary split-GFP fragments, one half expressed on the extracellular membranes of a neuron and the second half in the lumen of synaptic vesicles in another neuron. If the two neurons form synaptic connections, the two split-GFP fragments are combined to a functional fluorescent GFP protein within the synaptic cleft (Macpherson et al. 2015). To drive split-GFP fragments in PNs we used the lexA driver *line R68D02-lexA*, which labels a sparse subset of PNs (Fig. 7B, C), and the GAL4 driver *VT043924* for expression in APL (Fig. 7A). The experimental genotypes, either APL pre- or postsynaptic to PNs, displayed clear GFP reconstitution in the calyx, indicating that

processes are close enough to form functional synapses. No signal was detected in control brains (Fig. 7C, D).

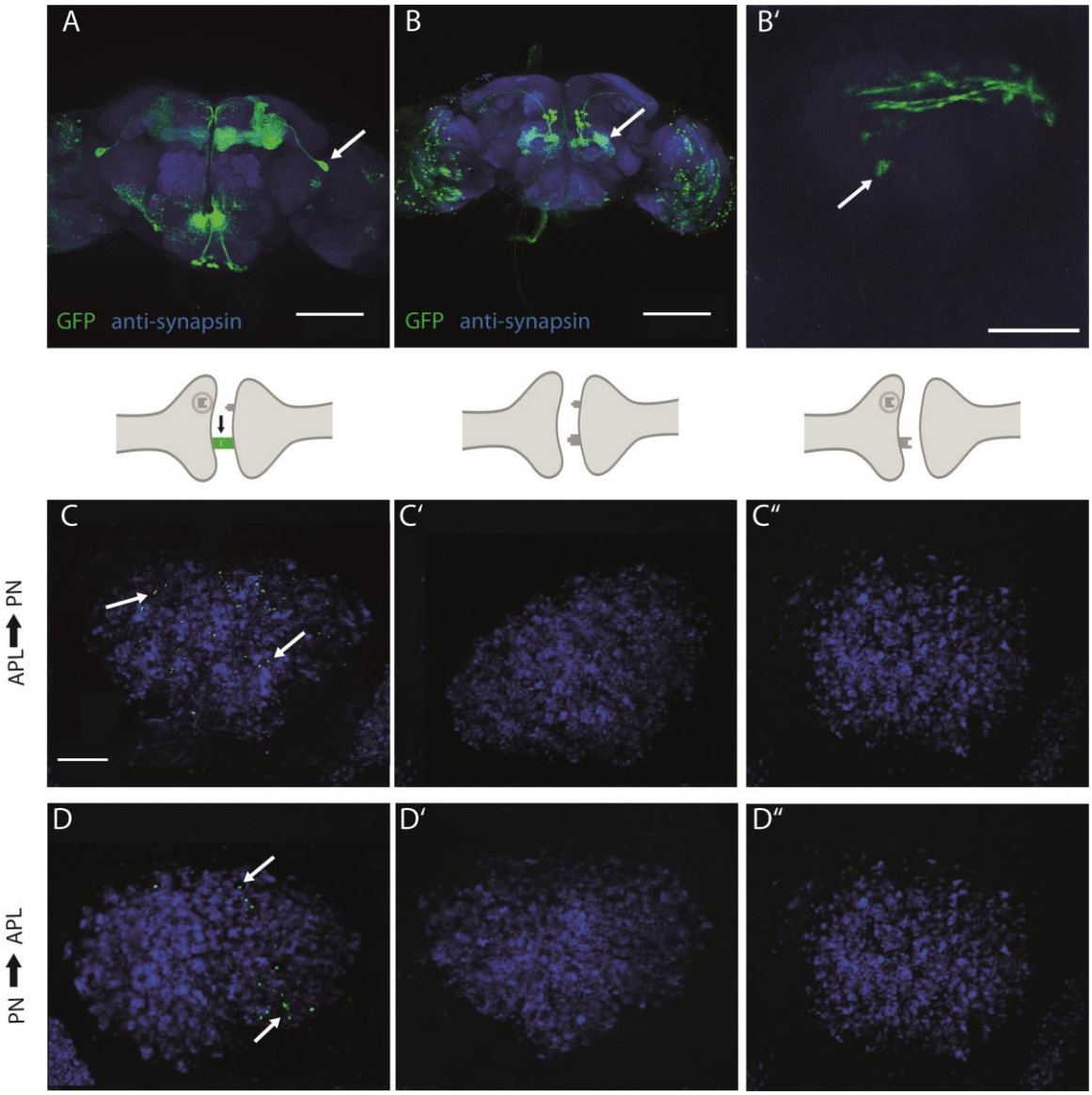

Figure 7: Activity dependent syb::GRASP to identify connections between APL and PNs across multiple animals. **A)** *VT043924* expressing *UAS-mCD8::GFP*. The only labeled neuron accessing the MB is APL. White arrow points to APL cell body. From the cell body a thick neurite projects to the MB calyx and branches extensively throughout the MB, including the lobes. Scale bar is 100µm **B)** lexA driver line *R68D02* expressing *UAS-mCD8::GFP*. White arrow points to the AL with three labeled glomeruli that extent PNs into the MB calyx (B'). Scale bar is 100 µm in B and 10µm in B'. **C)** syb::GRASP signal in the calyx (green puncta) with APL presynaptic to PNs (C) and the two genetic controls (C' and C") in which only either half of the two split-GFP fragments is expressed. White arrows point out single GFP puncta. Genotype and controls are represented in the schematic above the images. Images are representative of n=6. Scale bar is 10µm. **D)** syb::GRASP signal in the calyx with PNs presynaptic to APL (D) and the genetic controls (D', D"). White arrow points to GFP signal. Images are representative of n=6. Scale bar is 10µm. Illustration of synapses created in BioRender.

3.2 Pre- and postsynaptic structural plasticity in the MB calyx

To study whether the MB calyx undergoes plastic changes upon memory formation, we focused on the PN-KC connectivity within the MG. As shown here in our EM reconstruction of a MG, the innervation by the GABAergic neurons, APL and MB-C1, is rather sparse, compared to the dense synaptic connections between PNs and KCs.

The following data in this chapter were generated in a combined effort by Lothar Baltruschat and me. The initial concept of the study was designed by Gaia Tavosanis and Lothar Baltruschat, and a detailed description of the screen of driver lines and odors used in this chapter will be described elsewhere (Baltruschat, Ranft et al., in revision). This will also include testing the functional and structural convergence described here.

3.2.1 Visualizing olfactory information flow

For tracking potential plastic changes in the MB calyx, we needed to design a setup in which we could identify the odor responsive MGi after olfactory conditioning. The design had to ensure a high degree of cell specificity, as changes might be subtle and faint. Therefore, it was of great importance to screen on the one hand for a GAL4 driver line that is PN specific, and on the other hand for an odor that is specifically activating this particular set of PNs only. Our choice here was the *R37H08-GAL4* driver line. This driver labels PNs extending their dendrites in the DA1 and DL3 glomerulus of the AL, for simplicity from here on referred to as DA1 PNs (Fig. 8A, B). Our odor of choice was 11-cis-vaccenyl acetate (cVA), as it specifically stimulates olfactory sensory neurons (OSNs) innervating the DA1 and DL3 glomerulus and its corresponding PNs (Lebreton et al. 2014). This way, we were able to retrace the whole olfactory information flow from the AL to the MB calyx.

For investigating specifically the MGi active during odor stimulation, flies expressed under the control of *R37H08-GAL4* the presynaptic active zone (AZ) marker *Brp-short*^{mCherry} in DA1 PNs (Kittel et al. 2006; Wagh et al. 2006; Kremer et al. 2010). *R37H08-GAL4* labels 9 cells per hemisphere, which project from the DA1 glomerulus to the MB calyx. Here they form boutons, which are highly enriched with AZs. Thus, the boutons are unambiguously identifiable in the calyx. To study the postsynaptic KCs, we labeled the postsynaptic density zones (PSD) with *MB247-Dα7-GFP*; a fusion construct consisting of the *MB247* promoter, active in the majority of KCs, and the Dα7 subunit of the acetylcholine receptor tagged with eGFP (Kremer et al. 2010). The expression enabled to visualize the postsynaptic claw-like dendritic endings of multiple KCs, which appear as a rim around PN boutons (Fig. 8C).

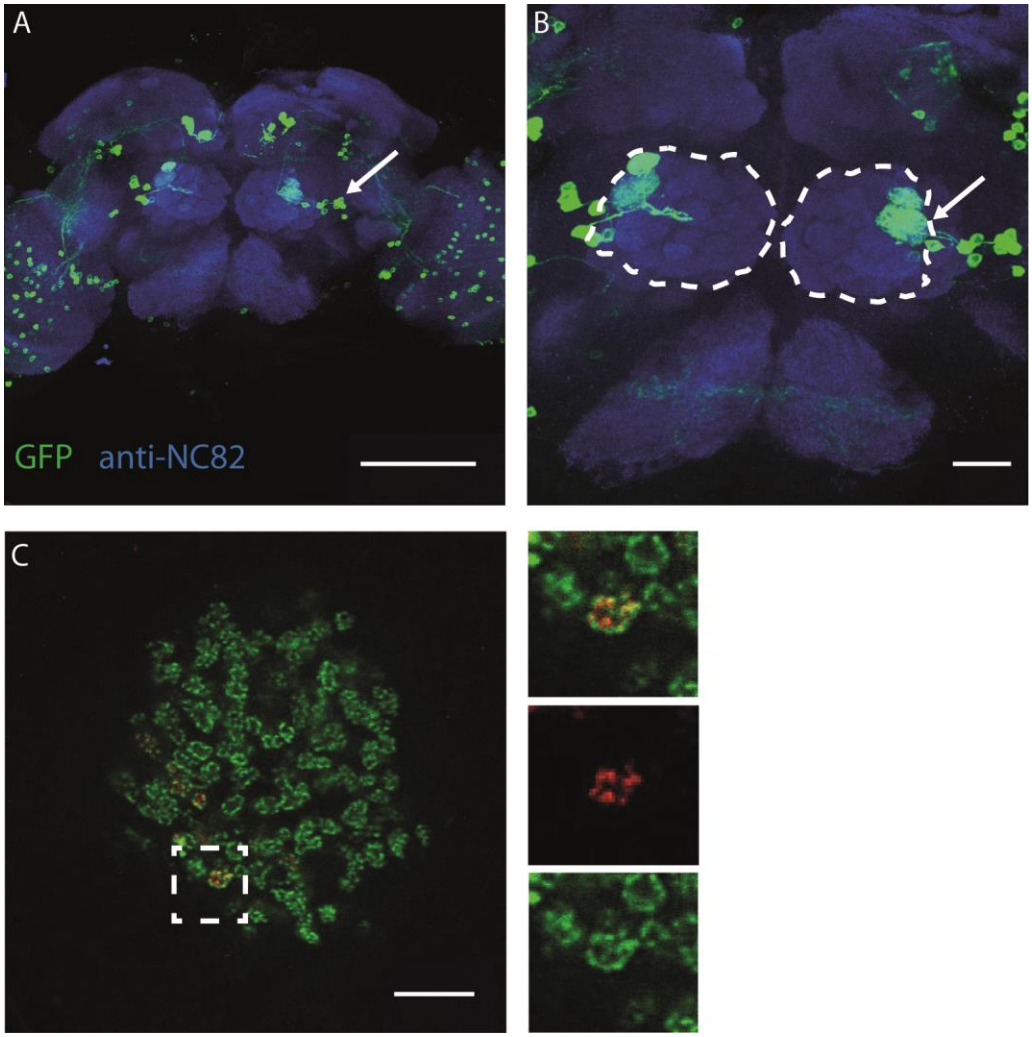

Figure 8: Genotype to visualize information flow. **A)** *R37H08-GAL4* expressing *UAS-mCD8::GFP*. Arrow points to PN cell bodies. Anti-NC82 staining is used to visualize the brain. Scale bar represents 100µm. **B)** Higher magnification on the AL, highlighted with dashed circle. Arrow points to DA1 and DL3 glomeruli. Scale bar represents 25µm. **C)** Posterior view on the MB calyx. *MB247-Dα7-GFP* labels PSD in KC claws in green. AZ marker *Brp-short*^{mCherry} in DA1 driven by *R37H08-GAL4* is shown in red. Box is magnified on the right and shows a single MG (below: *MB247-Dα7-GFP*, middle: *Brp-short*^{mCherry}, above: merge). Scale bar represents 10µm.

3.2.2 Conditioning flies with cVA

To induce learning and memory formation we trained flies in an appetitive memory assay. We applied a two-odor paradigm with cVA, the DA1 PN specific odor, and geranyl acetate (Ga), which stimulates a separate set of PNs (Bhandawat et al. 2007) that is not labeled by *R37H08-GAL4*. As the unconditioned stimulus (US) we used sucrose. Flies were simultaneously exposed to cVA and sucrose, thus forming the positive conditioned stimulus (CS+). Ga was presented to the flies without sucrose, forming the negative conditioned

stimulus (CS-). This way, a population of flies is trained to associate the CS+ odor with the sucrose reward. When tested, these flies approach the CS+ odor in the absence of the US sugar reward, rather than the CS- (Fig. 9A, B). We used two control conditions to determine memory formation. On the one hand the reciprocal control with Ga as the CS+, in which flies were trained to associate Ga with sucrose. On the other hand the unpaired control, in which neither odor was simultaneously delivered with sucrose, but separately after one another, to avoid appetitive association.

Prior to the actual experiment, we tested if female and male flies perform differently when trained with cVA. As cVA is a sex-pheromone (Datta et al. 2008), it might induce different behaviors in females and males, thus negatively influence the outcome of the conditioning paradigm. We trained mixed groups of wildtype CantonS flies in a short-term memory (STM) (Fig. 9B) paradigm and counted males and females independently. Both males and females successfully associated cVA with sucrose and showed no significant difference between each other or the combined total (Fig. 9C). Same was true for training with Ga (Fig. 9D).

Now we could train flies with the before mentioned reporter and driver units (*;;R37H08-GAL4/ MB247Dα7::GFP, UAS-Brp-short*^{mCherry}) in the STM paradigm. Here, testing odor preference was performed one minute after training. Flies successfully learned to associate cVA with the US, as the majority approached the CS+. Similarly in the reciprocal control with Ga as CS+, flies also approached more strongly the CS+. Both paradigms were significantly different from the unpaired control, which resulted in an odor neutral preference (Fig. 9E).

We also trained flies in the LTM paradigm (Fig. 9B), in which memory formation is tested 24 hours after training. Here as well, flies successfully formed a positive association with either cVA or Ga, which again were significantly different from the unpaired control (Fig. 9F).

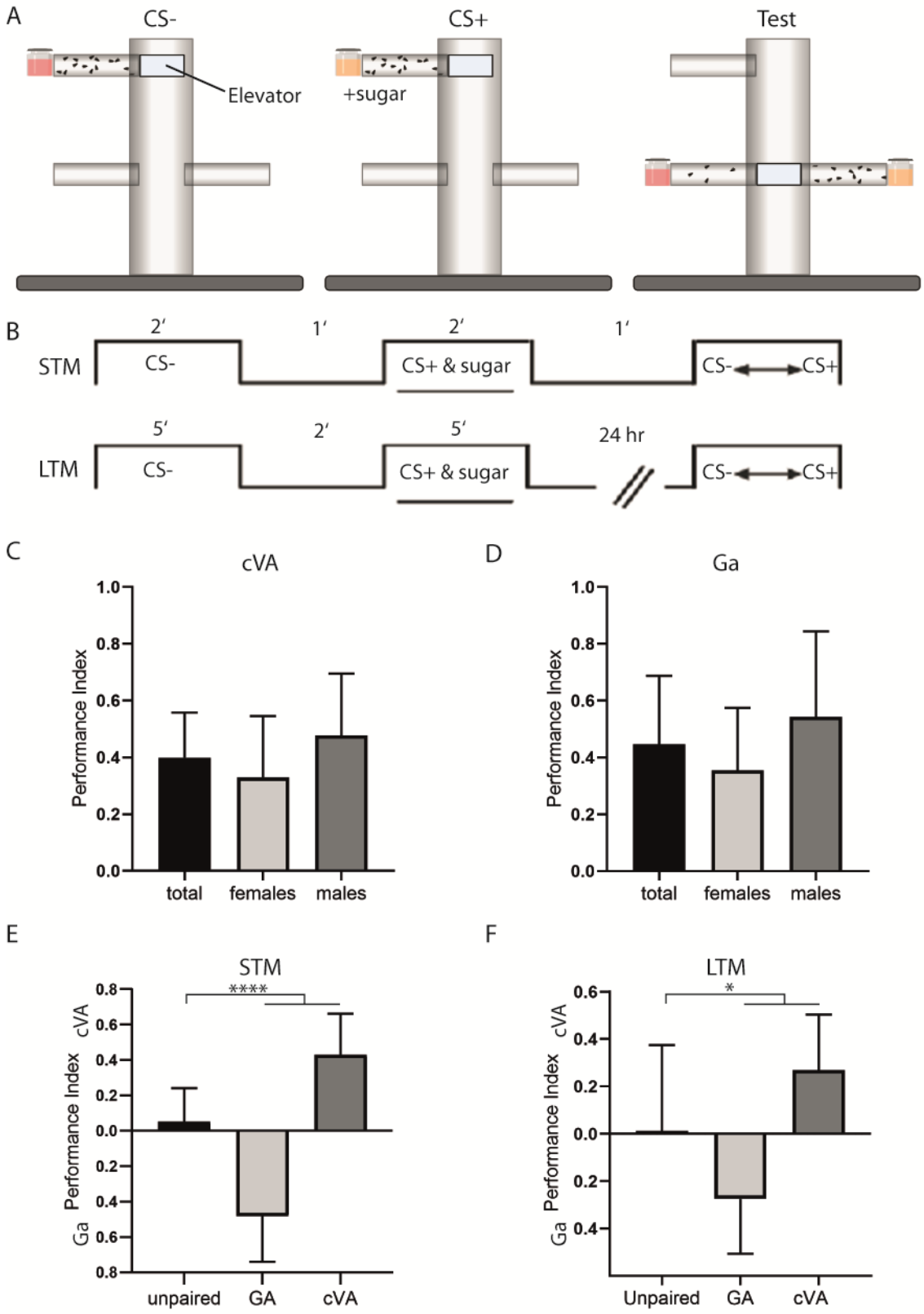

Figure 9: Flies learn in a STM and LTM to associate cVA with a sugar reward. **A)** Illustration of appetitive olfactory conditioning created in BioRender. **B)** Schematic protocol of appetitive olfactory conditioning for either STM or LTM. **C)** Female and male flies do not perform differently to each other or compared to total sum of flies, when conditioned with cVA in the STM paradigm. Each group consists of n=8. **D)** Female and male flies do not perform differently after appetitive conditioning with Ga in the STM paradigm. Each group consists of n=8. **E)** Performance index of *R37H08-GAL4/*

MB247Dα7::GFP, UAS-Brp-short^{mCherry} flies in STM. Flies conditioned with Ga or cVA scored significantly differently compared to an unpaired control group; n= 19-25. **F)** Performance index of *R37H08-Gal4/ MB247Dα7::GFP, UAS-Brp-short*^{mCherry} flies in LTM. Flies conditioned with Ga or cVA scored significantly differently compared to an unpaired control group; n= 14-19. Data are represented as the mean ± SD. Behavioral data were tested in a one-way ANOVA followed by a posthoc Bonferroni multiple comparisons test. Significance is set to $p<0.05$ = *, $p<0.005$ = **, $p<0.0005$ = ***, $p<0.0001$ = ****.

3.2.3 Plastic changes upon LTM

After we had established a system to visualize the DA1-PN pre- and postsynaptic connections specific to the odor activation in our conditioning assay with cVA, we could start investigating potential plastic changes in the MB calyx at the site of MGi.

For that matter, we prepared brains of flies (*;;R37H08-Gal4/ MB247Dα7::GFP, UAS-Brp-short*^{mCherry}) randomly picked from groups that had been successfully tested in the appetitive memory assay with cVA or from the control groups, unpaired and Ga conditioned. Unpaired conditioned flies control for the olfactory conditioning paradigm. Ga stimulates a separate set of PNs that does not overlap with *R37H08-Gal4*. Therefore these flies enable testing if potential changes are specific to activated synapses or training causes global changes in the calyx.

Per brain, the entire volume of one MB calyx was imaged. Image stacks were analyzed with a customized script in Definiens Developer XD™, an image analysis software which allowed an automated 3D- reconstruction of the calyx and precise 3D volumetric measurements of MGi. The 3D-reconstruction was based on the *MB247Dα7::GFP* signal, labeling the postsynaptic KC claws around the presynaptic PN bouton. The classification of DA1-PN MGi was based on the Brp-short^{mCherry} expression under the control of the DA1-PN specific driver line *R37H08-Gal4*. This way, we could analyze the volume of MGi, defined by the volume of the KC claws and the PN bouton, and the lumen of MGi, defined by the PN bouton size. Additionally, the number of DA1-PN MGi was determined and controlled by blindfolded manual counting of two experimenters.

After the STM paradigm, neither of the morphological parameters showed a measurable change between the differently trained groups, either trained with cVA or Ga, and the unpaired control (Fig. 10A-C). However, after the LTM paradigm, flies trained with cVA did show changes compared to Ga trained flies and the unpaired control group. The MG volume and the lumen were decreased, as was the number of DA1-PN MGi increased (Fig. 10D-F). These changes were only specific to the cVA trained group. Ga trained flies and unpaired

control flies showed similar scores compared to each other. Thus, LTM induces input-specific structural plasticity in the MB calyx, manifested in more but smaller MGi.

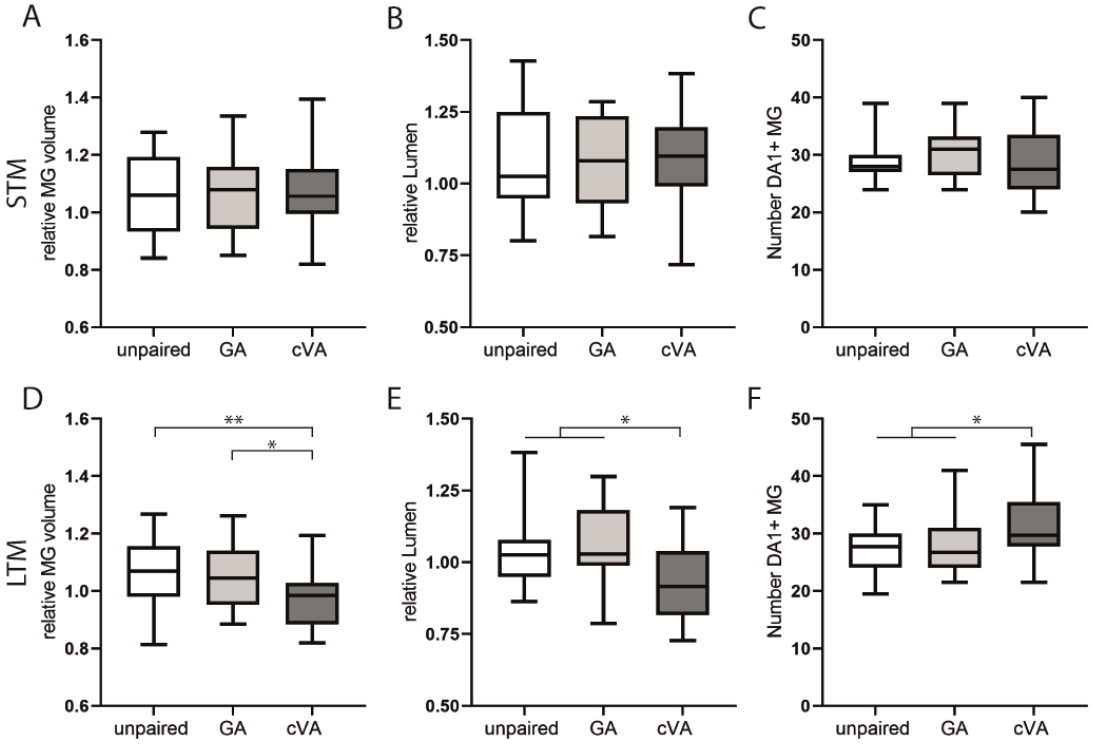

Figure 10: MGi undergo plastic changes in an appetitive LTM paradigm. **A-C)** MB calyxes analyzed after STM with unpaired n= 14, GA n = 15, cVA n = 18. **A)** The MG volume is defined by the GFP labeled PSDs in KC claws around the PN bouton. Between groups the relative MG volume of DA1 PN MGi does not change upon STM. **B)** The MG lumen is defined by the red $Brp^{mCherry}$ label expressed in the DA1 PN boutons. No changes in the size of the lumen between groups could be detected after STM. **C)** Number of positive DA1 MG did not show any difference between groups. **D-F)** MB calyxes analyzed after LTM with unpaired n= 25, GA n = 17, cVA n = 19. **D)** MG volume of DA1 PN MGi in flies trained with cVA is smaller compared to flies trained with Ga and unpaired control flies, **E)** as well is the MG lumen. **F)** The number of DA1 PN MGi is increased in flies trained with cVA after LTM. Data are represented in box plots representing with a thick line the median, a box the first and third quartiles and whiskers the minimum and maximum. Data were tested in a one-way ANOVA followed by a posthoc Bonferroni multiple comparisons test. Significance is set to $p<0.05$ = *, $p<0.005$ = **. Figure adapted from Baltruschat, Ranft et al., in revision.

3.3 Appetitive conditioning with optogenetic stimulation

As an alternative to the odor conditioning paradigm, we tried to make use of the neurogenetic tool kit of *D. melanogaster*. Instead of using an odor, we drove the optogenetic effector Cs-ChrimsonR (Klapoetke et al. 2014) in a subset of PNs. In temporal coincidence with a sugar reward and artificially induced neuronal activity, we tried to create a light-induced memory.

3.3.1 Fly genotype for optogenetic conditioning

For this purpose we designed a setup in which we could test whether flies had learned to associate the optogenetic stimulation with the sugar reward. Cs-ChrimsonR is an artificial light-gated cation channel of the channelrhodopsin channel family. It is optimally excited at a red wavelength of 617nm (Klapoetke et al. 2014). In brief, channelrhodopsin consists of seven transmembrane proteins called rhodopsin, which contain an all-trans-retinal molecule. Light exposure induces a conformational change of all-trans-retinal to 13-cis-retinal followed by a conformational change of the rhodopsin proteins. This leads to an influx of cations into the cell and its depolarization (Nagel et al. 2003) (Fig. 11A). We chose Cs-ChrimsonR for two reasons. First, the *Drosophila* visual system contains six forms of the visual pigment rhodopsin in eight photoreceptor cells. Their spectral sensitivity has been well described, with the longest wavelength maxima at 560 nm (Salcedo et al. 1999). Therefore, it has been suggested that flies have limited vision in the red shifted spectrum and it has limited innate behavioral meaning to them (Klapoetke et al. 2014). Second, with a red-shifted activation spectrum, Cs-ChrimsonR allows direct brain stimulation through the intact cuticle in freely moving flies (Klapoetke et al. 2014).

To ensure that only desired PNs would be activated by the red light stimulation, a highly specific driver line is required. Ruling out unwanted Cs-ChrimsonR expression was only possible with the splitGAL4 system, which, as mentioned before, only drives functional GAL4 expression in two overlapping driver lines (Pfeiffer et al. 2010). Therefore, we chose flies of the *SS01867-splitGAl4* line, which labels 10 PNs deriving from three AL glomeruli (DL1, DA1, DM2), (Fig. 11B). To investigate potential structural changes in the calyx, we simultaneously drove the expression of *MB247Dα7::GFP* and *UAS-Brp-short*^{mCherry}.

Flies of this genotype (*SS01867 x UAS-Cs-Chrimson-tdTomato; MB247Dα7::GFP, UAS-Brp-short*^{mCherry}) (Fig. 11D) were tested first in a regular appetitive olfactory LTM paradigm (for protocol see Fig. 9B), to ensure that they are capable of learning. Using 4-

methylcyclohexanol (MCH) and 3-octanol (Oct), flies scored significant positive performance indexes with both odors (Fig. 11C).

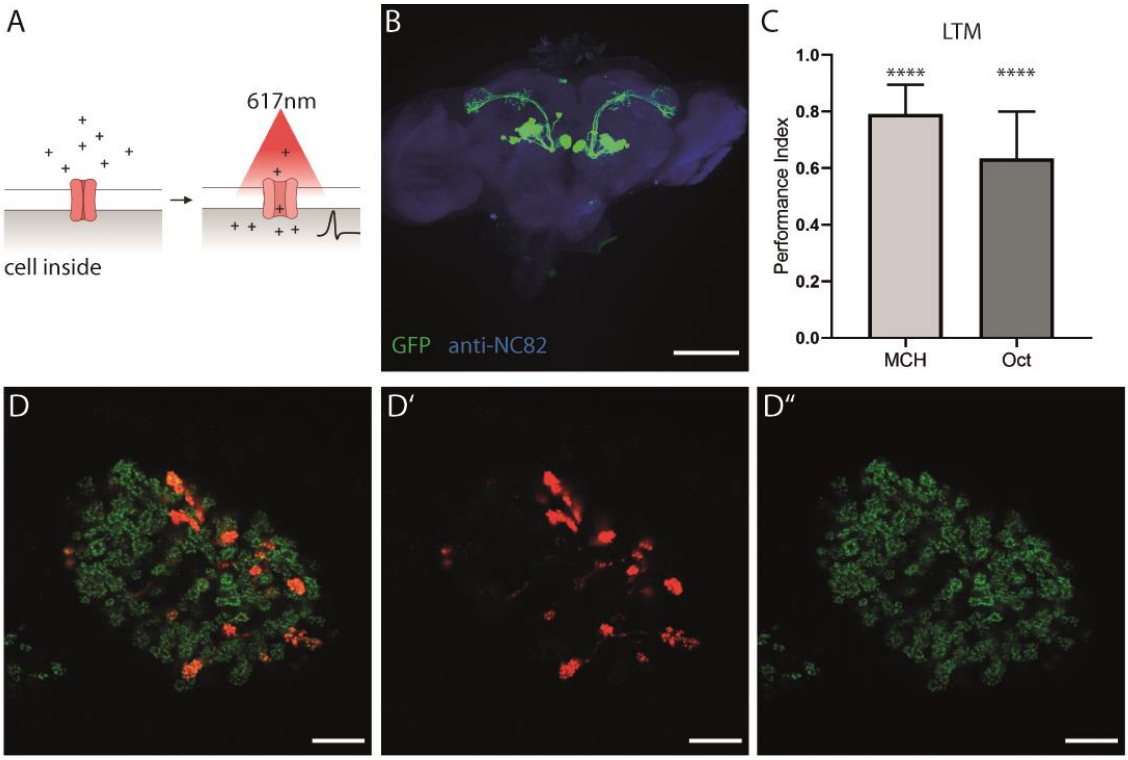

Figure 11: Genotype for optogenetic conditioning. **A)** Schematic drawing of the optogenetic tool Cs-ChrimsonR. Opening of the channelrhodopsin is induced by red light. This allows ions to flow through the channelrhodpsin into the neuron, resulting in a depolarization of the membrane potential and neuronal activation. Image created with BioRender. **B)** *SS01867* driving *UAS-mCD8::GFP* in PNs. Scale bar 100µm. **C)** Flies of the genotype *SS01867/UAS-Cs-Chrimson-tdTomato; MB247Dα7::GFP, UAS-Brp-short*^{mCherry} form appetitive LTM when trained with the odors MCH and Oct. Data are represented as the mean ± SD (One sample t test, $p<0.05$). Each group consists of n=8. **D)** Posterior view of the MB calyx in flies of the same genotype as in C. *MB247-Dα7::GFP* labels PSD in KC claws in green. *SS01867* drives Cs-ChrimsonR tagged with tdTomato in PNs visible in red. Scale bar is 10µm.

3.3.2 Place choice test arena

For evaluating flies' performance, we designed a place choice arena, in which freely moving flies could choose between two halves (Fig. 12A). One half was illuminated with IR light, the other additionally with a 625 nm λ far red light LED. Red light intensity was determined with flies expressing Cs-ChrimsonR under the control of the *GH146-GAL4* driver, which drives expression in approximately 65% of AL PNs, APL and also moonwalk descending neurons (MDN). Activation of MDNs triggers backward walking and spinning (Bidaye et al. 2014). Thus, increasing red light intensity until flies started walking backwards or spinning,

set the threshold for sufficient red light intensity to penetrate the intact cuticle and resulted in 1.45 mW/cm². We simultaneously tested, if starving after retinal feeding impacts Cs-ChrimsonR activity negatively. For this, flies were starved for 24 and 48 hours after 3 days of all-trans retinal feeding. Both groups still performed backward walking and spinning at 1.45 mW/cm² light intensity.

To ensure that flies do not have a bias for or against one of the two halves, we set wildtype CantonS flies into the arena for 5 minutes with only one half illuminated red. Flies distributed evenly in the arena throughout the complete recording time (Fig. 12B).

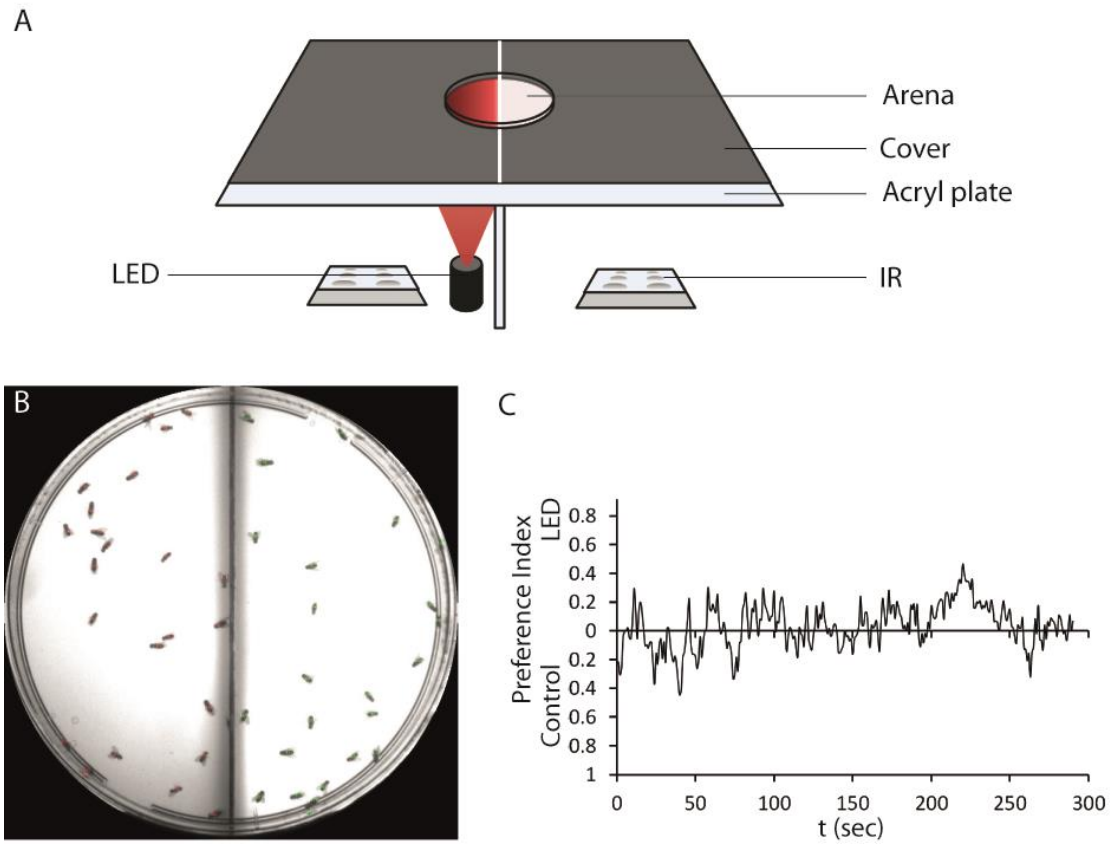

Figure 12: Design to test optogenetic conditioning. **A)** Illustration of a place choice test arena which enables optogenetic stimulation of neurons in one half. Image created in BioRender. **B)** Example of an image with flies in the arena recorded with a video camera from above. **C)** Flies do not show a bias for the red light illuminated half of the arena. Preference indexes were calculated for every second and plotted over time.

3.3.3 Optogenetic conditioning

Eventually, flies of the desired genotype (*SS01867 x UAS-Cs-Chrimson-tdTomato; MB247Dα7::GFP, UAS-Brp-short*^{mCherry}) were trained with optogenetic stimulation in a LTM appetitive memory assay. The place choice was recorded for 5 minutes, including 10 seconds of adjustment time to the arena in complete darkness at the start.

Initially with red light on, flies increased locomotion which returned to normal baseline behavior within 10 – 20 seconds. From then on trained flies (CS) spent slightly more time on the red illuminated half (PI range: -002 to 0.19, single PI: 0.04). Unpaired control flies showed to a small extent a preference for the dark half (PI range: 0.02 to -0.2, single PI: -0.1) (Fig. 13A, A'). The single PI was calculated by first averaging the PIs from 30 to 300 seconds, and afterwards averaging across groups. Data are normally distributed (D'Agostino and Pearson test). The two groups scored significantly different (Unpaired t-test: p-value 0.046) (Fig. 13A'). However, averaging within smaller time windows of 10 frames to calculate single PIs did not reveal significant differences.

To test whether new MGi were formed, brains were dissected right after testing of CS and unpaired control flies. As before (see chapter 3.2.3), the entire volume of one MB calyx per brain was imaged. The number of Cs-ChrimsonR positive MGi was determined and controlled by blindfolded manual counting of two experimenters. Here, no significant difference between the two groups could be detected with a mean of 58.13 and 58.45 Cs-ChrimsonR positive MGi for CS and unpaired control flies respectively (Fig. 13A").

As successful learning could not be conclusively detected, either in the optogeneitc conditioning paradigm or in the morphological evaluation of the calyx, the conditioning assay was altered to achieve unambiguous learning scores. In a first approach starvation time was doubled to ensure flies' motivation of coincidence detection of sugar and red light stimulus. Flies, however, did not score significantly better and no significant difference between CS and unpaired control groups could be detected (Fig. 13B).

One defining characteristic of LTM formation is its dependence on *de-novo* protein synthesis (Tully et al. 1994; Bailey, Bartsch, and Kandel 1996; Davis 2011). Hence, LTM is energy costly. To ensure enough nutrition supply, flies were given for 3 hours standard fly food supplemented with 100µl all-trans retinal 15 minutes after training (adopted protocol from (Gill et al. 2017)). They were transferred to plastic vials containing tissue paper soaked with water and re-starved for 21 hours before testing. Both training protocol with either 24 hours or 48 hours of food deprivation before conditioning were applied, but did not show unambiguous learning scores or differences between unpaired control and trained CS flies. (Fig. 13C, C')

Another explanation for the inconclusive results of the prior experiments could be the testing of flies. During testing, flies might simply stay in one place or groom themselves instead of exploring the arena and, therefore, do not find the illuminated half. To eliminate this possibility, the two halves of the arena were illuminated with red light alternating every 30 or 60 seconds. Trained flies were expected to migrate between the two halves with the back and forth switching of the red light. On the other hand, control flies should display an even distribution across the arena and stay unaffected from the red light alternations. This was, however, not the case. With an alternation rate of 30 seconds, a minor migration pattern in a similar fashion with the red light illumination was visible for both groups and additionally a PI above 0.19 could not be exceeded (Fig. 13D). Alternation of red light at 60 seconds interval did also not prove unambiguously learning. Trained flies spent more time on one half of the arena independently of the red light illumination, whereas control flies slightly preferred the other half. Flies seem to settle again in one position and do not follow red light illumination (Fig. 13D').

In a final approach, flies were trained in a space training paradigm. Instead of a single session of simultaneous sugar and red light exposure during training, flies were trained five times for 1 minute with a 15 minute interval and afterwards re-fed for 3 hours. Control flies were exposed to red light and sugar separately with 2 minutes apart. Again, flies did not score significantly better and no significant difference between CS and unpaired control groups could be detected. (Fig. 13E)

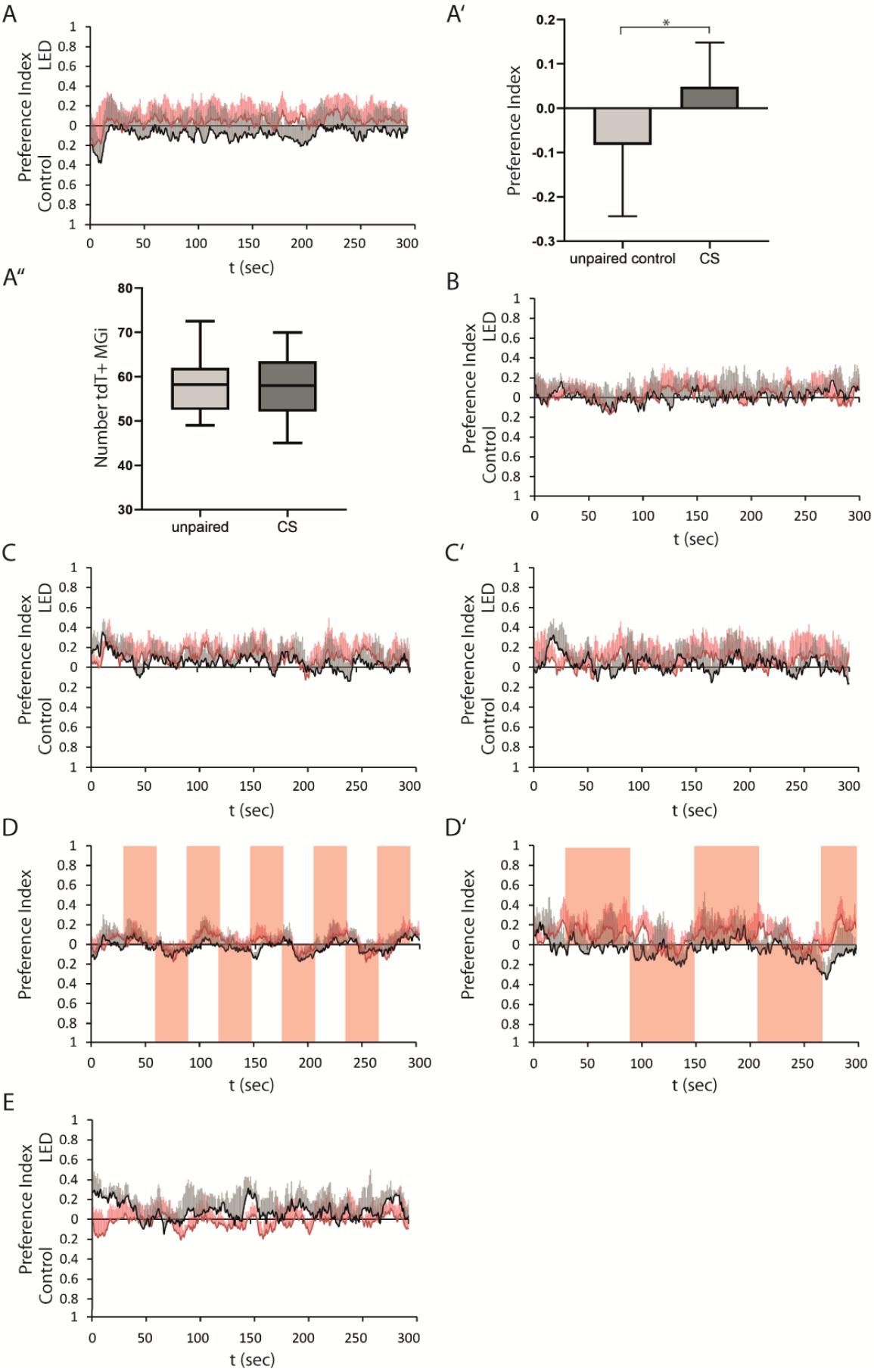
A
Preference Index
LED
Control
t (sec)
A′
Preference Index
unpaired control
CS
*
A″
Number tdT+ MGi
unpaired
CS
B
C
C′
D
D′
E

Figure 13: LTM conditioning by optogenetic activation of PNs. **A)** A graph of PI across time, where trained flies (CS, in red) are plotted against the unpaired control (gray). Upper half represents red light illuminated half of the arena, lower half of graph represents the control area. Flies were starved 24 hours before training. **A')** Bar graph showing the single value PIs of unpaired control and CS flies. Single value PIs were calculated by averaging the PIs from 30 seconds to 300 seconds per group and averaged per condition. A positive score represents red light attraction, a negative score avoidance. CS flies show a greater preference for the red light illuminated half of the arena compared to the unpaired control (Unpaired t-test: p-value= 0.046). **A")** Number of MGi with PN boutons expressing Cs-ChrimsonR tagged with tdTomato compared between unpaired control and CS flies. No difference was found between conditions. Data are represented in box plots representing with a thick line the median, a box the first and third quartiles and whiskers the minimum and maximum. Data were tested in a t-test with significance set to $p<0.05$; n= 20-28. **B)** Graph of PI across time with CS (red) plotted against unpaired control (gray). Flies were starved 48 hours before training. **C, C')** PIs are shown of CS (red) and unpaired control (gray) across time. Flies were fed with trans-Retinal food after training. In **C)** flies were starved 24 hours, in **C')** for 48 hours. **D, D')** PIs plotted as in A. Red rectangles indicate red light illumination alternating between halves of arena every **D)** 30 seconds or **D')** 60 seconds. **E)** Graph shown as in A. Flies were trained in a space training paradigm. No difference between CS and unpaired control is found.

3.4 Characterizing the MB calyx innervating neuron MB-C1

The MB calyx is the input site of the olfactory information delivered by PNs ascending from the AL. PNs and MB intrinsic KCs form here microglomerular synaptic complexes, which also include other neurons. In our previously discussed EM reconstruction of a MG, we could identify these neurons. One identified neuron type is Mushroom body calyx neuron 1 (MB-C1). Two neurons exist in each hemisphere. The somas are located laterally and ventrally of the LH. From here, they extend ventrally a single branch, turn dorsally to enter the LH. Here they send collaterals into the LH. The main branches project further into the MB calyx, where they branch extensively throughout the main calyx. The EM reconstruction shows that the MB-C1 neurons form pre- and postsynaptic connections with PN boutons and give input to KCs as well.
The role of MB-C1 in olfactory processing and learning is unknown. This chapter gives a first description of this neuron type

3.4.1 MB-C1 is GABAergic

To investigate MB-C1 (Fig. 14A), we first started examining the neurotransmitter type. Under the control of the splitGAL4 driver *GMR_MB380B* we expressed the membrane marker *UAS-mCD8::GFP* in MB-C1 (Fig. 14B) and performed immunohistochemical experiments with antibodies against different types of neurotransmitter or their precursor proteins. An anti-GABA antibody staining confirmed that the cell body of both MB-C1 neurons exhibited strong GABA immunoreactivity (Fig. 14C). To verify the specificity of the antibody and to exclude false labelling, we chose to knock down the expression of GABA in MB-C1 using RNA interference (RNAi). Driving the expression of a construct that can induce RNAi mediated glutamic acid decarboxylase 1 (GAD1) knock-down specifically in MB-C1 suppressed GABA expression (Fig. 14D). This confirmed the GABAergic identity of MB-C1. Other immunohistochemical experiments testing neurotransmitter expressions of Acetyl choline, Dopamine, Histamine, Glutamate, Serotonin and Octopamine were negative (Table 13).

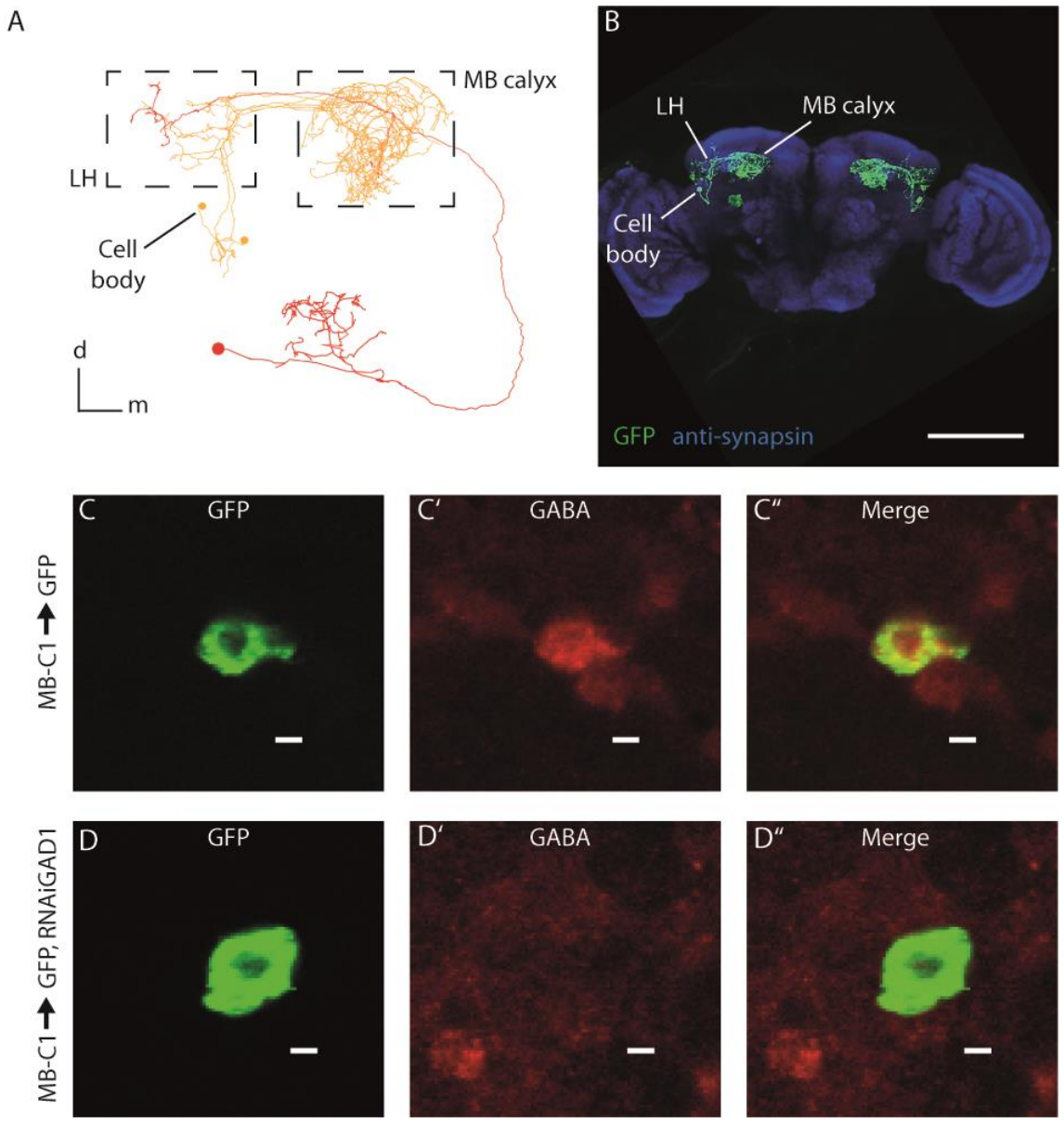

Figure 14: MB-C1 is GABAergic. **A)** Skeletonized tracing of MB-C1 neurons (orange) and a PN (red) in the FAFB data set. **B)** *GMR_MB380B* driving GFP in MB-C1 Anti-synapsin staining to visualize the brain. Scale bar = 100µm. **C-C")** High magnification image of one MB-C1 cell body expressing endogenous GFP labeled with anti-GABA staining. Scale bar 1µm. **D-D")** Cell specific knock-down of GABA synthesis by driving *RNAiGAD1* transgene in MB-C1 shows no anti-GABA labeling in MB-C1 cell body.

Table 13: Neurotransmitter expression in MB-C1.

Antigen	Antiserum	MB-C1
Choline acetyltransferase	CHAT4B1 mouse monoclonal	negative
Tyrosine Hydroxylase	AB152 mouse anti-tyrosine hydroxylase	negative
Histamine	PAN19c polyclonal rabbit	negative
Glutamate	Anti-Glutamate monoclonal mouse	negative
Serotonine	5HT-H209 mouse monoclonal	negative
Octopamine	Tyrosine decarboxylase rabbit polyclonal	negative
GABA	GABA polyclonal rabbit	positive

3.4.2 Pre- and postsynaptic connections in MB calyx and LH

The EM reconstruction of a MG showed pre- and postsynaptic connections of MB-C1 in the calyx. MB-C1 also extends branches into the LH. To confirm the finding in the calyx and further investigate the polarity in the LH we used genetic markers for dendritic and axonal compartments.

First we applied the genetically encoded somato-dendritic marker DenMark, which labels dendritic compartments without interfering with the neuronal function or development independently of neuronal subtype (Nicolai et al. 2010). Under the control of the splitGAL4 driver *GMR_MB380B* we expressed *UAS-DenMark* in combination with the membrane marker *UAS-mCD8::GFP* and examined the subcellular localization of DenMark expression. High levels of DenMark expression were detected in the somata and in neurites of MB-C1. These neurites were found in the MB calyx and in the LH, indicating that MB-C1 is not clearly polarized between LH and MB calyx. Whereas mCD8::GFP labels the entire membrane of the neuron, DenMark specifically marks dendritic compartments and postsynaptic sites; therefore a complete overlap was not expected (Fig. 15A-A"). To identify presynaptic sites, we expressed the presynaptic AZ marker *UAS-Brp-short*^{mCherry} and *UAS-mCD8::GFP* under the control of *GMR_MB380B*. MB-C1 expressed strong punctuated red fluorescent signal in the calyx and the LH, indicating that its collaterals are presynaptic in both neuropils (Fig. 15B-B").Taken together, MB-C1 is pre- and postsynaptic in the MB calyx and the LH.

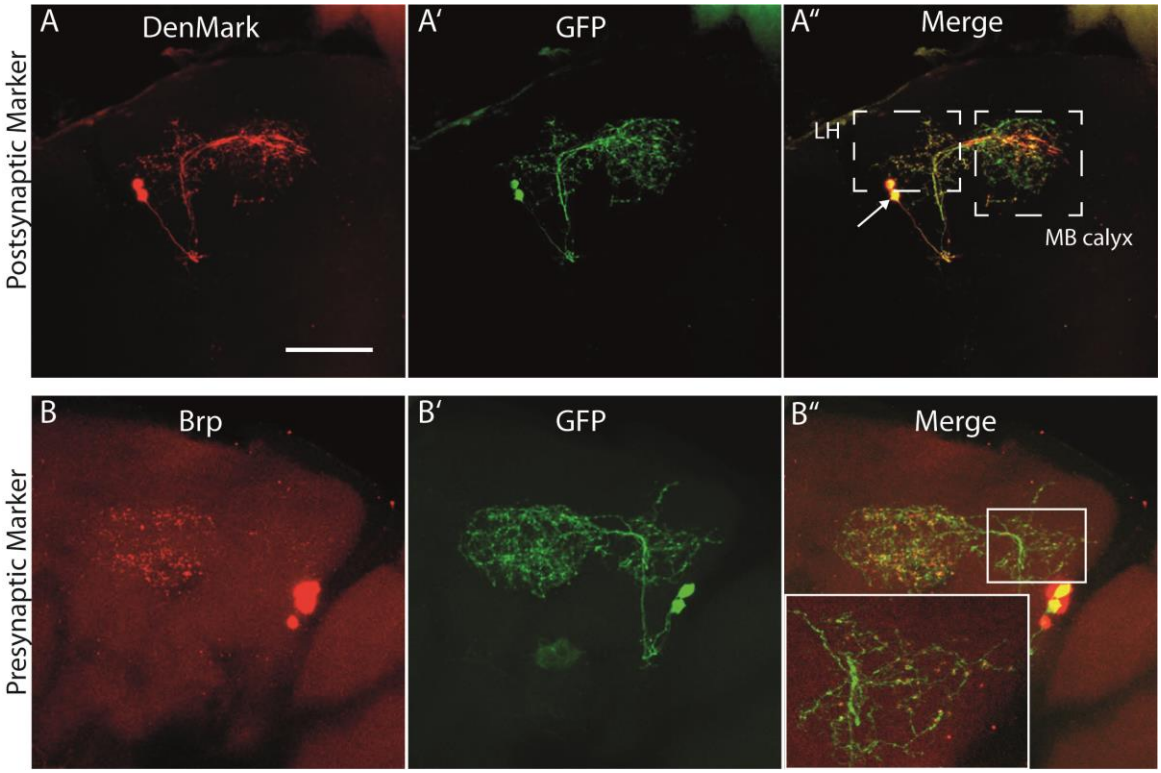

Figure 15: MB-C1 is pre- and postsynaptic in MB calyx and LH. **A-A")** Driving the postsynaptic marker DenMark in *GMR_MB380B* shows expression in the MB calyx and the LH. Arrow in A" points to the cell bodies. Dashed squares in A" indicate the positions of LH and MB calyx. **B-B")** The presynaptic marker Brp-short^{mCherry} is expressed in the MB calyx and the LH. **B")** The LH is marked with a square and magnified in the low left corner of the image. Scale bar in **A)** is 50µm and representative for all images.

3.4.3 MB-C1 innervating aversive LH region

Odors of attractive and aversive valence are separately represented in different clusters in the AL. This segregation is further reflected in two different regions in the LH. The dorsal region of the LH represents attractive odors, whereas the ventral region represents aversive odors (Seki et al. 2017). As MB-C1 innervates the LH, we examined the location of its collaterals in the LH.

The boundaries of the LH are determined by the PN innervation in the lateral protocerebrum (Schultzhaus et al. 2017). For this reason we used *GH146-QF* driving *QUAS-mCD8::GFP* expression in approximately 65% of AL PNs (Schwaerzel, Heisenberg, and Zars 2002) to define the LH and simultaneously expressed *UAS-tdTomato* under the control of *GMR_MB380B* in the MB-C1 neurons. This way, we were able to visualize the lateral innervation by MB-C1 in the LH. Interestingly, MB-C1 does not extend branches throughout the entire LH, but is limited to the ventral region (Fig. 16). Here, MB-C1 extends thin

branches that form bouton-like swellings (Fig. 16A). Thus, MB-C1 innervation is limited to the aversive coding LH region.

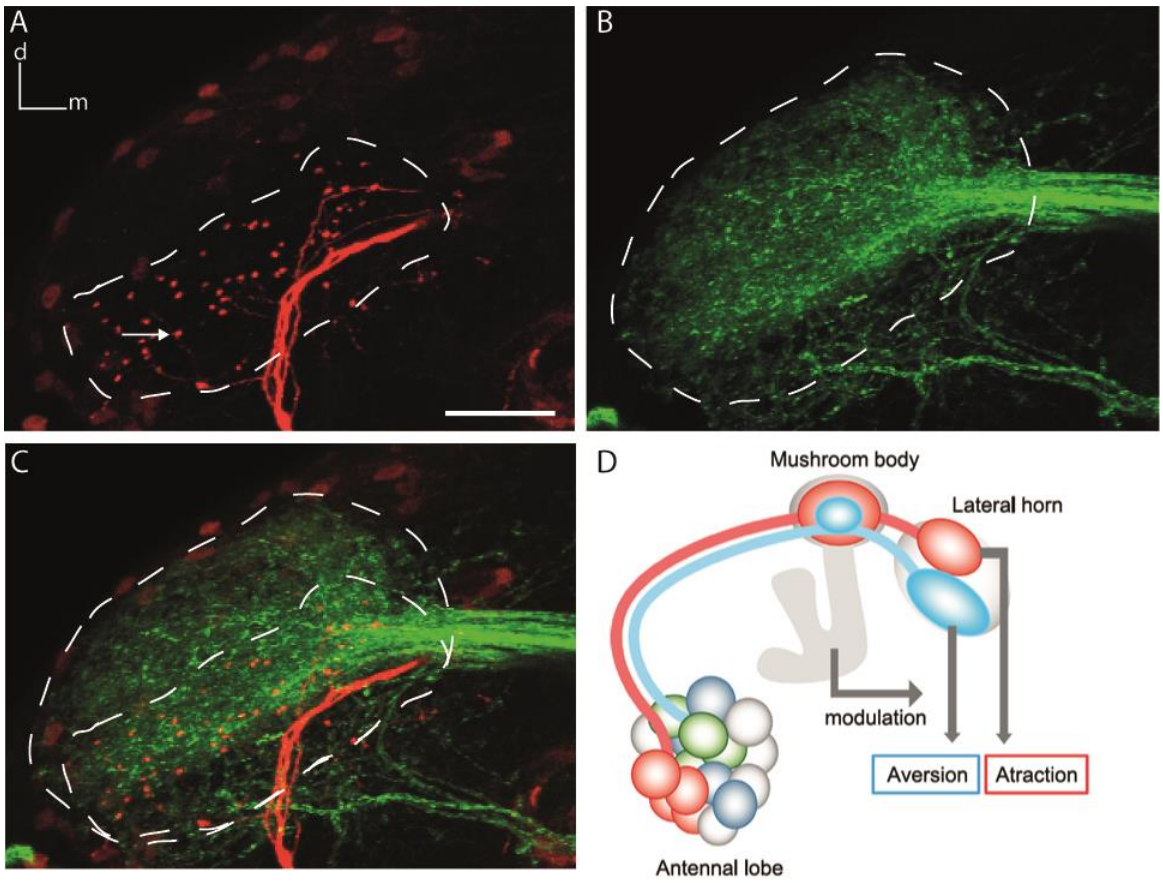

Figure 16: MB-C1 innervates the ventral LH. **A)** *GMR_MB380B* driving dtTomato (red) labeling MB-C1. Arrow points to bouton like swelling. Area innervated in the LH is outlined by dashed line. **B)** *GH146* driving GFP in PNs. Dashed line represents the boundaries of the LH. **C)** The merge shows the innervation of MB-C1 is limited to the ventral region of the LH. **D)** Illustration showing the regions for aversion and attraction in the MB and the LH. Illustration adopted from (Seki et al. 2017). Scale bar in **A)** represents 50µm and applies to all images. Images represent n=10.

3.4.4 Silencing MB-C1 synaptic output

Since MB-C1 enters the LH and the MB calyx, we wondered whether this neuron might influence innate olfactory behavior and olfactory learning. We chose to express *UAS-Shibire^{ts}* under the control of MB-C1-splitGAL4 driver *GMR_MB380B*. Shibire^{ts} is a temperature-sensitive mutation, which allows normal endocytosis to occur at temperatures below 22°C, but prevents membrane retrieval at temperatures exceeding 30°C, leading to reduced neurotransmitter release, thus blocking specifically synaptic output in the otherwise intact nervous system (Kitamoto 2001, 2002b, 2002a).

Flies expressing *UAS-Shibire^{ts}* in MB-C1 at a high temperature exhibited significant differences in their naïve responses to odors of aversive valence (Oct and MCH) compared to flies of the same genotype at low temperature, as well to genetic control flies with either the *GMR_MB380B* or *UAS-Shibire^{ts}* alone (Fig. 17A, B). Interestingly, no differences between temperatures or genotypes was found when flies were exposed to an attractive odor, here apple vinegar (Fig. 17 C).

We also tested whether olfactory learning is affected when MB-C1 output is blocked by Shibire^{ts}. We used an appetitive STM paradigm, in which we conditioned flies to associate sugar with either Oct or MCH. Flies expressing *UAS-Shibire^{ts}* in MB-C1 at a high temperature exhibited a significant impairment of performance after olfactory classical conditioning with both odors (Fig. 17D, E). To investigate how blocking synaptic output of MB-C1 interferes with learning, we tested whether memory acquisition or memory recall is affected. To block synaptic output via Shibire^{ts}, flies have to be incubated at high temperature for at least 2 hours. Therefore, we used an appetitive mid-term memory (MTM) paradigm, in which flies are tested 3 hours after regular training. First, we tested if flies, wildtype *CantonS* and expressing *UAS-Shibire^{ts}* in MB-C1, are able to perform in this paradigm. Again we used Oct and MCH as odors. Both groups, wildtype *CantonS* (Fig. 17 F) and mutant flies (Fig. 17G) showed significant positive preference scores. Second, we tested if blocking synaptic output during memory recall is affected. Flies expressing *UAS-Shibire^{ts}* in MB-C1 were transferred directly after training to high temperature and kept on during testing. Flies scored significantly lower when transferred to high temperature compared to flies kept constantly at low temperature and to genetic control flies (Fig. 17H, I). Next, we tested if learning is affected by blocking MB-C1 synaptic output. MTM was performed similarly, yet flies were exposed to high temperature 3 hours prior and during training. Afterwards flies were kept for 3 hours and tested on low temperature. This time, all groups exhibited similar performance and showed no significant differences in comparison to temperature control flies (Fig. 17J, K). Together, these findings suggest that MB-C1 function is important for the retrieval of memory, rather than during acquisition.

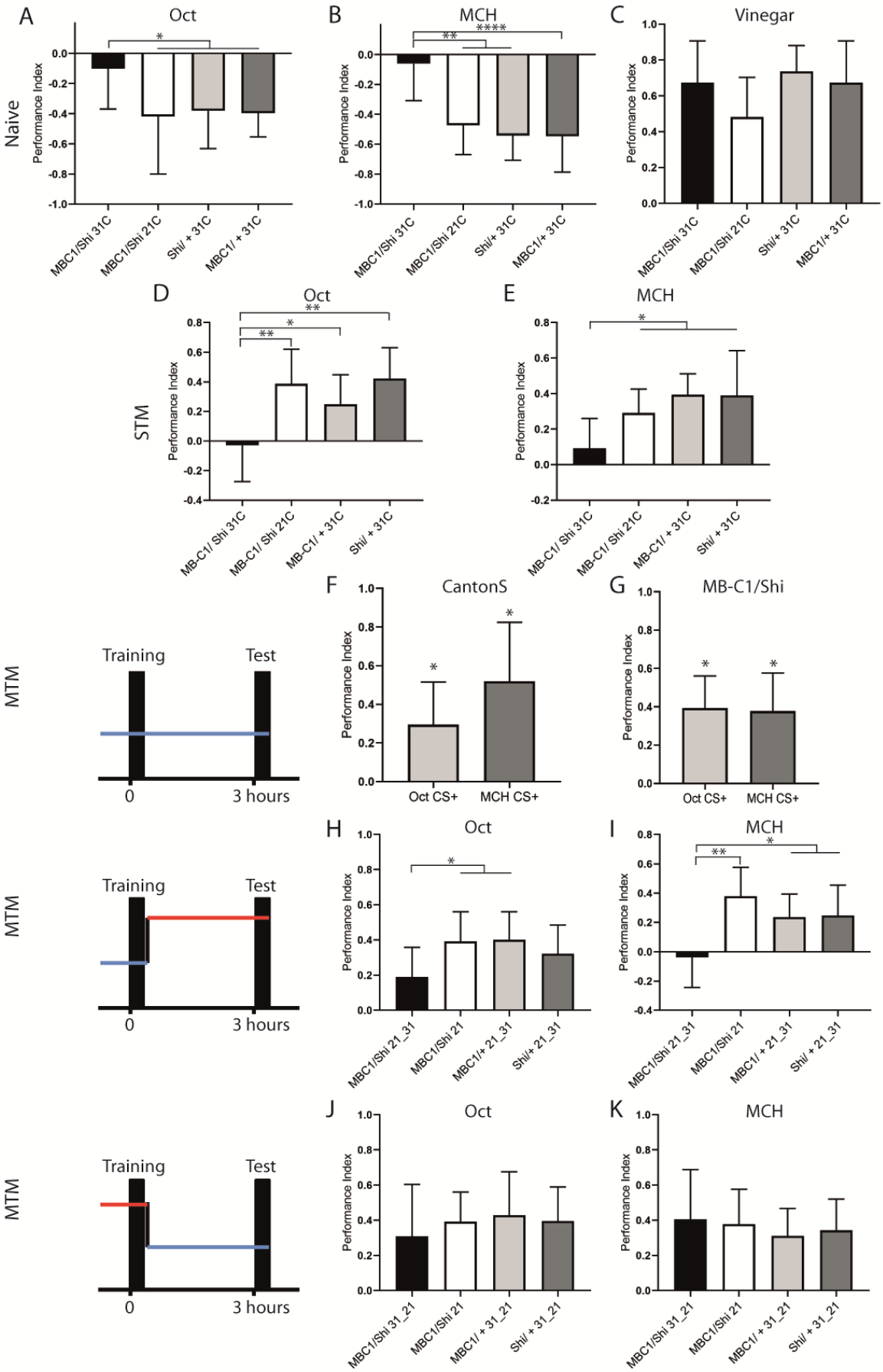
A
Oct
Naive
Performance Index
MBC1/Shi 31C
MBC1/Shi 21C
Shi/ + 31C
MBC1/ + 31C
B
MCH
C
Vinegar
D
Oct
STM
MB-C1/ Shi 31C
MB-C1/ Shi 21C
MB-C1/ + 31C
Shi/ + 31C
E
MCH
F
CantonS
Oct CS+
MCH CS+
G
MB-C1/Shi
MTM
Training
Test
0
3 hours
H
Oct
MBC1/Shi 21_31
MBC1/Shi 21
MBC1/+ 21_31
Shi/+ 21_31
I
MCH
J
Oct
MBC1/Shi 31_21
MBC1/Shi 21
MBC1/ + 31_21
Shi/ + 31_21
K
MCH

Figure 17: Blocking synaptic output in MB-C1. **A-C)** Naïve response to Oct **A)** and MCH **B)** is significantly reduced when synaptic output is blocked on 31°C by Shibire in MB-C1, but not when flies are exposed to vinegar **C)**. **D-E)** STM performance is significantly reduced when expression of Shibire in MB-C1 is induced on 31°C. Flies were trained with Oct **D)** and MCH **E)** and compared to the temperature and genotype controls. **F)** Wildtype *CantonS* flies form MTM on 21°C when trained with Oct and MCH. **G)** Flies of the genotype *GMR_MB380B/UAS-Shibire^{ts}* are able to form MTM when trained with Oct and MCH. **H-I)** Shibire expression in MB-C1 induced by 31°C during testing reduces performance scores when trained with Oct **H)** and MCH **I)**. J-K) When Shibire is expressed during training, flies do not show performance differences to control groups. Data are represented as the mean ± SD. Behavioral data were tested in a one-way ANOVA followed by a posthoc Bonferroni multiple comparisons test in a, b, c, d, e, h, i, j, and k; data in f and g were tested with a one-sample t-test. Significance is set to $p<0.05$. Each group in A, B and C consists of n=12; and in D, E, F, G, H, I, J, K of n=8.

Next, we decided to disrupt neurotransmitter synthesis in MB-C1 via GABA RNAi and test innate and learned olfactory responses. Although RNAi of GABA was successful (see chapter 3.4.1), innate responses were not different from control flies (Fig. 18A, B). When testing STM, performance was only impaired when flies were trained with MCH, but not with Oct (Fig. 18C, D). Neurons can express multiple neurotransmitter simultaneously, among them different neuropeptides (Pauls et al. 2014). Immunohistochemical analysis were negative for Acetylcholine, Dopamine, Histamine, Glutamate, Serotonin and Octopamine (see chapter 3.4.1). Therefore we used RNAi of prohormone convertase 2 (AMON), a single enzyme essential for peptide processing in the fruit fly (Pauls et al. 2014). Knocking down the expression of AMON inhibits neuropeptide expression. We tested the innate olfactory responses with the aversive odors, Oct and MCH, using two different UAS-RNAi constructs to knock down AMON. However, neither group exhibited significantly different behavior than the control group (Fig. 18E, F). Finally, we induced MB-C1 cell specific apoptosis by overexpressing the pro-apoptotic genes *reaper* (rpr) (White et al. 1994; White, Tahaoglu, and Steller 1996) or *head involution defective* (hid) (Grether et al. 1995) in *GMR_MB380B* and tested innate responses to Oct and MCH. Nevertheless, innate odor avoidance could not be suppressed (Fig. 18G, H).

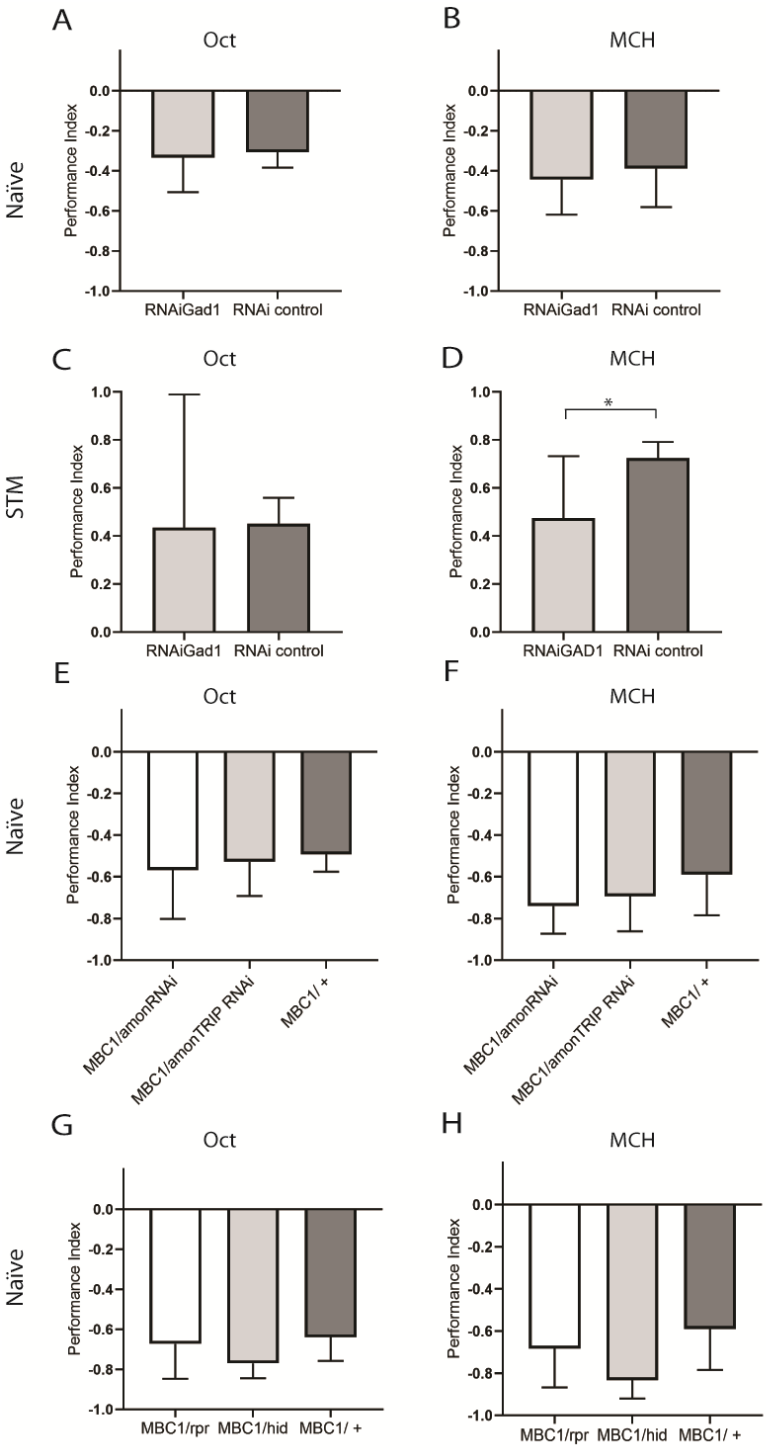

Figure 18: Neurotransmitter knock-down in MB-C1. **A-B)** Knocking down GABA in MB-C1 does not affect naïve responses to **A)** Oct and **B)** MCH. **C-D)** STM is not affected by GABA knock-down when trained with **C)** Oct but when trained with **D)** MCH. **E-F)** Knocking down AMON in MB-C1 does not influence flies naïve responses to **E)** Oct and **F)** MCH. **G-H)** Cell specific apoptosis of MB-C1 induced by *rpr* or *hid* does not affect naïve responses to either **G)** Oct or **H)** MCH.

Overall, silencing MB-C1 by blocking synaptic output with *UAS-Shibire^{ts}* showed a significant impact on flies innate and learned olfactory behavior. Nonetheless, these results could not

be replicated by neurotransmitter and neuropeptide RNAi and cell specific apoptosis. Although exciting, these results cannot be interpreted undoubtedly and the function of MB-C1 has yet to be investigated further.

4 Discussion

The drosophila mushroom body is a cerebellum-like structure that is essential for associative olfactory learning. In recent years, it has been extensively studied for understanding the neuronal mechanisms that enable the fly to form such associations. Great attention has been especially given to the MB lobes. This work sets its focus on the olfactory integration site of the MB, the calyx, with an emphasis on the connectome of the microglomerular synaptic complex, structural plasticity during memory consolidation and the MB-C1 neuron.

4.1 A complete reconstruction of a microglomerular synaptic complex

Here, we provide for the first time the complete wiring diagram of a single MG within the MB calyx with all its neuronal types and their synaptic contributions. In contrast to other studies that were primarily suggesting neuronal identities based on local morphological criteria, we traced the neurons and located their cell bodies to reveal their morphology. This enabled us to compare these tracings to existing LM data and to screen existing databases containing LM information of adult fly brain neurons. Except for a small number of synaptic profiles, we could unambiguously classify each cell type.

The PN bouton has a maximum diameter of 2.66µm and a volume of 5.77µm^3,

Our reconstructed MG consists of a DA1 PN bouton surrounded by 14 KCs claws of 5 different subtypes, two presynaptic KCs, APL and both MB-C1. A similar number of postsynaptic KC claws with an average of 11 have been reported before (Butcher et al. 2012). The PN bouton falls with 2.66µm in diameter into the previous reported range of 1-4µm (Butcher et al. 2012). We found 27 additional KCs making synaptic connections within the MG space, either with KC claws, APL or MB-C1. Altogether, the microcircuit consists of 47 neurons of 4 different cell types. The MG space is further passed through by three KCs not forming any synaptic connections.

4.1.1 Projection neuron bouton form pre- and postsynaptic connections with various KC subtypes

The postsynaptic KCs receive input at 8-25 postsynaptic sites, which is in accordance with a previous estimation of 18-24 postsynaptic sites (Butcher et al. 2012). DA1 PN boutons are reported to be located within a region of the MB calyx to be predominantly occupied by αβs KCs (Lin et al. 2007). However, the great majority of KCs in our reconstruction are of the γmain subtype, which is with approximately 600 cells the most frequent KC subtype in the MB (Aso, Hattori, et al. 2014). Together with the fact that we find 4 additional KC subtypes downstream of the PN bouton suggests that the output of individual PNs is more diverse than previously expected. Indeed, recent EM reconstruction from the *Drosophila* larva (Eichler et al. 2017) and data generated with LM in the adult (Caron et al. 2013) suggest random PN-to-KC connectivity. Another point to consider is the finding that different subsets of KCs serve different functions. For instance, α'β' KCs are necessary to acquire and stabilize aversive and appetitive memory, but dispensable during memory retrieval, which depends on αβ KCs (Krashes et al. 2007). Also, LTM depends on αβ KCs, but does not require α'β' KCs, which on the contrary are forming MTM (Pitman et al. 2011). Therefore, a PN output onto a mixed group of KC subtypes ensures that the sensory information is distributed over the whole MB and can be evaluated accordingly to a context, *e.g.* punishment or reward, but also novel or already learned stimulus.

Previous studies showed that KCs contain a mixture of pre- and postsynaptic connections in the MB calyx, with postsynaptic sites in the claws and presynaptic connections along the main branches. The presynapses were localized outside MGi and distant from PN boutons (Butcher et al. 2012; Christiansen et al. 2011). Yet, we show here for the first time that KCs also give input into PN boutons. These synapses were indeed along the main branches, which KCs extend from the soma through the calyx into the pedunculus. A feedback pathway

from the KCs to the AL has been described before (Hu, Zhang, and Wang 2010). Activation of KCs induced depolarization in PNs and local interneurons in the AL, indicating top-down modulation of olfactory processing. The authors suggest that the feedback is mediated by MB lobes, because activation of KC axons induced a greater response in the AL than activation of KC cell bodies. The difference might be caused by neurons projecting from the MB lobes to the AL (Hu, Zhang, and Wang 2010). Nevertheless, the KC synapses onto PN boutons could to some extent contribute to this feedback loop. Likewise, these synaptic connections could perhaps promote odor processing in the calyx, either globally or locally in individual MGi. The latter assumption is further supported by our reconstruction with two presynapses in two KC claws connecting with the APL.

4.1.2 Integration of GABAergic neurons in the MG

Past studies describing the neuronal network within the MB calyx reported a great number of ENs, among them octopaminergic (Aso, Hattori, et al. 2014; Busch et al. 2009; Burke et al. 2012; Wu et al. 2013), GABAergic (Tanaka, Tanimoto, and Ito 2008; Liu and Davis 2009), serotonergic (Roy et al. 2007), dopaminergic (Aso, Hattori, et al. 2014; Mao and Davis 2009; Chen et al. 2012) neurons and yet to be determined neurons (Tanaka, Tanimoto, and Ito 2008; Zheng et al. 2018). Therefore, we were surprised to find only APL and MB-C1 in the MG complex. APL is a large GABAergic (Liu and Davis 2009) and octopaminergic (Wu et al. 2013) neuron broadly innervating the MB. Each hemisphere contains one APL neuron with the cell body located lateral to the MB calyx and near the LH (Tanaka, Tanimoto, and Ito 2008). From the cell body it extends a single neurite dorso-medially that splits into two branches. One branch projects to the mushroom body at the vertical lobe (Liu and Davis 2009), while the second enters the calyx and the pedunculus (Tanaka, Tanimoto, and Ito 2008). Although the neuron innervates the calyx, pedunculus and the MB lobes entirely, developmental data suggest that the MB is solely innervated through the MB calyx (Mayseless et al. 2018). It is part of a functional loop with KCs, as it is activated by KCs and itself simultaneously inhibits KCs (Lin et al. 2014). This is facilitated by a negative feedback circuit between the APL and the KCs, suggested to be important for the maintenance of KCs' sparse activity and thereby promotes odor discrimination (Lin et al. 2014) Reducing GABA synthesis in APL enhances short term memory olfactory learning. On the other hand, odor discrimination is reduced, yet not abolished (Liu and Davis 2009). Further, Octopamine release of APL onto KCs promotes anesthesia-resistant memory consolidation of an odor conditioned stimulus (Wu et al. 2013). Although, MB-C1 had not been sufficiently studied in Drosophila, it is suggested to be GABAergic based on morphological comparison with the

Calycal giants (CGs) neurons in *Periplaneta Americana* (Tanaka, Tanimoto, and Ito 2008; Nishino and Mizunami 1998). Four CGs per hemisphere exist in *P. americana* connecting the LH with the MB calyx. Their activity is suppressed by olfactory, visual, tactile or air current stimulation, but CGs themselves suppress the activity of KCs, leading to the suggestion that disinhibition of CGs may facilitate the transmission of sensory signals to KCs (Nishino and Mizunami 1998).

The role of these neurons in the MB calyx specifically and in particular in the MG has not been investigated, yet. The finding that APL and MB-C1 make synapses onto both PN boutons and KCs, and that PN bouton synapses onto APL and MB-C1 resembles the circuitry of inhibitory GABAergic neurons in the lib region of the MB calyx in honey bees (Ganeshina and Menzel 2001). Here, the presynapses of GABAergic neurons on PN boutons and KCs suggest that the transmission of the odor stimulus is inhibited by both pre- and postsynaptic inhibition. Simultaneously, the cholinergic PN boutons are excitatory and synapse onto the GABAergic neurons, which may represent a short negative feedback loop (Ganeshina and Menzel 2001). The here demonstrated connections in the MG indicate a microcircuit with local inhibition by GABAergic neurons. These microcircuits are also found in the brains of vertebrates, such as rats (Zipp et al. 1989), and mouse (Porter, Johnson, and Agmon 2001), and potentially stabilize and regulate the excitation level of neuronal networks (Ganeshina and Menzel 2001; Menzel 2014). Whether this is also the case for the MB calyx in the fruit fly needs to be further tested. In particular, further research has to investigate, firstly, if the connections of APL and MB-C1 in the MB calyx act independently of their connections in other regions; that is for APL in the MB lobes, and for MB-C1 in the LH. This could imply that these neurons have spatially distinct functions. Secondly, it is necessary to investigate, if the neurons act locally within individual MGi or globally throughout the whole MB calyx. Local inhibition of individual MGi could potentially explain the sparse coding mechanism of KCs.

4.1.3 Comparison with previous EM studies of the MG complex

Previous EM studies mentioned that within the MG complex small profiles with clear free of vesicle cytoplasm are exclusively KCs (Butcher et al. 2012). In our data set we find that such small profiles can also belong to postsynaptic sites of APL and MB-C1. Bigger profiles are only presynaptic to the bouton and belong to APL, MB-C1 and the two γmain KCs, which do not form postsynaptic claws around the bouton. Another criterion for identifying ENs was based on a sparsely filled cytoplasm not seen in PN profiles (Yasuyama, Meinertzhagen, and Schurmann 2002), which in our EM data set does not become obvious.

In our reconstruction we were able to associate every synaptic cleft with a T-bar. This is in contrast to previous EM studies, which reported two types of AZ, with ribbon and without T-bar ribbons (Leiss et al. 2009; Butcher et al. 2012). However, these studies utilized EM data sets of thicker sections with 50 nm (Leiss et al. 2009) or 1-2 µm (Butcher et al. 2012) thickness, whereas the data set generated in the Bock laboratory consists of 35-40 nm thick sections (Zheng et al. 2018). Studies describing the AZ in Drosophila report that the mean Bruchpilot (Brp) ring diameter of the T-bar in the in the MB calyx is between 160 nm to 190 nm (Gupta et al. 2016), and has a height of 98 ± 26 nm in the neuromuscular junctions (NMJ), measured between the BRP C terminus and DRBP C terminus (Liu et al. 2011). Thus, it might be possible that previous studies missed T-bar specializations due to section thickness.

Overall, our reconstruction of a MG suggests a complex microcircuit within the calyx that includes feedforward and feedback pathways between multiple neuron types. The circuitry includes cholinergic excitatory neurons and GABAergic inhibitory neurons. These microcircuits could potentially modulate and compute olfactory processing and memory formation in the MB calyx.

4.2 Rewiring upon LTM in the MB calyx

Much evidence indicates that the formation of LTM involves enduring alteration of synaptic responses to the learned stimulus. These changes serve memory storage and ensure its retrieval. A central question derived from these observations is, what are the cellular and molecular events that lead to such plastic changes? Here we established an appetitive LTM paradigm in which for the first time pre- and postsynaptic connection are visible and detectible, thus in the future will serve as a model to help answer this question.

4.2.1 Input specific reorganization

In particular, we report that the MB calyx in the adult fly undergoes input-specific pre- and postsynaptic plastic changes during memory consolidation. We successfully trained flies to associate cVA with a sugar reward in a STM and LTM training paradigm. Although, cVA is a sex-pheromone (Datta et al. 2008), we could show that both male and female flies successfully associated cVA with sucrose and showed no significant difference between each other in their learning behavior (Fig. 9). Upon LTM formation, the MGi specifically activated by cVA decreased in volume, but increased in number. When flies were trained with Ga or in an unpaired control, the cVA specific MGi did not undergo these changes. Similarly, we did not find these changes when flies were trained in a STM paradigm with cVA, Ga or in an unpaired control (Fig. 10).

The current model for associative learning in the fruit fly is based on the compartmentalization of the MB and the finding that the synaptic connections between KC axons and MBONs in MB lobes are weakened by presynaptic depression upon the release of Dopamine by DANs. An odor activates a specific subset of KCs and an US activates either reward or punishment coding DANs. The reward coding DANs alter the synaptic connections between KCs and avoidance driving MBONs, whereas the punishment coding DANs act on the connections between KCs and approach promoting MBONs. Thus, the balance of the network is shifted in favor of either avoidance or approach behavior (Aso, Sitaraman, et al. 2014; Bouzaiane et al. 2015; Cohn, Morantte, and Ruta 2015; Hige et al. 2015; Owald and Waddell 2015; Perisse et al. 2016; Cognigni, Felsenberg, and Waddell 2018) (see also chapter 1.5 and Fig. 3). Furthermore, the activation of KCs by odor is regulated through sparse coding, as only a restricted number of approximately 5% of KCs respond to odor stimulation independently of the number of activated PNs (Perez-Orive et al. 2002; Honegger, Campbell, and Turner 2011; Turner, Bazhenov, and Laurent 2008). In addition, the spatial organization of the MB calyx suggests that different KC subtypes

predominantly, yet not exclusively, occupy specific zones (Lin et al. 2007), as do PNs (Lin et al. 2007; Seki et al. 2017; Zheng et al. 2018).

By considering these three hypotheses, our findings in the study presented here can be interpreted as follows. LTM formation leads to rewiring of the MB calyx circuitry. As the number of boutons increases, the size of MGi decreases. This presumably suggests that each bouton would have less KC claws on average and, thus, leading to the reduction in MGi size. If the number of odor activated KCs remains the same, sparse coding should thus not be affected. Yet, the smaller number of KC claws could indicate a refinement of the odor specific KC code with more odor specific PN boutons projecting onto a specific subtype of KCs. In other words, new specific KCs could be recruited. This would lead to a more distinct representation of the memory in the MB lobes and in the different output behavior compartments. This drastic rearrangement of odor representation in the MB input site is further supported by findings in the lip region of the MB calyx in honey bee, *Apis mellifera*. Here, new experience and learning leads to an increase in the number of MGi (Krofczik et al. 2008; Hourcade et al. 2010) (see also chapter 1.7.2). In addition, functional imaging of KCs in the lip region of the honey bee calyx suggests that KCs are either specifically recruited or eliminated from responding during odor learning (Szyszka, Galkin, and Menzel 2008).

Altogether, the here presented data suggest structural reorganization of pre- and postsynaptic partners upon LTM formation in the MB calyx. The changes are specific to the odor stimulated MGi, hence activity dependent. The data are consistent with findings in honey bees and ants (Krofczik et al. 2008; Hourcade et al. 2010; Stieb et al. 2010; Szyszka, Galkin, and Menzel 2008; Szyszka et al. 2011).

4.3 Optogenetic PN stimulation in a LTM paradigm

To investigate whether the structural plastic changes with LTM formation in the PNs is specific to the cVA conditioning paradigm or can be universally applied to PN-KC connections, we tried to establish an alternative conditioning paradigm. Moreover, in order to deliver cVA to the fly, it has to be diluted in a carrier, here ethanol (EtOH), which itself activates KCs. Also, cVA is a sex pheromone that activates a sexually dimorphic circuit (Datta et al. 2008) and has a strong biological significance to flies (Bartelt, Schaner, and Jackson 1985). However, we did not find difference between males and females in our appetitive conditioning paradigm with cVA (Fig. 9C).

Due to a missing additional PN-driver line that could be specifically activated by odor stimulation and that assures a convergence in function and structure, we explored the possibility of artificially substituting the odor stimulation. Similar approaches to manipulate the neurons of the olfactory perception system and influence the behavior of flies have been reported before, e.g. by using thermogenetic activation with the transient receptor potential cation channel A 1 (TRPA1) in KCs (Vasmer et al. 2014) and the dopaminergic PAM cluster (Aso et al. 2010), or optogenetic activity in dopaminergic PPL1 neurons (Riemensperger, Kittel, and Fiala 2016), in KCs (Lyutova et al. 2019), and in a MBON (Konig et al. 2019). Yet to date, nobody has reported a light-induced memory by simulating artificially the olfactory input into the MB, the PNs.

Our tool of choice was Cs-ChrimsonR, because it is a red-shifted version of the channelrhodopsin family, with an excitation peak at 617nm (Klapoetke et al. 2014). The shift to the red spectrum is of great importance, as flies cannot see red light (Klapoetke et al. 2014; Salcedo et al. 1999). Moreover, red light is able to pass through the cuticula (also known as exoskeleton) around the head. Cs-ChrimsonR has sufficient light sensitivity and stability to be activated by the red light passing through the cuticula and depolarize central brain neurons (Klapoetke et al. 2014).

4.3.1 Induction of memory formation by optogenetic activation of PNs could not be demonstrated

For this purpose, groups of flies were trained by pairing a sugar reward with the optogenetic stimulation of PNs. To test memory formation, a set-up in which flies can choose between two halves of a place choice arena was designed. Trained flies were expected to show greater preference over time for the red illuminated half over the other not illuminated half. Unpaired control flies were expected to distribute randomly. We tested

several different training protocols, which included different levels of starvation to motivate the flies to learn, refeeding, and space training. We also tested different test situations, in which either one half was permanently illuminated for the duration of testing, or the arena was illuminated with red light alternating between the two halves. However, the different protocols could not unquestionably proof memory formation. Neither did the flies show significant preference scores, nor did the evaluation of MB calyces show an increase in MGi.

One reason why the optogenetic conditioning paradigm was not successful could be the lack of day light. Fruit flies are diurnal (active during daytime) animals and rhythmic light-dark cycles have been proven to significantly impact animal behavior and physiology. Light acts as a powerful modulator of different brain functions, such as circadian rhythm, hormone secretion, and various cognitive functions. Just recently, a study could show elegantly that LTM was severely impaired in flies kept in constant darkness. The impairment was independent of stress reactions and sleep deprivation, thus the experimenters suggest that LTM is light-dependent (Inami et al. 2020). Furthermore, in fruit flies, environmental light activates photoreceptors in a set of brain neurons expressing a neuropeptide called Pigment-dispersing factor (Pdf) and increases their spontaneous firing rate (Sheeba et al. 2008; Fogle et al. 2011; Ni et al. 2017). Pdf neurons play a critical role in LTM maintenance, as Pdf reactivates the memory modulator CREB (cAMP response element-binding protein), which is essential for LTM maintenance (Inami et al. 2020). Taken together, Drosophila has a light-dependent memory maintenance system regulated by Pdf signaling (Inami et al. 2020). In our optogenetic conditioning experiment, flies were kept in constant darkness to avoid unnecessary light stimulated activation of PNs. This is essential for two reasons. First, uncontrolled light exposure stimulates the PNs and could lead to forming unwanted associations that could compete with the wanted trained stimulus. Second, flies have to be kept in darkness to avoid the extinction of the trained associative memory. Repeated exposure of the trained CS without the expected biological significant US, reduces the behavioral response of the animal through a process called extinction learning (Bouton 2004; Felsenberg et al. 2018). However, in a control experiment, we tested flies expressing *UAS-Cs-ChrimsonR* in the PN subset SS01867 kept in constant darkness in the well-established odor paradigm. Although, never been exposed to light, these flies showed strong learning scores (Fig. 11C).

Another point to consider is that we used a defined set of PNs, namely 12 cells of the DA1, DL1 and DM2 AL glomeruli. The number of cells might not have been sufficient enough. A previous study investigated, if flies can learn any input pattern into the MB, irrespective of the exact identity of the activated PNs, exact odor representation, or of symmetry between the hemispheres. Here, the experimenters expressed the thermogenetic tool TRPA1 in

random sets of PNs. Afterwards flies were trained in an aversive STM paradigm, in which heat activation of TRPA1 was paired with an electric shock. Flies were only successfully performing, if the number of TRAP1 expressing PNs was greater than 31 cells. Lower numbers were not sufficient enough (Warth Perez Arias et al. 2020). This is almost three times more cells artificially activated than we could activate in our flies. Thus, creating new splitGAL4 lines that label a number of greater than 31 cells, but still only drive expression in PNs could potentially evoke memory formation upon optogenetic activation.

4.4 The GABAergic Mushroom body neuron 1

In our MG reconstruction, we identified next to KCs, PN and APL also MB-C1 as a component of the circuitry. Two MB-C1 neurons per hemisphere exist. They extend branches out into the LH and project onwards to the MB calyx, where they arborize excessively. To our surprise, up to now MB-C1 has been overlooked and no studies have been performed. Meanwhile, the connections between LH and the MB have caught more interest eventually. Some findings suggest that the MB also contributes to innate behavior and, vice versa, LH odor processing contributes to olfactory learning in the MB (Dolan et al. 2018; Dolan et al. 2019; Lewis et al. 2015; Tsao et al. 2018; Bates 2020). Consequently, investigating MB-C1 could add new information to the understanding of odor processing in the MB calyx.

4.4.1 Morphology of MB-C1

We identified MB-C1 as a GABAergic neuron and demonstrated by means of our EM reconstruction and with genetic markers to be pre- and postsynaptic in its target areas, LH and MB calyx. Whereas MB-C1 is innervating the whole main calyx, the innervation into the LH is limited to the ventral area. This restricted LH innervation was further confirmed by a recent study, which systematically mapped the LH with its intrinsic and extrinsic neurons by generating a large splitGAL4 driver line collection (Dolan et al. 2019). The LH is subdivided into a ventral and a dorsal region, with the ventral region suggested to be predominantly responsible for promoting innate behavior for aversive odors (Seki et al. 2017). MB-C1 may thus act to normalize, *e.g.* to synchronize, the activity between the MB calyx and the ventral LH region. This scenario would further suggest an additional separated processing step of aversive and attractive odors. Either the dorsal region of the LH, which represents the innate attractive behavior (Seki et al. 2017), is not normalized with the MB calyx, or normalizing could be promoted by a separate neuronal circuit. Another interpretation of the MB-C1 connectivity could be that MB-C1 is important for integrating aversive odor processing of the LH into the MB, or conversely, the odor processing in the MB can influence the information processing in the LH.

4.4.2 Blocking MB-C1

By expressing *UAS-Shibire^{ts}* in MB-C1, we blocked synaptic output at a temperature of 31°C. This led to a significant reduced innate avoidance behavior towards the aversive odors Oct

and MCH. Conversely, innate attraction behavior to the odor of vinegar was not affected. Furthermore, blocking MB-C1 synaptic output interfered with the positive association of Oct and MCH with a positive sugar reward in a STM paradigm. To investigate, if either learning or memory retrieval is affected by the suppression of MB-C1 synaptic output, we utilized a MTM paradigm. Thus, we were able to block MB-C1 during training and testing of memory separately. Here, blocking during learning did not show a significant affect, whereas blocking during memory retrieval inhibited the association between an aversive odor and a positive sugar reward. These findings suggest the above mentioned scenario, in which MB-C1 is promoting the integration of the innate aversive information of the odor into the MB. When MB-C1 is blocked during testing, the flies might lack the innate information or the integration is disrupted. In order for the fly to perform an accurate response to the trained odor, the fly has potentially to compare the innate odor processing in the LH with the newly learned information. More precisely, this would mean in our conditioning paradigm that the naive representation of the aversive odor is essential to recall the learned positive association with the reward.

However, neither the innate nor the conditioned behavior could be reproduced by specifically knocking down the expression of GABA or AMON in MB-C1, nor did cell specific apoptosis of MB-C1. The temperature dependency of *UAS-Shibire*^{ts} has certainly its disadvantage, because the internal temperature of flies varies considerably with the outside temperature. Therefore, an unambiguous and final conclusion about the function of MB-C1 cannot be drawn, yet.

How innate and learned behaviors are interacting with each other is still not known sufficiently, yet. Therefore, further investigation of these connections is certainly of great importance for the understanding of learning in general.

5 Statement of Contributions

Statement for: 3.1 Microglomerulus reconstruction

Task	Names
Conceptualization	Philipp Ranft, Gaia Tavosanis, Davi Bock
Methodology	Philipp Ranft, Gaia Tavosanis, Davi Bock
Formal analysis	Philipp Ranft, Gaia Tavosanis, Davi Bock
Investigation	Philipp Ranft
Proof reading of neuron tracing	Scott Lauritzen, Feng Li, Steven A. Calle-Schuler, Lucia Kmecova, Iqbal J. Ali, Nadiya Sharifi, Corey B. Fisher, Benjamin Gorko, Najila Masoodpanah, Joseph Hsu
Resources and funding acquisition	Gaia Tavosanis, Davi Bock
Supervision	Gaia Tavosanis

Statement for: 3.2 Pre- and postsynaptic structural plasticity in the MB calyx

Task	Names
Conceptualization	Lothar Baltruschat, Gaia Tavosanis
Methodology	Lothar Baltruschat, Gaia Tavosanis
Formal analysis	Philipp Ranft, Lothar Baltruschat, Gaia Tavosanis
Investigation	Philipp Ranft, Lothar Baltruschat
Software	Christoph Möhl
Resources and supervision	Gaia Tavosanis

Statement for: 3.3 Appetitive conditioning with optogenetic stimulation

Task	Names
Conceptualization	Philipp Ranft, Gaia Tavosanis
Methodology	Philipp Ranft, Gaia Tavosanis
Formal analysis	Philipp Ranft, Gaia Tavosanis
Behavioral experiments	Philipp Ranft
Place choice arena	Philipp Ranft, Lothar Baltruschat
Image acquisition and analysis	Philipp Ranft, Luigi Prisco
Resources and supervision	Gaia Tavosanis

Statement for: 3.4 Characterizing the MB calyx innervating neuron MB-C1

Task	**Names**
Conceptualization	Philipp Ranft, Gaia Tavosanis
Methodology	Philipp Ranft, Gaia Tavosanis
Formal analysis	Philipp Ranft, Gaia Tavosanis
Investigation	Philipp Ranft
Resources and supervision	Gaia Tavosanis

6 Acronyms

°C	degrees Celsius
#	number
αβ KC	alpha beta subtype of Kenyon cells
α'β' KC	alpha prime beta prime subtype of Kenyon cells
γ KC	gama subtype of Kenyon cells
3D	three-dimensional
Ach	Acetylcholine
AL	Antennal lobe
ANOVA	analysis of variance
AMON	Prohormone convertase 2, *amontillado*
APL	Anterior paired lateral neuron
AZ	Active zone
Brp	Bruchpilot
CREB	cAMP response element-binding protein
CG	Calycal giant neuron
CNS	Central nervous system
CS	Conditioned stimulus
CS+	odorant paired with sucrose
CS-	odorant not paired with sucrose
Cs-ChrimsonR	light-gated cation channelrhodopsin, excitation 617nm
cVA	11-cis-Vaccenyl acetate
DA1	Dorso-anterior glomerulus 1 of the adult antennal lobe
DAN	Dopaminergic neuron
DL1	Dorso-lateral glomerulus 1 of the adult antennal lobe
DL3	Dorso-lateral glomerulus 3 of the adult antennal lobe
DM2	Dorso-medial glomerulus 2 of the adult antennal lobe
DRBP	Drosophila Rab3-interacting molecule binding protein
eGFP	enhanced Green-fluorescent protein
EM	Electron microscopy
EN	Extrinsic neuron
EtOH	Ethanol
FAFB	Female Adult Fly Brain

Ga	Geranyl acetate
GABA	γ-Aminobutyric acid
GAD1	glutamic acid decarboxylase 1
GAL4	Galactose-responsive transcription factor
GFP	Green-fluorescent protein
GRASP	GFP-reconstitution across synaptic partners
hid	*head involution defective* gene
KC	Kenyon cell
LH	Lateral horn
LED	Light-emitting diode
LexA	real name of a DNA binding protein
LexAop	LexA DNA-binding sequence
LM	Light microscopy
LTM	Long-term memory
mALT	medial antennal lobe tract
MB	Mushroom body
MB-C1	Mushroom body calyx neuron 1
MBON	Mushroom body output neuron
MCH	4-methylcyclohexanol
MDN	moonwalk descending neuron
MG	Microglomerulus
MGi	Microglomeruli, plural of MG
MTM	Mid-term memory
NMJ	Neuromuscular junctions
OAN	Octopaminergic neuron
Oct	3-Octanol
OSN	Olfactory sensory neuron
PAM	DANs innervating MB lobes, coding for reward
PBS	Phosphate buffered saline
Pdf	Pigment-dispersing factor
PI	Preference index
PN	Projection neuron
PPL1	DANs innervating MB lobes, coding for punishment
PSD	Postsynaptic density zone
RNA	Ribonucleic acid
RNAi	Ribonucleic acid (RNA) interference

rpr	*reaper* gene
sec	seconds
Shi^{ts}	Temperature-sensitive Shibire
splitGAL4	driver line with GAL4 coding region split between two enhancer
ssTEM	serial section transmission electron microscopy
STM	Short-term memory
t	time
tdT	tandem dimer Tomato fluorescent protein
TRPA1	Transient receptor potential cation channel, A 1
UAS	Upstream activating sequence
US	Unconditioned stimulus

7 References

Amin, H., and A. C. Lin. 2019. 'Neuronal mechanisms underlying innate and learned olfactory processing in Drosophila', *Curr Opin Insect Sci*, 36: 9-17.

Aso, Y., D. Hattori, Y. Yu, R. M. Johnston, N. A. Iyer, T. T. Ngo, H. Dionne, L. F. Abbott, R. Axel, H. Tanimoto, and G. M. Rubin. 2014. 'The neuronal architecture of the mushroom body provides a logic for associative learning', *Elife*, 3: e04577.

Aso, Y., and G. M. Rubin. 2016. 'Dopaminergic neurons write and update memories with cell-type-specific rules', *Elife*, 5.

Aso, Y., D. Sitaraman, T. Ichinose, K. R. Kaun, K. Vogt, G. Belliart-Guerin, P. Y. Placais, A. A. Robie, N. Yamagata, C. Schnaitmann, W. J. Rowell, R. M. Johnston, T. T. Ngo, N. Chen, W. Korff, M. N. Nitabach, U. Heberlein, T. Preat, K. M. Branson, H. Tanimoto, and G. M. Rubin. 2014. 'Mushroom body output neurons encode valence and guide memory-based action selection in Drosophila', *Elife*, 3: e04580.

Aso, Y., I. Siwanowicz, L. Bracker, K. Ito, T. Kitamoto, and H. Tanimoto. 2010. 'Specific dopaminergic neurons for the formation of labile aversive memory', *Curr Biol*, 20: 1445-51.

Bailey, C. H., D. Bartsch, and E. R. Kandel. 1996. 'Toward a molecular definition of long-term memory storage', *Proc Natl Acad Sci U S A*, 93: 13445-52.

Bartelt, R. J., A. M. Schaner, and L. L. Jackson. 1985. 'cis-Vaccenyl acetate as an aggregation pheromone inDrosophila melanogaster', *J Chem Ecol*, 11: 1747-56.

Bates, A. S.; Schlegel, P.; et al. 2020. 'Complete connectomic reconstruction of olfactory projection neurons in the fly brain', *Biorxiv*.

Benton, R., K. S. Vannice, C. Gomez-Diaz, and L. B. Vosshall. 2009. 'Variant ionotropic glutamate receptors as chemosensory receptors in Drosophila', *Cell*, 136: 149-62.

Bhandawat, V., S. R. Olsen, N. W. Gouwens, M. L. Schlief, and R. I. Wilson. 2007. 'Sensory processing in the Drosophila antennal lobe increases reliability and separability of ensemble odor representations', *Nat Neurosci*, 10: 1474-82.

Bidaye, S. S., C. Machacek, Y. Wu, and B. J. Dickson. 2014. 'Neuronal control of Drosophila walking direction', *Science*, 344: 97-101.

Bouton, M. E. 2004. 'Context and behavioral processes in extinction', *Learn Mem*, 11: 485-94.

Bouzaiane, E., S. Trannoy, L. Scheunemann, P. Y. Placais, and T. Preat. 2015. 'Two independent mushroom body output circuits retrieve the six discrete components of Drosophila aversive memory', *Cell Rep*, 11: 1280-92.

Brand, A. H., and N. Perrimon. 1993. 'Targeted gene expression as a means of altering cell fates and generating dominant phenotypes', *Development*, 118: 401-15.

Burke, C. J., W. Huetteroth, D. Owald, E. Perisse, M. J. Krashes, G. Das, D. Gohl, M. Silies, S. Certel, and S. Waddell. 2012. 'Layered reward signalling through octopamine and dopamine in Drosophila', *Nature*, 492: 433-7.

Busch, S., M. Selcho, K. Ito, and H. Tanimoto. 2009. 'A map of octopaminergic neurons in the Drosophila brain', *J Comp Neurol*, 513: 643-67.

Butcher, N. J., A. B. Friedrich, Z. Lu, H. Tanimoto, and I. A. Meinertzhagen. 2012. 'Different classes of input and output neurons reveal new features in microglomeruli of the adult Drosophila mushroom body calyx', *J Comp Neurol*, 520: 2185-201.

Cardona, A., S. Saalfeld, J. Schindelin, I. Arganda-Carreras, S. Preibisch, M. Longair, P. Tomancak, V. Hartenstein, and R. J. Douglas. 2012. 'TrakEM2 software for neural circuit reconstruction', *PLoS One*, 7: e38011.

Caron, S. J., V. Ruta, L. F. Abbott, and R. Axel. 2013. 'Random convergence of olfactory inputs in the Drosophila mushroom body', *Nature*, 497: 113-7.

Chen, C. C., J. K. Wu, H. W. Lin, T. P. Pai, T. F. Fu, C. L. Wu, T. Tully, and A. S. Chiang. 2012. 'Visualizing long-term memory formation in two neurons of the Drosophila brain', *Science*, 335: 678-85.

Chiang, A. S., C. Y. Lin, C. C. Chuang, H. M. Chang, C. H. Hsieh, C. W. Yeh, C. T. Shih, J. J. Wu, G. T. Wang, Y. C. Chen, C. C. Wu, G. Y. Chen, Y. T. Ching, P. C. Lee, C. Y. Lin, H. H. Lin, C. C. Wu, H. W. Hsu, Y. A. Huang, J. Y. Chen, H. J. Chiang, C. F. Lu, R. F. Ni, C. Y. Yeh, and J. K. Hwang. 2011. 'Three-dimensional reconstruction of brain-wide wiring networks in Drosophila at single-cell resolution', *Curr Biol*, 21: 1-11.

Christiansen, F., C. Zube, T. F. Andlauer, C. Wichmann, W. Fouquet, D. Owald, S. Mertel, F. Leiss, G. Tavosanis, A. J. Luna, A. Fiala, and S. J. Sigrist. 2011. 'Presynapses in Kenyon cell dendrites in the mushroom body calyx of Drosophila', *J Neurosci*, 31: 9696-707.

Claridge-Chang, A., R. D. Roorda, E. Vrontou, L. Sjulson, H. Li, J. Hirsh, and G. Miesenbock. 2009. 'Writing memories with light-addressable reinforcement circuitry', *Cell*, 139: 405-15.

Cognigni, P., J. Felsenberg, and S. Waddell. 2018. 'Do the right thing: neural network mechanisms of memory formation, expression and update in Drosophila', *Curr Opin Neurobiol*, 49: 51-58.

Cohn, R., I. Morantte, and V. Ruta. 2015. 'Coordinated and Compartmentalized Neuromodulation Shapes Sensory Processing in Drosophila', *Cell*, 163: 1742-55.

Costa, M., J. D. Manton, A. D. Ostrovsky, S. Prohaska, and G. S. Jefferis. 2016. 'NBLAST: Rapid, Sensitive Comparison of Neuronal Structure and Construction of Neuron Family Databases', *Neuron*, 91: 293-311.

Couto, A., M. Alenius, and B. J. Dickson. 2005. 'Molecular, anatomical, and functional organization of the Drosophila olfactory system', *Curr Biol*, 15: 1535-47.

Crittenden, J. R., E. M. Skoulakis, K. A. Han, D. Kalderon, and R. L. Davis. 1998. 'Tripartite mushroom body architecture revealed by antigenic markers', *Learn Mem*, 5: 38-51.

Datta, S. R., M. L. Vasconcelos, V. Ruta, S. Luo, A. Wong, E. Demir, J. Flores, K. Balonze, B. J. Dickson, and R. Axel. 2008. 'The Drosophila pheromone cVA activates a sexually dimorphic neural circuit', *Nature*, 452: 473-7.

Davis, R. L. 2011. 'Traces of Drosophila memory', *Neuron*, 70: 8-19.

de Belle, J. S., and M. Heisenberg. 1994. 'Associative odor learning in Drosophila abolished by chemical ablation of mushroom bodies', *Science*, 263: 692-5.

de Bruyne, M., P. J. Clyne, and J. R. Carlson. 1999. 'Odor coding in a model olfactory organ: the Drosophila maxillary palp', *J Neurosci*, 19: 4520-32.

de Bruyne, M., K. Foster, and J. R. Carlson. 2001. 'Odor coding in the Drosophila antenna', *Neuron*, 30: 537-52.

Dolan, M. J., G. Belliart-Guerin, A. S. Bates, S. Frechter, A. Lampin-Saint-Amaux, Y. Aso, R. J. V. Roberts, P. Schlegel, A. Wong, A. Hammad, D. Bock, G. M. Rubin, T. Preat, P. Y. Placais, and Gsxe Jefferis. 2018. 'Communication from Learned to Innate Olfactory Processing Centers Is Required for Memory Retrieval in Drosophila', *Neuron*, 100: 651-68 e8.

Dolan, M. J., S. Frechter, A. S. Bates, C. Dan, P. Huoviala, R. J. Roberts, P. Schlegel, S. Dhawan, R. Tabano, H. Dionne, C. Christoforou, K. Close, B. Sutcliffe, B. Giuliani, F. Li, M. Costa, G. Ihrke, G. W. Meissner, D. D. Bock, Y. Aso, G. M. Rubin, and G. S. Jefferis. 2019. 'Neurogenetic dissection of the Drosophila lateral horn reveals major outputs, diverse behavioural functions, and interactions with the mushroom body', *Elife*, 8.

Dubnau, J., L. Grady, T. Kitamoto, and T. Tully. 2001. 'Disruption of neurotransmission in Drosophila mushroom body blocks retrieval but not acquisition of memory', *Nature*, 411: 476-80.

Dujardin, F. 1850. 'Mémoire sur le système nerveux des insectes', *Ann Sci Nat Zool*, 14: 195-206.

Eichler, K., F. Li, A. Litwin-Kumar, Y. Park, I. Andrade, C. M. Schneider-Mizell, T. Saumweber, A. Huser, C. Eschbach, B. Gerber, R. D. Fetter, J. W. Truman, C. E. Priebe, L. F. Abbott, A. S. Thum, M. Zlatic, and A. Cardona. 2017. 'The complete connectome of a learning and memory centre in an insect brain', *Nature*, 548: 175-82.

Felsenberg, J., P. F. Jacob, T. Walker, O. Barnstedt, A. J. Edmondson-Stait, M. W. Pleijzier, N. Otto, P. Schlegel, N. Sharifi, E. Perisse, C. S. Smith, J. S. Lauritzen, M. Costa, Gsxe Jefferis, D. D. Bock, and S. Waddell. 2018. 'Integration of Parallel Opposing Memories Underlies Memory Extinction', *Cell*, 175: 709-22 e15.

Fisek, M., and R. I. Wilson. 2014. 'Stereotyped connectivity and computations in higher-order olfactory neurons', *Nat Neurosci*, 17: 280-8.

Fishilevich, E., and L. B. Vosshall. 2005. 'Genetic and functional subdivision of the Drosophila antennal lobe', *Curr Biol*, 15: 1548-53.

Fogle, K. J., K. G. Parson, N. A. Dahm, and T. C. Holmes. 2011. 'CRYPTOCHROME is a blue-light sensor that regulates neuronal firing rate', *Science*, 331: 1409-13.

Frechter, S., A. S. Bates, S. Tootoonian, M. J. Dolan, J. Manton, A. R. Jamasb, J. Kohl, D. Bock, and G. Jefferis. 2019. 'Functional and anatomical specificity in a higher olfactory centre', *Elife*, 8.

Ganeshina, O., and R. Menzel. 2001. 'GABA-immunoreactive neurons in the mushroom bodies of the honeybee: an electron microscopic study', *J Comp Neurol*, 437: 335-49.

Gill, J., Y. Park, J. P. McGinnis, C. Perez-Sanchez, M. Blanchette, and K. Si. 2017. 'Regulated Intron Removal Integrates Motivational State and Experience', *Cell*, 169: 836-48 e15.

Grabe, V., A. Strutz, A. Baschwitz, B. S. Hansson, and S. Sachse. 2015. 'Digital in vivo 3D atlas of the antennal lobe of Drosophila melanogaster', *J Comp Neurol*, 523: 530-44.

Grether, M. E., J. M. Abrams, J. Agapite, K. White, and H. Steller. 1995. 'The head involution defective gene of Drosophila melanogaster functions in programmed cell death', *Genes Dev*, 9: 1694-708.

Gruntman, E., and G. C. Turner. 2013. 'Integration of the olfactory code across dendritic claws of single mushroom body neurons', *Nat Neurosci*, 16: 1821-9.

Gupta, V. K., U. Pech, A. Bhukel, A. Fulterer, A. Ender, S. F. Mauermann, T. F. Andlauer, E. Antwi-Adjei, C. Beuschel, K. Thriene, M. Maglione, C. Quentin, R. Bushow, M. Schwarzel, T. Mielke, F. Madeo, J. Dengjel, A. Fiala, and S. J. Sigrist. 2016. 'Spermidine Suppresses Age-Associated Memory Impairment by Preventing Adverse Increase of Presynaptic Active Zone Size and Release', *PLoS Biol*, 14: e1002563.

Hallem, E. A., and J. R. Carlson. 2006. 'Coding of odors by a receptor repertoire', *Cell*, 125: 143-60.

Heimbeck, G., V. Bugnon, N. Gendre, A. Keller, and R. F. Stocker. 2001. 'A central neural circuit for experience-independent olfactory and courtship behavior in Drosophila melanogaster', *Proc Natl Acad Sci U S A*, 98: 15336-41.

Heisenberg, M., A. Borst, S. Wagner, and D. Byers. 1985. 'Drosophila mushroom body mutants are deficient in olfactory learning', *J Neurogenet*, 2: 1-30.

Herculano-Houzel, S. 2009. 'The human brain in numbers: a linearly scaled-up primate brain', *Front Hum Neurosci*, 3: 31.

Hige, T., Y. Aso, M. N. Modi, G. M. Rubin, and G. C. Turner. 2015. 'Heterosynaptic Plasticity Underlies Aversive Olfactory Learning in Drosophila', *Neuron*, 88: 985-98.

Honegger, K. S., R. A. Campbell, and G. C. Turner. 2011. 'Cellular-resolution population imaging reveals robust sparse coding in the Drosophila mushroom body', *J Neurosci*, 31: 11772-85.

Hourcade, B., T. S. Muenz, J. C. Sandoz, W. Rossler, and J. M. Devaud. 2010. 'Long-term memory leads to synaptic reorganization in the mushroom bodies: a memory trace in the insect brain?', *J Neurosci*, 30: 6461-5.

Hu, A., W. Zhang, and Z. Wang. 2010. 'Functional feedback from mushroom bodies to antennal lobes in the Drosophila olfactory pathway', *Proc Natl Acad Sci U S A*, 107: 10262-7.

Inami, S., S. Sato, S. Kondo, H. Tanimoto, T. Kitamoto, and T. Sakai. 2020. 'Environmental light is required for maintenance of long-term memory in Drosophila', *J Neurosci*.

J. Erber, TH. Masuhr, R. Menzel. 1980. 'Localization of short-term memory in the brain of the bee, Apis mellifera', *Physiological Entomology*, 5: 343-58.

Jeanne, J. M., M. Fisek, and R. I. Wilson. 2018. 'The Organization of Projections from Olfactory Glomeruli onto Higher-Order Neurons', *Neuron*, 98: 1198-213 e6.

Jefferis, G. S., C. J. Potter, A. M. Chan, E. C. Marin, T. Rohlfing, C. R. Maurer, Jr., and L. Luo. 2007. 'Comprehensive maps of Drosophila higher olfactory centers: spatially segregated fruit and pheromone representation', *Cell*, 128: 1187-203.

Kitamoto, T. 2001. 'Conditional modification of behavior in Drosophila by targeted expression of a temperature-sensitive shibire allele in defined neurons', *J Neurobiol*, 47: 81-92.

———. 2002a. 'Conditional disruption of synaptic transmission induces male-male courtship behavior in Drosophila', *Proc Natl Acad Sci U S A*, 99: 13232-7.

———. 2002b. 'Targeted expression of temperature-sensitive dynamin to study neural mechanisms of complex behavior in Drosophila', *J Neurogenet*, 16: 205-28.

Kittel, R. J., C. Wichmann, T. M. Rasse, W. Fouquet, M. Schmidt, A. Schmid, D. A. Wagh, C. Pawlu, R. R. Kellner, K. I. Willig, S. W. Hell, E. Buchner, M. Heckmann, and S. J. Sigrist. 2006. 'Bruchpilot promotes active zone assembly, Ca2+ channel clustering, and vesicle release', *Science*, 312: 1051-4.

Klapoetke, N. C., Y. Murata, S. S. Kim, S. R. Pulver, A. Birdsey-Benson, Y. K. Cho, T. K. Morimoto, A. S. Chuong, E. J. Carpenter, Z. Tian, J. Wang, Y. Xie, Z. Yan, Y. Zhang, B. Y. Chow, B. Surek, M. Melkonian, V. Jayaraman, M. Constantine-Paton, G. K. Wong, and E. S. Boyden. 2014. 'Independent optical excitation of distinct neural populations', *Nat Methods*, 11: 338-46.

Konig, C., A. Khalili, T. Niewalda, S. Gao, and B. Gerber. 2019. 'An optogenetic analogue of second-order reinforcement in Drosophila', *Biol Lett*, 15: 20190084.

Krashes, M. J., A. C. Keene, B. Leung, J. D. Armstrong, and S. Waddell. 2007. 'Sequential use of mushroom body neuron subsets during drosophila odor memory processing', *Neuron*, 53: 103-15.

Krashes, M. J., and S. Waddell. 2011. 'Drosophila appetitive olfactory conditioning', *Cold Spring Harb Protoc*, 2011: pdb prot5609.

Kremer, M. C., F. Christiansen, F. Leiss, M. Paehler, S. Knapek, T. F. Andlauer, F. Forstner, P. Kloppenburg, S. J. Sigrist, and G. Tavosanis. 2010. 'Structural long-term changes at mushroom body input synapses', *Curr Biol*, 20: 1938-44.

Krofczik, S., U. Khojasteh, N. H. de Ibarra, and R. Menzel. 2008. 'Adaptation of microglomerular complexes in the honeybee mushroom body lip to manipulations of behavioral maturation and sensory experience', *Dev Neurobiol*, 68: 1007-17.

Lai, S. L., and T. Lee. 2006. 'Genetic mosaic with dual binary transcriptional systems in Drosophila', *Nat Neurosci*, 9: 703-9.

Lebreton, S., V. Grabe, A. B. Omondi, R. Ignell, P. G. Becher, B. S. Hansson, S. Sachse, and P. Witzgall. 2014. 'Love makes smell blind: mating suppresses pheromone attraction in Drosophila females via Or65a olfactory neurons', *Sci Rep*, 4: 7119.

Leiss, F., C. Groh, N. J. Butcher, I. A. Meinertzhagen, and G. Tavosanis. 2009. 'Synaptic organization in the adult Drosophila mushroom body calyx', *J Comp Neurol*, 517: 808-24.

Lewis, L. P., K. P. Siju, Y. Aso, A. B. Friedrich, A. J. Bulteel, G. M. Rubin, and I. C. Grunwald Kadow. 2015. 'A Higher Brain Circuit for Immediate Integration of Conflicting Sensory Information in Drosophila', *Curr Biol*, 25: 2203-14.

Lin, A. C., A. M. Bygrave, A. de Calignon, T. Lee, and G. Miesenbock. 2014. 'Sparse, decorrelated odor coding in the mushroom body enhances learned odor discrimination', *Nat Neurosci*, 17: 559-68.

Lin, H. H., J. S. Lai, A. L. Chin, Y. C. Chen, and A. S. Chiang. 2007. 'A map of olfactory representation in the Drosophila mushroom body', *Cell*, 128: 1205-17.

Liu, C., P. Y. Placais, N. Yamagata, B. D. Pfeiffer, Y. Aso, A. B. Friedrich, I. Siwanowicz, G. M. Rubin, T. Preat, and H. Tanimoto. 2012. 'A subset of dopamine neurons signals reward for odour memory in Drosophila', *Nature*, 488: 512-6.

Liu, K. S., M. Siebert, S. Mertel, E. Knoche, S. Wegener, C. Wichmann, T. Matkovic, K. Muhammad, H. Depner, C. Mettke, J. Buckers, S. W. Hell, M. Muller, G. W. Davis, D. Schmitz, and S. J. Sigrist. 2011. 'RIM-binding protein, a central part of the active zone, is essential for neurotransmitter release', *Science*, 334: 1565-9.

Liu, X., and R. L. Davis. 2009. 'The GABAergic anterior paired lateral neuron suppresses and is suppressed by olfactory learning', *Nat Neurosci*, 12: 53-9.

Luo, S. X., R. Axel, and L. F. Abbott. 2010. 'Generating sparse and selective third-order responses in the olfactory system of the fly', *Proc Natl Acad Sci U S A*, 107: 10713-8.

Lyutova, R., M. Selcho, M. Pfeuffer, D. Segebarth, J. Habenstein, A. Rohwedder, F. Frantzmann, C. Wegener, A. S. Thum, and D. Pauls. 2019. 'Reward signaling in a recurrent circuit of dopaminergic neurons and peptidergic Kenyon cells', *Nat Commun*, 10: 3097.

Macpherson, L. J., E. E. Zaharieva, P. J. Kearney, M. H. Alpert, T. Y. Lin, Z. Turan, C. H. Lee, and M. Gallio. 2015. 'Dynamic labelling of neural connections in multiple colours by trans-synaptic fluorescence complementation', *Nat Commun*, 6: 10024.

Mao, Z., and R. L. Davis. 2009. 'Eight different types of dopaminergic neurons innervate the Drosophila mushroom body neuropil: anatomical and physiological heterogeneity', *Front Neural Circuits*, 3: 5.

Marin, E. C., G. S. Jefferis, T. Komiyama, H. Zhu, and L. Luo. 2002. 'Representation of the glomerular olfactory map in the Drosophila brain', *Cell*, 109: 243-55.

Mayseless, O., D. S. Berns, X. M. Yu, T. Riemensperger, A. Fiala, and O. Schuldiner. 2018. 'Developmental Coordination during Olfactory Circuit Remodeling in Drosophila', *Neuron*, 99: 1204-15 e5.

McGuire, S. E., P. T. Le, and R. L. Davis. 2001. 'The role of Drosophila mushroom body signaling in olfactory memory', *Science*, 293: 1330-3.

McGuire, S. E., P. T. Le, A. J. Osborn, K. Matsumoto, and R. L. Davis. 2003. 'Spatiotemporal rescue of memory dysfunction in Drosophila', *Science*, 302: 1765-8.

Menzel, R. 2014. 'The insect mushroom body, an experience-dependent recoding device', *J Physiol Paris*, 108: 84-95.

Nagel, G., T. Szellas, W. Huhn, S. Kateriya, N. Adeishvili, P. Berthold, D. Ollig, P. Hegemann, and E. Bamberg. 2003. 'Channelrhodopsin-2, a directly light-gated cation-selective membrane channel', *Proc Natl Acad Sci U S A*, 100: 13940-5.

Ni, J. D., L. S. Baik, T. C. Holmes, and C. Montell. 2017. 'A rhodopsin in the brain functions in circadian photoentrainment in Drosophila', *Nature*, 545: 340-44.

Nicolai, L. J., A. Ramaekers, T. Raemaekers, A. Drozdzecki, A. S. Mauss, J. Yan, M. Landgraf, W. Annaert, and B. A. Hassan. 2010. 'Genetically encoded dendritic marker sheds light on neuronal connectivity in Drosophila', *Proc Natl Acad Sci U S A*, 107: 20553-8.

Nishino, H., and M. Mizunami. 1998. 'Giant input neurons of the mushroom body: intracellular recording and staining in the cockroach', *Neurosci Lett*, 246: 57-60.

Olsen, S. R., V. Bhandawat, and R. I. Wilson. 2010. 'Divisive normalization in olfactory population codes', *Neuron*, 66: 287-99.

Olsen, S. R., and R. I. Wilson. 2008. 'Lateral presynaptic inhibition mediates gain control in an olfactory circuit', *Nature*, 452: 956-60.

Owald, D., and S. Waddell. 2015. 'Olfactory learning skews mushroom body output pathways to steer behavioral choice in Drosophila', *Curr Opin Neurobiol*, 35: 178-84.

Papadopoulou, M., S. Cassenaer, T. Nowotny, and G. Laurent. 2011. 'Normalization for sparse encoding of odors by a wide-field interneuron', *Science*, 332: 721-5.

Parnas, M., A. C. Lin, W. Huetteroth, and G. Miesenbock. 2013. 'Odor discrimination in Drosophila: from neural population codes to behavior', *Neuron*, 79: 932-44.

Pascual, A., and T. Preat. 2001. 'Localization of long-term memory within the Drosophila mushroom body', *Science*, 294: 1115-7.

Pauls, D. , J. Chen, W. Reiher, J.T. Vanselow, A. Schlosser, J. Kahnt, and C. Wegener. 2014. 'Peptidomics and processing of regulatory peptides in the fruit fly Drosophila', *EuPA OPEN Proteomics*, 3: 114-27.

Pavlov, I. 1927. 'Conditioned reflexes: an investigation of the physiological activity of the cerebral cortex', *Oxford University Press*.

Perez-Orive, J., O. Mazor, G. C. Turner, S. Cassenaer, R. I. Wilson, and G. Laurent. 2002. 'Oscillations and sparsening of odor representations in the mushroom body', *Science*, 297: 359-65.

Perisse, E., D. Owald, O. Barnstedt, C. B. Talbot, W. Huetteroth, and S. Waddell. 2016. 'Aversive Learning and Appetitive Motivation Toggle Feed-Forward Inhibition in the Drosophila Mushroom Body', *Neuron*, 90: 1086-99.

Pfeiffer, B. D., T. T. Ngo, K. L. Hibbard, C. Murphy, A. Jenett, J. W. Truman, and G. M. Rubin. 2010. 'Refinement of tools for targeted gene expression in Drosophila', *Genetics*, 186: 735-55.

Phelps, C. B., and A. H. Brand. 1998. 'Ectopic gene expression in Drosophila using GAL4 system', *Methods*, 14: 367-79.

Pitman, J. L., W. Huetteroth, C. J. Burke, M. J. Krashes, S. L. Lai, T. Lee, and S. Waddell. 2011. 'A pair of inhibitory neurons are required to sustain labile memory in the Drosophila mushroom body', *Curr Biol*, 21: 855-61.

Porter, J. T., C. K. Johnson, and A. Agmon. 2001. 'Diverse types of interneurons generate thalamus-evoked feedforward inhibition in the mouse barrel cortex', *J Neurosci*, 21: 2699-710.

Prokop, A., and I. A. Meinertzhagen. 2006. 'Development and structure of synaptic contacts in Drosophila', *Semin Cell Dev Biol*, 17: 20-30.

Quinn, W. G., W. A. Harris, and S. Benzer. 1974. 'Conditioned behavior in Drosophila melanogaster', *Proc Natl Acad Sci U S A*, 71: 708-12.

Riemensperger, T., R. J. Kittel, and A. Fiala. 2016. 'Optogenetics in Drosophila Neuroscience', *Methods Mol Biol*, 1408: 167-75.

Root, C. M., K. Masuyama, D. S. Green, L. E. Enell, D. R. Nassel, C. H. Lee, and J. W. Wang. 2008. 'A presynaptic gain control mechanism fine-tunes olfactory behavior', *Neuron*, 59: 311-21.

Roy, B., A. P. Singh, C. Shetty, V. Chaudhary, A. North, M. Landgraf, K. Vijayraghavan, and V. Rodrigues. 2007. 'Metamorphosis of an identified serotonergic neuron in the Drosophila olfactory system', *Neural Dev*, 2: 20.

Saalfeld, S., A. Cardona, V. Hartenstein, and P. Tomancak. 2009. 'CATMAID: collaborative annotation toolkit for massive amounts of image data', *Bioinformatics*, 25: 1984-6.

Salcedo, E., A. Huber, S. Henrich, L. V. Chadwell, W. H. Chou, R. Paulsen, and S. G. Britt. 1999. 'Blue- and green-absorbing visual pigments of Drosophila: ectopic expression and physiological characterization of the R8 photoreceptor cell-specific Rh5 and Rh6 rhodopsins', *J Neurosci*, 19: 10716-26.

Schlegel, P., M. J. Texada, A. Miroschnikow, A. Schoofs, S. Huckesfeld, M. Peters, C. M. Schneider-Mizell, H. Lacin, F. Li, R. D. Fetter, J. W. Truman, A. Cardona, and M. J. Pankratz. 2016. 'Synaptic transmission parallels neuromodulation in a central food-intake circuit', *Elife*, 5.

Schultzhaus, J. N., S. Saleem, H. Iftikhar, and G. E. Carney. 2017. 'The role of the Drosophila lateral horn in olfactory information processing and behavioral response', *J Insect Physiol*, 98: 29-37.

Schwaerzel, M., M. Heisenberg, and T. Zars. 2002. 'Extinction antagonizes olfactory memory at the subcellular level', *Neuron*, 35: 951-60.

Seki, Y., H. K. M. Dweck, J. Rybak, D. Wicher, S. Sachse, and B. S. Hansson. 2017. 'Olfactory coding from the periphery to higher brain centers in the Drosophila brain', *BMC Biol*, 15: 56.

Sheeba, V., H. Gu, V. K. Sharma, D. K. O'Dowd, and T. C. Holmes. 2008. 'Circadian- and light-dependent regulation of resting membrane potential and spontaneous action potential firing of Drosophila circadian pacemaker neurons', *J Neurophysiol*, 99: 976-88.

Stieb, S. M., T. S. Muenz, R. Wehner, and W. Rossler. 2010. 'Visual experience and age affect synaptic organization in the mushroom bodies of the desert ant Cataglyphis fortis', *Dev Neurobiol*, 70: 408-23.

Stocker, R. F., G. Heimbeck, N. Gendre, and J. S. de Belle. 1997. 'Neuroblast ablation in Drosophila P[GAL4] lines reveals origins of olfactory interneurons', *J Neurobiol*, 32: 443-56.

Strausfeld, N. J., L. Hansen, Y. Li, R. S. Gomez, and K. Ito. 1998. 'Evolution, discovery, and interpretations of arthropod mushroom bodies', *Learn Mem*, 5: 11-37.

Su, C. Y., K. Menuz, and J. R. Carlson. 2009. 'Olfactory perception: receptors, cells, and circuits', *Cell*, 139: 45-59.

Szyszka, P., C. Demmler, M. Oemisch, L. Sommer, S. Biergans, B. Birnbach, A. F. Silbering, and C. G. Galizia. 2011. 'Mind the gap: olfactory trace conditioning in honeybees', *J Neurosci*, 31: 7229-39.

Szyszka, P., A. Galkin, and R. Menzel. 2008. 'Associative and non-associative plasticity in kenyon cells of the honeybee mushroom body', *Front Syst Neurosci*, 2: 3.

Tanaka, N. K., H. Tanimoto, and K. Ito. 2008. 'Neuronal assemblies of the Drosophila mushroom body', *J Comp Neurol*, 508: 711-55.

Tsao, C. H., C. C. Chen, C. H. Lin, H. Y. Yang, and S. Lin. 2018. 'Drosophila mushroom bodies integrate hunger and satiety signals to control innate food-seeking behavior', *Elife*, 7.

Tully, T., T. Preat, S. C. Boynton, and M. Del Vecchio. 1994. 'Genetic dissection of consolidated memory in Drosophila', *Cell*, 79: 35-47.

Tully, T., and W. G. Quinn. 1985. 'Classical conditioning and retention in normal and mutant Drosophila melanogaster', *J Comp Physiol A*, 157: 263-77.

Turner, G. C., M. Bazhenov, and G. Laurent. 2008. 'Olfactory representations by Drosophila mushroom body neurons', *J Neurophysiol*, 99: 734-46.

Vasmer, D., A. Pooryasin, T. Riemensperger, and A. Fiala. 2014. 'Induction of aversive learning through thermogenetic activation of Kenyon cell ensembles in Drosophila', *Front Behav Neurosci*, 8: 174.

Waddell, S. 2010. 'Dopamine reveals neural circuit mechanisms of fly memory', *Trends Neurosci*, 33: 457-64.

Wagh, D. A., T. M. Rasse, E. Asan, A. Hofbauer, I. Schwenkert, H. Durrbeck, S. Buchner, M. C. Dabauvalle, M. Schmidt, G. Qin, C. Wichmann, R. Kittel, S. J. Sigrist, and E. Buchner. 2006. 'Bruchpilot, a protein with homology to ELKS/CAST, is required for structural integrity and function of synaptic active zones in Drosophila', *Neuron*, 49: 833-44.

Warth Perez Arias, C. C., P. Frosch, A. Fiala, and T. D. Riemensperger. 2020. 'Stochastic and Arbitrarily Generated Input Patterns to the Mushroom Bodies Can Serve as Conditioned Stimuli in Drosophila', *Front Physiol*, 11: 53.

White, K., M. E. Grether, J. M. Abrams, L. Young, K. Farrell, and H. Steller. 1994. 'Genetic control of programmed cell death in Drosophila', *Science*, 264: 677-83.

White, K., E. Tahaoglu, and H. Steller. 1996. 'Cell killing by the Drosophila gene reaper', *Science*, 271: 805-7.

Wu, C. L., M. F. Shih, P. T. Lee, and A. S. Chiang. 2013. 'An octopamine-mushroom body circuit modulates the formation of anesthesia-resistant memory in Drosophila', *Curr Biol*, 23: 2346-54.

Xu, C.S., M. Januszewski, Z. Lu, S. Tamemura, K.J. Hayworth, G. Huang, K. Shinomiya, J. Maitin-Shepard, D. Ackerman, S. Berg, T. Blakely, J. A. Bogovic, J. Clements, T. Dolafi, P. Hubbard, D. Kainmueller, W. Katz, T. Kawase, K.A. Khairy, L. Leavitt, P.H. Li, L. Lindsey, N. Neubarth, D.J. Olbris, H. Otsuna, E.T. Troutman, L. Umayam, T. Zhao, M. Ito, J. Goldammer, T. Wolff, R. Svirskas, P. Schlegel, E.R. Neace, C.J. Knecht, C.X. Alvarado, D.A. Bailey, S. Ballinger, J.A. Borycz, B.S. Canion, N. Cheatham, M. Cook, M. Dreher, O. Duclos, B. Eubanks, K. Fairbanks, S. Finley, N. Forknoll, A. Francis, G.P. Hopkins, E.M. Joyce, S. S. Kim, N.A. Kirk, J. Kovalyak, S.A. Lauchie, A. Lohff, C. Maldonado, E. Manley, S. McLin, C. Mooney, M. Ndama, O. Ogundeyi, N. Okeoma, C. Ordish, N. Padilla, C. Patrick, T. Paterson, E.E. Phillips, E.M. Philips, N. PRampally, C. Ribeiro, M.K. Robertson, J.T. Rymer, S.M. Ryan, M. Sammons, A.K. Scott, A.L. Scott, A. Shinomiya, C. Smith, K. Smith, N.L. Smith, M.A. Sobeski, A. Suleiman, J. Swift, S. Takemura, I. Talebi, D. Tarnogorska, E. Tenshaw, T. Tokhi, J.J. Walsh, T. Yang, J.A. Horne, F. Li, R. Parekh, P.K. Rivlin, V. Jayaraman, K. Ito, S. Saalfeld, R. George, I. Meinertzhagen, G.M. Rubin, H.F. Hess, L.K. Scheffer, V. Jain, and S.M. Plaza. 2020. 'A Connectome of the Adult Drosophila Central Brain', *Biorxiv*.

Yao, C. A., R. Ignell, and J. R. Carlson. 2005. 'Chemosensory coding by neurons in the coeloconic sensilla of the Drosophila antenna', *J Neurosci*, 25: 8359-67.

Yasuyama, K., I. A. Meinertzhagen, and F. W. Schurmann. 2002. 'Synaptic organization of the mushroom body calyx in Drosophila melanogaster', *J Comp Neurol*, 445: 211-26.

Zars, T., M. Fischer, R. Schulz, and M. Heisenberg. 2000. 'Localization of a short-term memory in Drosophila', *Science*, 288: 672-5.

Zheng, Z., J. S. Lauritzen, E. Perlman, C. G. Robinson, M. Nichols, D. Milkie, O. Torrens, J. Price, C. B. Fisher, N. Sharifi, S. A. Calle-Schuler, L. Kmecova, I. J. Ali, B. Karsh, E. T. Trautman, J. A. Bogovic, P. Hanslovsky, Gsxe Jefferis, M. Kazhdan, K. Khairy, S. Saalfeld, R. D. Fetter, and D. D. Bock. 2018. 'A Complete Electron Microscopy Volume of the Brain of Adult Drosophila melanogaster', *Cell*, 174: 730-43 e22.

Zipp, F., R. Nitsch, E. Soriano, and M. Frotscher. 1989. 'Entorhinal fibers form synaptic contacts on parvalbumin-immunoreactive neurons in the rat fascia dentata', *Brain Res*, 495: 161-6.

8 Acknowledgments

This work would not have been possible without the help and support of numerous people. First I would like to thank Prof. Dr. Gaia Tavosanis for her excellent scientific guidance throughout my doctorate. I am very grateful that I had the opportunity to join your lab and for sending me abroad to work on the reconstruction project. Of course, I would also like to thank the whole Tavosanis lab for your help and support.

Secondly, I would like to thank Dr. Davi Bock and his lab members for the collaboration on the EM reconstruction and letting me work in your lab in Janelia.

I thank Prof. Dr. Michael Pankratz for acting as my second referee and Prof. Dr. Gerhard von der Emde and Prof. Dr. Peter Vöhringer for participating in the PhD committee.

A very special thank you goes to my family. Especially, thank you to my parents and siblings for your support and for being my role models.

Finally, I would like to say thank you to all the people that supported me over the years of my PhD in Bonn from the PhD students, from the DZNE and from within and outside the scientific community.